ORNL/SPR-2021/2373 Rev. 1

A Study on the Characteristics of the Radiation Source Terms of Spent Fuel and Various Non-Fuel Hardware for Shielding Applications

Georgeta Radulescu
Peter Stefanovic

November 2023

OAK RIDGE National Laboratory

ORNL IS MANAGED BY UT-BATTELLE LLC FOR THE US DEPARTMENT OF ENERGY

ORNL/SPR-2021/2373 Rev. 1

Nuclear Energy and Fuel Cycle Division

A STUDY ON THE CHARACTERISTICS OF THE RADIATION SOURCE TERMS OF SPENT FUEL AND VARIOUS NON-FUEL HARDWARE FOR SHIELDING APPLICATIONS

Georgeta Radulescu
Peter Stefanovic

November 2023

Prepared by
OAK RIDGE NATIONAL LABORATORY
Oak Ridge, TN 37831-6283
managed by
UT-BATTELLE, LLC
for the
US DEPARTMENT OF ENERGY
under contract DE-AC05-00OR22725

CONTENTS

LIST OF FIGURES

LIST OF TABLES

ABBREVIATIONS

APSR	axial power shaping rod
B&W	Babcock & Wilcox
BPR	burnable poison rod
BPRA	burnable poison rod assembly
BWR	boiling water reactor
CE	Combustion Engineering
EFPD	effective full-power day
GE	General Electric
GP	gas plenum
LEF	lower end fitting
LOPAR	low parasitic
MTU	metric ton of initial uranium
NCT	normal conditions of transport
NFH	non-fuel hardware
PWR	pressurized water reactor
OFA	optimized fuel assembly
ORA	orifice rod assembly
SNF	spent nuclear fuel
TPD	thimble plug device
UEF	upper end fitting
WE	Westinghouse

ABSTRACT

Spent nuclear fuel (SNF) cask systems are typically designed for storage and transportation of a variety of fuel assembly and non-fuel hardware (NFH) types (e.g., control rod and burnable absorber rod assemblies) with a wide range of irradiation and decay characteristics. This report analyzes the dependencies of SNF radiation source terms, activated cobalt in hardware materials, and external cask dose rate, with a focus on fuel depletion parameters. This study employed several modeling approaches to help identify the bounding input parameters for shielding analyses. The calculations presented in this report were performed with the analysis sequences within the SCALE code system, which include ORIGEN, ORIGAMI, OPUS, POLARIS, and TRITON for depletion/decay calculations, and MAVRIC for dose rate calculations. MAVRIC uses the Monte Carlo method to solve particle transport problems involved in shielding calculations. Generic cask designs were used in the various MAVRIC calculations.

A parametric study was performed to determine the qualitative and quantitative changes over a full range of parameters which impact primary gamma*, neutron, and ^{60}Co source terms, as well as dose rates. The depletion-related parameters were specific power, initial enrichment, fuel density, fuel temperature, moderator density for both pressurized water reactor (PWR) and boiling water reactor (BWR) fuel. An additional parameter, specific for PWR fuel, was added, cycle-average soluble boron loading. Because multiple radionuclides with different half-lives contribute to the primary gamma and neutron source terms, the trends are shown as a function of selected cooling times from 1 to 40 years. The study extended the range of depletion parameters, previously analyzed in NUREG/CR-6802, for the treatment of PWR and BWR fuel with increased enrichment and higher burnup. The analyzed average fuel assembly burnup and maximum initial UO_2 fuel enrichment values were 80 GWd/MTU and 12%, respectively. The parametric study shows that the neutron source terms and dose rate increase with (1) increasing specific power; (2) decreasing initial enrichment; (3) increasing fuel temperature; (4) decreasing moderator density; and (5) increasing soluble boron concentration (PWR fuel only) for a given burnup and cooling time. The trends were consistent throughout the cooling time interval analyzed. The ^{60}Co activation source terms associated with irradiated fuel hardware and NFH increased with (1) increasing specific power; (2) decreasing initial enrichment; (3) decreasing moderator density; and (4) increasing soluble boron concentration (PWR fuel only) for a given burnup and cooling time. The effects of depletion parameter values on the primary gamma radiation sources are relatively complex because several fission products with various half-lives contribute gamma and bremsstrahlung radiation. As a result, the rate of change in the primary gamma source term/dose rate varies significantly as a function of cooling time for the analyzed ranges of specific power, initial enrichment, and moderator density values at constant burnup. This parametric study showed that a higher fuel enrichment produces conservative primary gamma source terms/dose rate only for cooling times longer than 10 years, whereas a lower fuel enrichment produces conservative primary gamma source terms/dose rate for cooling times shorter than 10 years. Fuel temperature had negligible effects and soluble boron content had relatively small effects (i.e., less than 4% variation over full range of parameters) on primary gamma and ^{60}Co source terms/dose rates. The evaluated fuel density range, 10.0–10.75 g/cm^3 for PWR fuel and 10.26–10.96 g/cm^3 for BWR fuel, had negligible effects on SNF neutron, primary gamma, and ^{60}Co source terms. Ultimately, the

* Gamma radiation is originating from the following sources

1. Decay of radioactive fission products
2. Secondary photons from neutron capture in fissile and non-fissile nuclides
3. Hardware activation products generated during core operations

In this report, the "primary gamma" refers to gamma radiation from "decay of radioactive fission products". This is in literature also referred to as "fuel gamma". In this report, the "secondary gamma" refers to "secondary photons from neutron capture in fissile and non-fissile nuclides". In this report, "^{60}Co source" refers to the activation product of the cobalt impurity in fuel hardware materials, which is the dominating "hardware activation product generated during core operations".

validation of source terms for increased enrichment and higher burnup values approaching 80 GWd/MTU will need to be demonstrated via the use of assay measurements. As these enhanced burnup measurements become available, their results should be factored into future analyses.

Dose rates produced by the generic vertical concrete cask model with PWR SNF were analyzed as a function of fuel assembly burnup (45, 60, and 75 GWd/MTU), cooling time (1, 5, and 40 years), and the air density (1.2 kg/m^3 and 1.108 kg/m^3) for distances up to 1,600 m from the cask center. The far-field dose rates decrease as fuel burnup decreases, cooling time increases, and distance from the cask increases. Air density is a major factor affecting contributions of both direct and skyshine radiation to far-field dose rates. Far-field dose rates increase when air density decreases. For the analyzed cask model, the external total dose rate decreased by approximately 3–10 orders of magnitude between 100 m to 1,600 m from the cask. The dose rate produced by fuel assemblies with an assembly average burnup of 70 GWd/MTU and a one-year cooling time was dominated by primary gamma radiation and ^{60}Co activation sources in fuel hardware materials. At 1 m from the cask surface, the percentage contributions of the primary gamma radiation and the ^{60}Co activation sources are 82% and 17%, respectively, of the total dose rate. The contribution from the primary gamma radiation increases to 89% of the total dose rate, whereas the contribution from the ^{60}Co activation sources decreases to ~4% of the total dose rate, at 1,600 m from the cask center. Primary gamma radiation also dominated the total dose rates at locations up to 1,600 m from the cask center for the five-year cooling time and up to 500–700 m from the cask center for the 40-year cooling time. The contribution of the secondary gamma radiation to the total dose rate increased with increasing distance from the cask. This contribution significantly increased with increasing burnup and cooling time. For a fuel assembly with an average assembly burnup of 70 GWd/MTU and with a 40-year cooling time, secondary gamma radiation dominated the total dose rate at distances beyond 700 m. To further highlight the significance of secondary gamma rays on external dose, dose rates at further distances from the cask were analyzed for cask loadings with similar near-field doses but different fuel assembly average burnup values, initial enrichment, and cooling time. In this report, two fuel assemblies of different irradiation and cooling time characteristics producing the same dose rate at a distance of up to 400 m were analyzed. The dose rates for the higher burnup fuel assembly were higher at distances greater than 400 m, primarily because the neutron and secondary gamma contributions to the total dose rate increase for distances beyond 400 meters.

The effects of several other input parameters and modeling approaches on the external cask dose rates were also examined. These parameters/approaches include fuel assembly design, geometry representation of the active fuel zone in the fuel assembly model (i.e., pin-by-pin or homogeneous material), fuel composition specification (i.e., fresh or irradiated fuel composition), neutrons produced by subcritical multiplication, fuel exposure to burnable absorber or control blade during irradiation, reconstituted fuel assemblies containing irradiated steel replacement rods, and radiation source terms for BWR fuel assemblies with partial-length fuel rods. A summary of the results of these analyses is provided in Section 6 of this report.

Several fuel assembly designs were evaluated to determine the effects of the specified assembly design on the external dose rate of a hypothetical transportation package. The evaluated PWR fuel types include the Babcock & Wilcox (B&W) 15 × 15, Westinghouse (WE) 17 × 17 low parasitic (LOPAR), WE 17 × 17 optimized fuel assembly (OFA), and Combustion Engineering (CE) 16 × 16 fuel types. This study identified the B&W 15 × 15 fuel assembly type as the bounding assembly among the four PWR fuel assembly types in a generic transportation cask. However, the Westinghouse WE 17 × 17 LOPAR fuel assembly produced approximately the same maximum radial dose rate values, within the range of statistical uncertainty, as the B&W 15 × 15 fuel assembly type. The evaluated BWR fuel types, including the 7 × 7, 8 × 8, 9 × 9, and 10 × 10 fuel types with full-length rods and uniform axial enrichment, practically produced the same maximum dose rates within the statistical uncertainty. For each reactor

type, the same set of depletion parameters, fuel initial enrichment, average assembly burnup, cooling time, and axial burnup profile were used in these calculations.

The gamma dose rate produced by a pin-by-pin assembly model was lower by ~5% than that produced by a homogeneous material model. The contributions of neutrons and secondary gamma radiation to the total dose rate were practically identical for the two models. Therefore, the homogeneous material model was slightly conservative than the pin-by-pin model.

The total dose rate values from irradiated fuel and fresh fuel compositions were identical within statistical uncertainty for a hypothetical storage cask model. In both cases the initial enrichment was 4%. However, the irradiated fuel composition produced a slightly higher dose rate value from primary gamma radiation (i.e., by ~2%) and lower dose rate values from neutrons (i.e., by ~15%) and secondary gamma radiation (i.e., by ~17%) than the fresh fuel composition. The two different fuel compositions produced approximately the same maximum external dose rate values because the gamma radiation typically dominates the external dose rates of dry storage casks.

Subcritical neutron multiplication refers to the neutron source produced in the fission reactions induced by neutrons from spontaneous fissions and (alpha,n) reactions in spent fuel. This neutron source is not included in the neutron source terms determined with depletion and decay codes and must be considered as an additional neutron source in dose rate calculations. As indicated in the NUREG/CR-6802, the neutron source multiplication for systems that are subcritical is typically approximated as $1/(1-k_{eff})$ (i.e., subcritical multiplication factor), where k_{eff} is the effective neutron multiplication factor of the spent fuel. However, current Monte Carlo radiation transport codes can include explicit simulations of neutron source multiplications. The contributions that neutrons from subcritical multiplication make to the external neutron dose rate were determined in this study for a generic storage cask with fresh fuel using MAVRIC calculations. The percentage contribution made by the neutron source from subcritical multiplication to the total neutron dose rate was approximately 37% and the percentage contribution to the total secondary gamma dose rate of the secondary gamma radiation associated with the neutrons from subcritical multiplication was approximately 60%.

The neutron source strength of a PWR fuel assembly exposed to a burnable poison rod assembly during irradiation was significantly higher than that of an assembly with no such exposure. The neutron source strength was significantly higher and the ^{60}Co activation source was significantly lower for a BWR fuel assembly exposed to a control blade during irradiation relative to a BWR fuel assembly with no such exposure. However, the difference between assembly neutron source strengths with and without absorber exposures significantly decreased with increasing fuel assembly average burnup and cooling time. Burnable absorber exposure had little effect on primary gamma radiation source terms.

The effects of ^{60}Co in irradiated steel replacement rods in reconstituted PWR fuel assemblies on the external dose rate of a hypothetical storage cask model were evaluated for different canister loading scenarios and selected fuel cooling times from 2 to 75 years. These effects were evaluated relative to dose rate produced by regular PWR fuel assemblies with the same irradiation characteristics as the fuel assemblies containing irradiated replacement rods. The cask capacity was 37 fuel assemblies. Two different PWR canister models with different spatial distributions for the irradiated steel replacement rods inside assemblies were analyzed. In one canister model, each fuel assembly contained 8 to 10 irradiated steel replacement rods, for a total of 366 steel rods per canister (i.e., 4.75% of the total rods in the canister). In the other canister model, each fuel assembly contained 3 to 4 irradiated steel replacement rods, for a total of 136 steel rods per canister (i.e., 1.8% of the total rods in the canister). Additionally, two irradiation scenarios for the steel replacement rods were analyzed for each canister model. In these scenarios, the ^{60}Co source intensities were based on burnup values of 60 GWd/MTU and 40 GWd/MTU for the reconstituted fuel assembly, where the reconstituted fuel assembly discharge burnup is 60

GWd/MTU. The fuel assemblies containing irradiated replacement steel rods produced a maximum of approximately 30% to 130% increase in the external dose rate relative to regular fuel assemblies, depending on the number of steel rods and reconstituted assembly average burnup. The study also showed that a cask containing 9 reconstituted fuel assemblies in the innermost basket locations and regular fuel assemblies in the other basket locations has the same external dose rate, within statistical uncertainty, as a cask loaded with regular assemblies.

A study showed that a full-length fuel rod BWR assembly produces the same maximum radial dose rate as a BWR fuel assembly with partial-length fuel rods, for a given assembly average burnup, axial burnup profile, and cooling time, primarily because of the location of the axial burnup profile peak within the dominant lattice region.

Calculations of ^{60}Co activation sources associated with ^{59}Co impurity in BPRs, orifice rod assemblies (ORAs), and thimble plug devices (TPDs)—which often serve as bounding PWR NFH radiation sources in cask shielding analyses—are also provided. These calculations identified irradiated ORA as the bounding component among ORA and various TPDs because of its slightly higher weight.

1. INTRODUCTION

SNF cask systems are designed for the storage and/or transportation of a variety of fuel assembly and NFH types with a wide range of irradiation characteristics. This report provides radiation source term and dose rate analyses to help identify conservative input parameters with respect to external dose rates of storage and transportation casks. All calculations were performed with depletion, decay, and shielding modules in the SCALE 6.2.4 computer code system [1]. These modules are briefly described in Section 2, and hypothetical transportation and storage cask models are described in Section 3. The contents of this report are as follows.

- A parametric study evaluating the effects of various depletion-related parameters on radiation source terms and dose rates. The study, documented in Section 4, extends the range of parameters previously analyzed in NUREG/CR-6802 [2] to include depletion parameter values anticipated for increased enrichment and higher burnup PWR and BWR fuel. The analyzed average assembly burnup was 80 GWd/MTU and the range of fuel initial enrichment in the parametric study was 1 to 12 %.

- Far-field dose rate from a vertical concrete cask loaded with PWR fuel as a function of distance up to 1,600 m from the cask with varying parameters in these analyses that include the average fuel assembly burnup (45 GWd/MTU, 60 GWd/MTU, and 70 GWd/MTU), fuel cooling time (1, 5, and 40 years), and air density (1.2 kg/m^3 and 1.108 kg/m^3). These analyses are presented in Section 5.

- Radiation source term and dose rate analyses that help identify conservative and yet realistic input parameters and modeling approaches with respect to external dose rates of storage and/or transportation casks (see Section 6). The analyzed parameters are:

  - PWR and BWR fuel assembly designs.
  - Active fuel region models, including pin-by-pin and homogeneous material representations.
  - Fresh fuel composition versus irradiated fuel composition.
  - Contribution to total dose rate of neutron and associated secondary gamma radiation from subcritical neutron multiplication.
  - Fuel assembly exposure to a removable burnable absorber rod (BPR) assembly or a control blade during irradiation versus no exposure. A study is provided to show the effects of these inserts on radiation source terms. However, information about fuel assembly exposure to BPRs or a control blade during operation is in general not publicly available. For example, information on fuel assembly exposure to these inserts is not reported on the GC-859 form [3]. For this reason, the analyses performed for this report are considered as sensitivity of these irradiation parameters to the source terms or dose rates.
  - Fuel assemblies with irradiated steel replacement rods versus regular fuel assemblies.
  - BWR fuel assemblies with partial fuel length rods versus fuel assemblies with full-length rods.

- Source calculations for various NFH, as presented in Section 7.

- Conclusions and recommendations for shielding review of spent fuel dry storage systems and transportation packages (Section 8).

- Future work (Section 9).

2. COMPUTER CODES USED IN DEPLETION, DECAY, AND SHIELDING ANALYSES

The analyses in this report are based on source term and dose rate calculations performed with the SCALE 6.2.4 computer code system [1]. Several computer codes and analyses sequences within the SCALE code system, including ORIGEN, ORIGAMI, POLARIS, TRITON, and MAVRIC, were used to perform radiation source term and dose rate calculation calculations.

2.1 SOURCE TERM CALCULATIONS

The ORIGEN module in the SCALE computer code system calculates time-dependent material concentrations, activities, and radiation source terms for many isotopes produced by neutron transmutation, fission, and radioactive decay during fuel irradiation in the reactors.

POLARIS is a 2D light water reactor lattice physics module in the SCALE computer code system. This module uses a multigroup self-shielding method called the embedded self-shielding method and a transport solver based on the method of characteristics. POLARIS was used to perform depletion calculations. Section 4 of this report provides more detailed discussion on this module.

TRITON is a multipurpose transport-theory based computer module in the SCALE computer code system that is designed to perform depletion and sensitivity and uncertainty analyses. The NEWT (T-DEPL) analysis sequence in the TRITON module was used to generate ORIGEN cross section libraries for various fuel assembly types. These libraries were subsequently used in ORIGAMI calculations to perform fast radiation source term calculations for irradiated fuel and NFH. The TRITON sequence invokes SCALE functional modules for resonance cross section processing, 2D discrete ordinates transport calculations (NEWT), burnup-dependent cross section preparation (COUPLE), and depletion calculations (ORIGEN).

The depletion/decay modules in the SCALE code system have been extensively validated using available radiochemical assay data for UO_2 fuel samples with enrichment up to 4.7% and burnup up to 70.4 GWd/MTU [4, 5]. The methodology used to calculate source terms in ORIGEN module is therefore expected to be applicable to assemblies analyzed in this report. Ultimately, the validation of source terms for fuel enrichments above 5% and burnup values approaching 80 GWd/MTU will need to be demonstrated via the use of assay measurements. As these measurements become available, their results should be factored into future analyses.

2.2 DOSE RATE CALCULATIONS

Dose rate calculations were performed with the MAVRIC shielding analysis sequence in SCALE, which employs the state-of-the-art hybrid variance reduction capabilities [6, 7] developed at Oak Ridge National Laboratory (ORNL) to generate high-fidelity shielding calculation results. A variance reduction method referred to as *forward-weighted consistent adjoint driven importance sampling* was used to estimate dose rates. This method (respWeighting) performs both forward and adjoint discrete ordinates calculations with the Denovo discrete ordinates code [8] to determine energy- and space-dependent source biasing and particle importance parameters.

The American National Standards Institute/American Nuclear Society 6.1.1-1977 neutron and photon flux-to-dose-rate conversion factors [9] were applied to the particle flux estimated by the Monte Carlo method to obtain the dose rate for all dose rate calculations described in this report.

3. CASK MODELS USED IN ANALYSES

This section describes the characteristics of the fuel assembly and cask models used to perform the various dose rate calculations documented in this report. The selection of these models would likely not change the conclusions of the analyses presented in the report.

3.1 FUEL ASSEMBLY MODEL

The fuel assembly model has four axial regions: the lower end fitting (LEF), active fuel, gas plenum (GP), and upper end fitting (UEF) regions. The active fuel region is represented as either a pin-by-pin model or as homogeneous material within the boundary of the active fuel region, depending on the study. The materials in each fuel assembly hardware region were homogenized within the boundary of the hardware region. The physical characteristics of these fuel assemblies are documented in ORNL/SPR-2021/2093 [10]. The fuel assembly hardware regions contain activation sources. The fuel source terms are based on the axial burnup distributions described in Section 3.2.

3.2 AXIAL BURNUP PROFILES

Radiation source terms of the fuel assemblies are dependent on axial burnup value. The axial burnup distribution is typically calculated by multiplying the average fuel burnup with a normalized axial burnup distribution, which is commonly referred as axial burnup profile. The axial burnup profiles used in the dose rate calculations documented in Sections 5 and 6 are presented in Table 1 for the PWR fuel and in Table 2 for the BWR fuel. The PWR axial burnup profile was selected from the YAEC-1937 database [11]. This profile characterizes a B&W 15x15 fuel assembly with an initial enrichment of 3.8% and an average assembly burnup of approximately 49 GWd/MTU. The BWR axial burnup profile was selected from the axial burnup profiles provided in the ANP 32-5045751-00 report [12] for BWR fuel assemblies with burnup greater than 34 GWd/MTU. The profile, originally provided for 25 equally divided axial zones, was collapsed to 10 axial zones [13] to reduce the number of source terms for shielding calculations. Table 2 presents the BWR axial burnup profile collapsed to 10 axial zones.

Table 1. Axial burnup profile for PWR fuel assemblies used in dose rate calculations.

PWR fuel	
Equally divided axial fuel zones	**Axial burnup profile**
1 (bottom)	0.727
2	0.959
3	1.042
4	1.067
5	1.072
6	1.071
7	1.068
8	1.064
9	1.063
10	1.062
11	1.062
12	1.061
13	1.060
14	1.056
15	1.044
16	1.008
17	0.898
18 (top)	0.616

Table 2. Axial burnup profile for BWR fuel assemblies used in dose rate calculations.

BWR fuel		
Axial fuel zone	**Fuel fractional length**	**Axial burnup profile**
1 (bottom)	0.00 – 0.04	0.237
2	0.04 – 0.16	1.074
3	0.16 – 0.24	1.295
4	0.24 – 0.36	1.291
5	0.36 – 0.48	1.244
6	0.48 – 0.60	1.159
7	0.60 – 0.72	1.088
8	0.72 – 0.84	0.957
9	0.84 – 0.92	0.663
10 (top)	0.92 – 1.00	0.203

3.3 HYPOTHETICAL TRANSPORTATION PACKAGE MODEL

This study used two hypothetical transportation packages under normal conditions of transport (NCT), one is for PWR fuel, and the other is for BWR fuel. The PWR canister accommodates 37 PWR fuel assemblies and the BWR canister accommodates 68 BWR fuel assemblies. The model for the PWR fuel package, as depicted in Figure 1, was used in the PWR dose rate analyses. The transportation cask model features two upper and two lower trunnions that penetrate the gamma and neutron shielding materials, thereby decreasing radiation attenuation at these locations. Dose rates were calculated at the cask radial surface and at two meters from the radial surface using a mesh tally. The tally mesh includes 36 azimuthal

and 50 axial equidistant segments between the top and bottom of the active fuel region. Section 6.1 of this report provides more details on the model, shielding calculation, and the calculated dose rates.

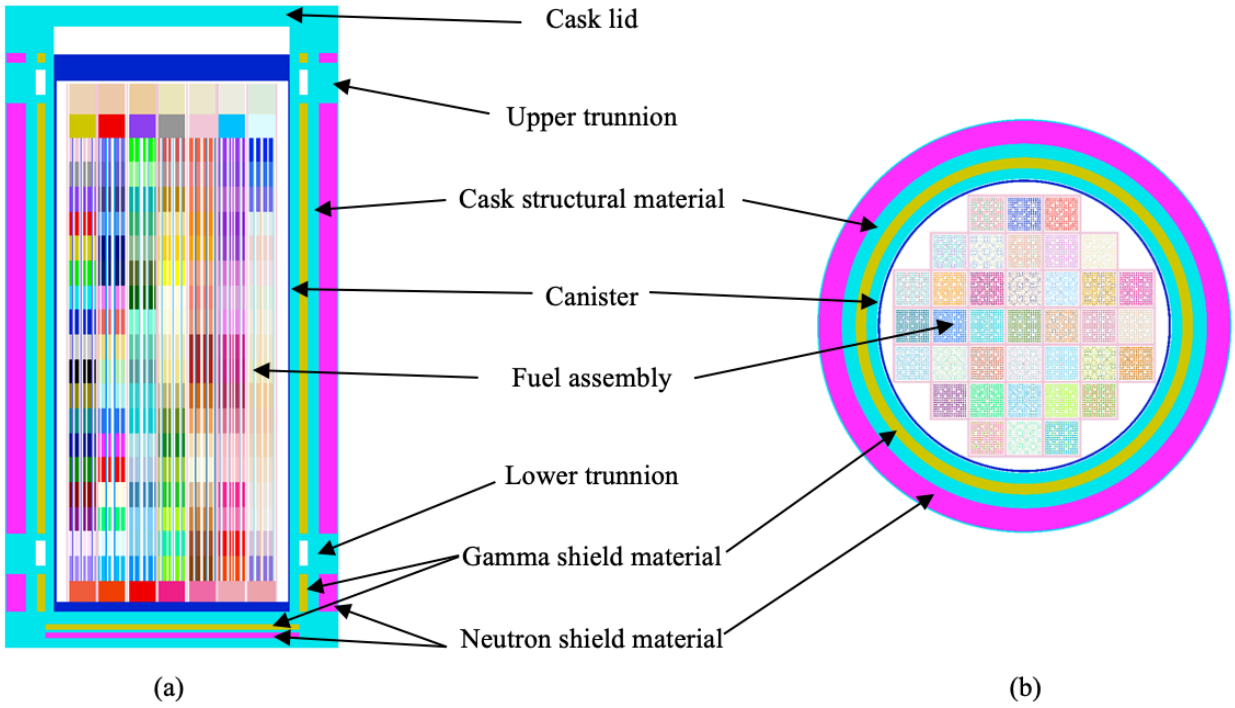

Figure 1. Vertical (a) and horizontal (b) cross-sectional views of the model for the PWR transportation package under NCT.

3.4 HYPOTHETICAL STORAGE CASK MODEL

The hypothetical storage cask model used in dose rate analyses is illustrated in Figure 2. The model features an above-ground vertical concrete storage cask with inlet/outlet air ducts that create radiation streaming paths at cask lower and upper regions. The thickness of the cask concrete in the radial direction is 71 cm. The dose rates were calculated at 1 m from the cask radial surface using a cylindrical tally mesh (see Figure 3) and as a function of distance up to 1,600 m from the cask center using cylindrical tally regions. The skyshine model is illustrated in Figure 3 (b). A cylindrical tally region is located above the ground and has a height of 2 m and a width of 1 m. The radius and the height of the air volume in the skyshine model were 1,900 m and 1,500 m, respectively, to ensure that skyshine radiation was properly accounted for at the various tally locations. The maximum dose rate value within the tally mesh and the average dose rate value within the tally region are used in analyses.

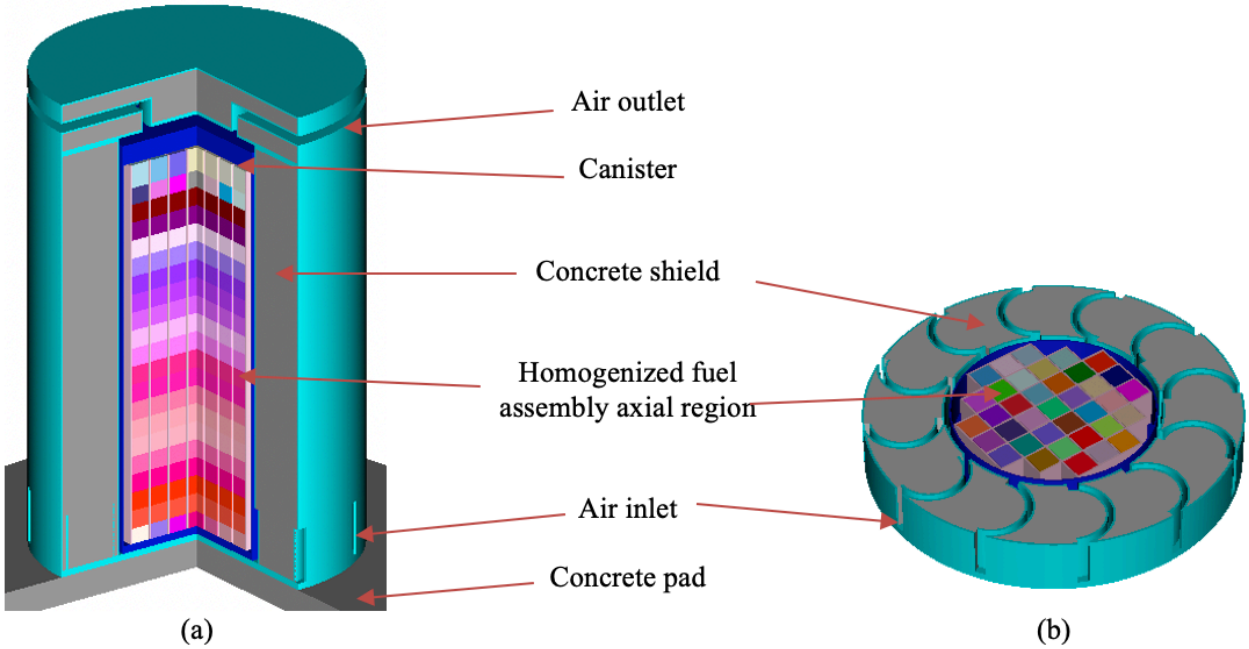

Figure 2. Hypothetical storage cask model with front-right quarter removed (a) and the cask inlet model (b).

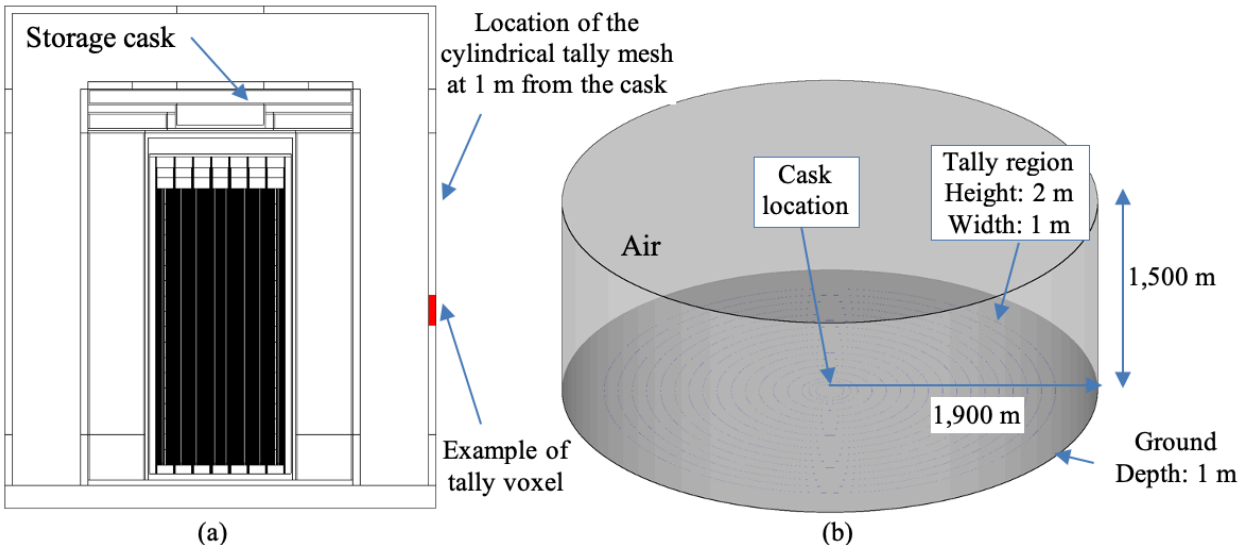

Figure 3. Dose rate tally region at 1 m from the radial surface of the cask (a) and the skyshine model (b).

3.5 SIMPLE SHIELDED FUEL ASSEMBLY MODEL

A model consisting of a single fuel assembly surrounded by 65 cm of concrete (see Figure 4) was used in the parametric study presented in Section 4, for more intuitive results. The maximum dose rates at the surface of the concrete shield and at 1 m from the surface of the concrete shield were calculated for a single source photon or a single source neutron with an energy within the energy groups presented in Table 3 and Table 4. These discrete energy groups are part of the SCALE 27 neutron, 19 gamma energy group structures [1]. The effectiveness of these energy groups is presented in Section 4. For simplicity, the energy groups that produce negligible contribution to dose rates are excluded in this calculation. The

radiation source was sampled uniformly within the volume of the fuel assembly. The dose rates produced by a single source particle are provided as a function of particle energy in Table 3 for primary gamma radiation and Table 4 for neutron and secondary gamma radiation.

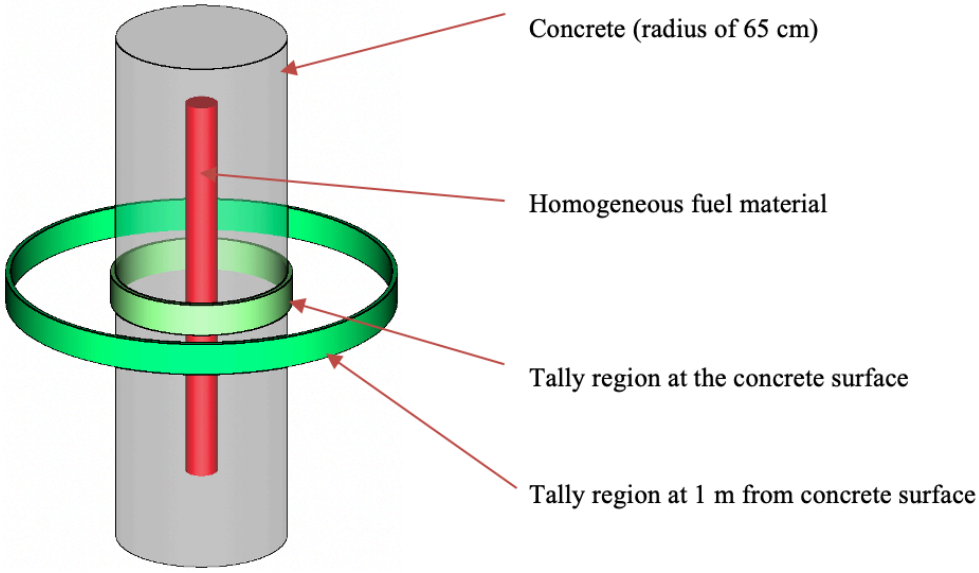

Figure 4. Illustration of the simple shielded assembly model for source term sensitivity studies.

Table 3. Primary gamma dose rate produced by a single source photon as a function of photon energy.

	Surface		1 m from surface	
Energy (eV) range	**Dose rate (mrem/h)**	**Relative error**	**Dose rate (mrem/h)**	**Relative error**
3.0E+05 – 2.0E+05	1.53E-16	0.001	5.51E-17	0.0006
4.0E+05 – 3.0E+05	1.87E-15	0.001	6.78E-16	0.0006
6.0E+05 – 4.0E+05	2.49E-14	0.0008	9.16E-15	0.0005
8.0E+05 – 6.0E+05	1.76E-13	0.0008	6.58E-14	0.0005
1.0E+06 – 8.0E+05	6.77E-13	0.0007	2.56E-13	0.0004
1.33E+06 – 1.0E+06	2.51E-12	0.0007	9.65E-13	0.0004
1.66E+06 – 1.33E+06	7.46E-12	0.0006	2.91E-12	0.0004
2.0E+06 – 1.66E+06	1.65E-11	0.0006	6.52E-12	0.0004
2.5E+06 – 2.0E+06	3.43E-11	0.0006	1.37E-11	0.0004
3.0E+06 – 2.5E+06	6.44E-11	0.0005	2.60E-11	0.0004
4.0E+06 – 3.0E+06	1.25E-10	0.0005	5.13E-11	0.0004

Table 4. Neutron and secondary gamma dose rate produced by a single source neutron as a function of neutron energy.

	Neutrons				Secondary gamma			
	Surface		1 m from surface		Surface		1 m from surface	
Energy (eV) range	DR [a] (mrem/h)	RE [b]	DR [a] (mrem/h)	RE [b]	DR [a] (mrem/h)	RE [b]	DR [a] (mrem/h)	RE [b]
3.0354E+03 – 5.8295E+02	3.01E-10	0.0038	1.06E-10	0.0022	7.07E-10	0.0022	2.79E-10	0.0015
1.5034E+04 – 3.0354E+03	2.80E-10	0.0035	9.88E-11	0.0023	6.84E-10	0.0019	2.70E-10	0.0015
1.1109E+05 – 1.5034E+04	2.58E-10	0.0036	9.16E-11	0.0024	6.63E-10	0.0022	2.62E-10	0.0017
4.0762E+05 – 1.1109E+05	2.41E-10	0.0034	8.48E-11	0.0022	6.48E-10	0.002	2.55E-10	0.0016
9.0718E+05 – 4.0762E+05	2.15E-10	0.0036	7.58E-11	0.0026	6.26E-10	0.002	2.47E-10	0.0015
1.4227E+06 – 9.0718E+05	2.04E-10	0.0039	7.18E-11	0.0024	6.23E-10	0.0023	2.45E-10	0.0017
1.8268E+06 – 1.4227E+06	2.05E-10	0.0042	7.21E-11	0.0025	6.44E-10	0.002	2.53E-10	0.0018
3.0119E+06 – 1.8268E+06	3.10E-10	0.0036	1.10E-10	0.0023	6.93E-10	0.0021	2.71E-10	0.0016
6.3763E+06 – 3.0119E+06	1.05E-09	0.002	3.71E-10	0.0012	7.64E-10	0.0021	2.94E-10	0.0016
2.0000E+07 – 6.3763E+06	5.03E-09	0.001	1.82E-09	0.0006	1.28E-09	0.0019	4.89E-10	0.0015

[a]Dose rate.
[b]Relative error.

4. RADIATION SOURCE SENSITIVITY TO DEPLETION PARAMETERS

Fuel vendors and power reactor licensees are exploring the possibility of an increase in the maximum enrichment of fuel up to 10% and an increase in the burnup limit to 80 GWd/MTU. A parametric study was performed to evaluate the dependencies of the radiation source terms and dose rate on the various depletion parameters. The study extends the range of depletion parameters previously analyzed in NUREG/CR-6802 [2] to include depletion parameter values anticipated for increased enrichment and higher burnup fuel operation. This study used the POLARIS PWR and BWR fuel assembly models documented in ORNL/TM-2020/1833 [14] and ORNL/TM-2020/1835 [15], respectively. The PWR fuel assembly analyzed is a Westinghouse (WE) 17 × 17 fuel assembly containing 104 integral fuel burnable absorbers. The BWR fuel assembly analyzed is a General Electric (GE)14 10 × 10 fuel assembly with two large water tubes. Only the dominant lattice of the BWR assembly (i.e., 92 fuel rods) was analyzed in this 2D parametric study. The parameter variations and the reference values are given in Table 5 for the PWR case and in Table 6 for the BWR case. Only one parameter at a time was varied; the other parameters remain the same as shown in Table 5 and Table 6. The broadness of these ranges is not physical, but the values were chosen such that the values expected for increased enrichment and higher burnup PWR and BWR fuel should be sufficiently included in these ranges. For each variation of the parameters, a POLARIS calculation is performed. The fuel assembly average burnup was 80 GWd/MTU in all depletion calculations. The results of the POLARIS calculations were used as an input to ORIGEN to obtain decay source terms over a 40-year decay scenario. In some cases, a dose rate calculation was performed using the model described in Section 3.5.

Table 5. Parameter ranges of variation for the PWR fuel assembly.

Parameter	**Range of values (reference value)** (Note 1)
Specific power (W/g of initial heavy metal)	10–50 (40)
Enrichment (wt %)	1–12 (8)
Fuel density (g/cm^3) (Note 2)	10.0–10.75 (10.26)
Fuel temperature (K)	500–1,100 (900)
Soluble boron loadings (ppm of B in light water)	0–1,700 (550)
Moderator density (g/cm^3) (Note 3)	0.6611–0.9996 (0.7048)

Note 1: Reference value for burnup was 80 GWd/MTU to represent higher burnup fuel.
Note 2: Fuel mass is maintained constant, and the varying pellet radius is limited to the inner radius of the fuel cladding.
Note 3: Moderator density is varied as a function of temperature for a typical PWR reactor pressure of 2,225 PSI.

Table 6. Parameter ranges of variation for the BWR fuel assembly.

Parameter	**Range of values (reference value)** (Note 1)
Specific power (W/g of initial heavy metal)	10–50 (25)
Enrichment (wt %)	1–12 (10)
Fuel density (g/cm^3) (Note 2)	10.26–10.96 (10.64)
Fuel temperature (K)	500–1,300 (1,100)
Moderator density (g/cm^3)	0.2–1.0 (0.68)
Moderator temperature (K)	383.15–783.15 (583.15)

Note 1: Reference value for burnup was 80 GWd/MTU to represent higher burnup fuel.
Note 2: Fuel mass is maintained constant, and the varying pellet radius is limited to the inner radius of the fuel cladding.

Principal gamma emitters in spent fuel include ^{144}Ce ($T_{1/2}$=284.89 days)/^{144}Pr ($T_{1/2}$=17.29 min), ^{106}Ru ($T_{1/2}$=1.02 years)/^{106}Rh ($T_{1/2}$=2.18 h), ^{134}Cs ($T_{1/2}$=2.0652 years), ^{154}Eu ($T_{1/2}$=8.593 years), and ^{137}Cs ($T_{1/2}$=30.1 years)/^{137m}Ba ($T_{1/2}$=2.6 min) [16]. The analyzed neutron source consists of spontaneous fission neutrons and neutrons from (α,n) reactions within the UO_2 matrix. Principal neutron emitters in spent fuel include ^{244}Cm ($T_{1/2}$=18.1 years) and ^{242}Cm ($T_{1/2}$=0.45 years). The neutron source produced by subcritical

multiplication and the corresponding secondary gammas are treated separately. Section 6.3 of this report provides discussions on how this neutron source and the associated secondary gammas are accounted for in the shielding calculations. Electrons and positrons from fission product decay—such as ^{90}Sr ($T_{1/2}$=28.78 years)/^{90}Y ($T_{1/2}$=64 h)—that are decelerated in the Coulomb field of nuclei produce bremsstrahlung radiation. Percentage contribution of the bremsstrahlung radiation to the total photon dose rate was estimated to 10–20% [17]. Activation of fuel hardware and NFH can significantly contribute to the cask dose rates depending on the exposure history and cooling time. One of the main sources of the activations is ^{60}Co from activated cobalt impurities in hardware materials. The neutron irradiation of iron isotopes (mainly ^{56}Fe) is also a well-known ^{60}Co production pathway. However, the production of ^{60}Co through activation of iron isotopes is much lower than the activation of ^{59}Co impurity. Therefore, only activation of ^{59}Co impurity was evaluated in this parametric study. The results are based on one gram of ^{59}Co irradiated in the active fuel region. For ^{59}Co impurities other than one gram, the ^{60}Co activity can be scaled up by multiplying the activity of 1 gram by the actual amount of impurity in the hardware.

In the next sections, neutron, primary gamma, and ^{60}Co decay source terms are presented as a function of parameter variations indicated in Table 5 and Table 6 for PWR and BWR fuel, respectively. A mathematical description of the normalized source term and dose rate plots is provided in Appendix B. For completeness, the trends for secondary gamma radiation are presented in Appendix A. The primary gamma and neutron strength values shown in the various graphs in the following sections represent source strength per metric ton of initial uranium (s^{-1}/MTU) determined with POLARIS. The ^{60}Co activity values on the various graphs in this section represent ^{60}Co activity per one gram of ^{59}Co (s^{-1}/g) per MTU.

The selected energy range for the gamma radiation source terms analyzed in this parametric study is 0.2 MeV – 4 MeV, which is slightly wider than the typically recommended 0.4 MeV – 3 MeV range for shielding evaluation of SNF in dry storage or transportation casks [18]. Low-energy gamma radiation is not a significant contributor to external cask dose rate because this radiation is easily absorbed in fuel and shielding materials. Gamma radiation with an energy greater than approximately 3 MeV is associated with ^{244}Cm spontaneous fission [19] and typically has a much lower source strength (i.e., by more than five orders of magnitude) than gamma radiation originating from fission product decay. Therefore, the contribution of high-energy gamma radiation to external cask dose rate is shown to be negligible. However, gamma energy greater than 3 MeV is analyzed in this parametric study because higher burnup SNF produces a larger amount of curium that current fuel.

A summary of primary production paths and cumulative thermal fission yields of the main gamma emitters in spent fuel is provided in Table 7 [20,21]. Most of the trending curves in the graphs provided in the next sections for the group-wise primary gamma source terms can be explained by the cumulative fission yields of the individual fission products from ^{235}U and ^{239}Pu and the impact of the varying depletion parameters on the neutron flux/energy spectrum. The production path of ^{244}Cm includes resonance and radiative capture reactions. ^{60}Co has a large capture resonance at ~100 eV [22] that dominates neutron capture.

Table 7. Summary information for main gamma emitters in spent fuel.

Radionuclide	Half-life	Primary production path	Cumulative thermal fission yield from ^{235}U	Cumulative thermal fission yield from ^{239}Pu
^{144}Ce	284.89 days	Fission	5.474	3.75
^{106}Ru	1.02 years	Fission	0.41	4.188
^{134}Cs	2.0652 years	^{133}Cs thermal capture	6.60	6.99
^{154}Eu	8.593 years	^{153}Eu thermal capture	0.1477	0.38
^{90}Sr	28.78 years	Fission	5.73	2.013
^{137}Cs	30.1 years	Fission	6.221	6.588

4.1 PWR ASSEMBLY STUDY

4.1.1 Specific Power

This section analyzes trends of variation with specific power for the radiation source terms of a PWR fuel assembly with an average assembly burnup of 80 GWd/MTU. Specific power affects the rate at which fission products are produced from fission events. The equilibrium level of unstable nuclides where the decay rate approaches the production rate is directly proportional to the specific power. The neutron flux increases with increasing specific power. Neutron energy spectrum hardening is also caused by an increase in the specific power [23].

4.1.1.1 Primary Gamma Radiation

In Figure 5(h), the total gamma radiation source terms are plotted as a function of specific power and cooling times. In this plot, the maximum total source strength over the whole range of evaluated specific power values is found for each cooling time. The results for that cooling time are then normalized by its respective maximum value. This figure shows that the total strength of the gamma source terms increases with increasing specific power, whereas it decreases with increasing cooling time. Furthermore, the effect of specific power on source terms reduces significantly as the cooling time increases. At shorter cooling times, the difference in source terms between the lowest and highest specific power values is approximately 50–60%. After 20 years of cooling, this difference reduces to less than 20%.

For shielding problems, the source strength within the individual energy range may impact the total dose rates outside a transportation package or a storage cask. To illustrate this effect, Figure 5(a–g) shows the trend of gamma source variation as a function of specific power for the energy groups in the range of 0.2 MeV to 4 MeV. The maximum source strength over the entire range of evaluated specific powers is found for each energy group source term, and the results within the energy group are then normalized by this maximum source term value to illustrate the trend of variation with specific power, as shown in Figure 5(a–g). The results show that the per energy group source terms follow a similar trend to the total source term: increasing with increasing specific power. This trend is produced by an increase in the production rate of fission products as fission rate increases. At longer cooling times, the source terms for photons in the energy group 2.5–3.0 MeV show the opposite trend. The reason for this behavior is that the gamma emitters with contributions to the energy group 2.5–3.0 MeV are ^{106}Rh, a short-lived nuclide in secular equilibrium with ^{106}Ru ($T_{1/2}$=1.02 years), and ^{208}Tl, a nuclide in the decay chain of minor actinide ^{232}U ($T_{1/2}$=68.9 years). ^{106}Ru decays away after approximately 10 years of cooling and ^{208}Tl remains the principal gamma emitter contributing to this energy group. During beta decay of ^{208}Tl gamma radiation with energy of 2,614 keV is emitted. The concentrations of ^{232}U and ^{208}Tl in fuel decreases with increasing specific power. However, this effect does not impact total source strength beyond the statistical uncertainties, as shown in Figure 5(h), because the ^{208}Tl gamma source strength is approximately five orders of magnitude lower when compared with the source terms from dominating energy groups. The results in Figure 6 show a negligible contribution to total dose rate from photons with energies below 0.4 MeV and above 3 MeV.

As a confirmation, a dose rate calculation was performed using the simple shielded assembly model described in Section 3.5. The external gamma dose rate values are plotted in Figure 6. The evaluation confirms the similar trends as the source terms described above, in which external dose rates increase with increasing specific power. Further examination of the dose rate contribution from individual radioisotopes is provided in Figure 7. For spent fuel with five years or less cooling time, the fractional dose contributions of ^{106}Ru/^{106}Rh, ^{144}Ce/^{144}Pr and ^{134}Cs (> 1 year) increase as specific power increases, whereas the fractional contributions of ^{154}Eu and ^{137}Cs/^{137m}Ba decrease as specific power increase.

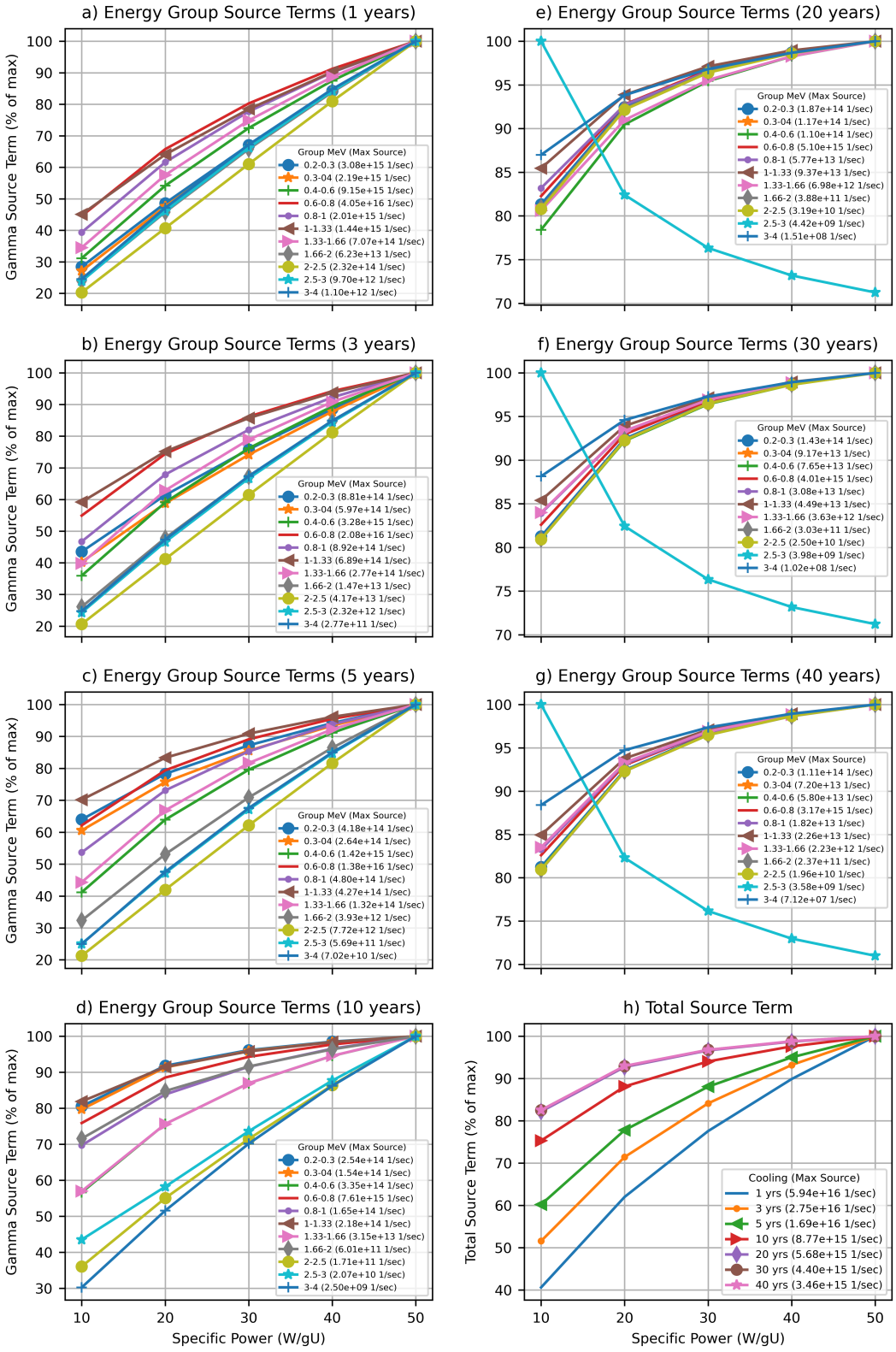

Figure 5. Gamma source terms as a function of specific power.

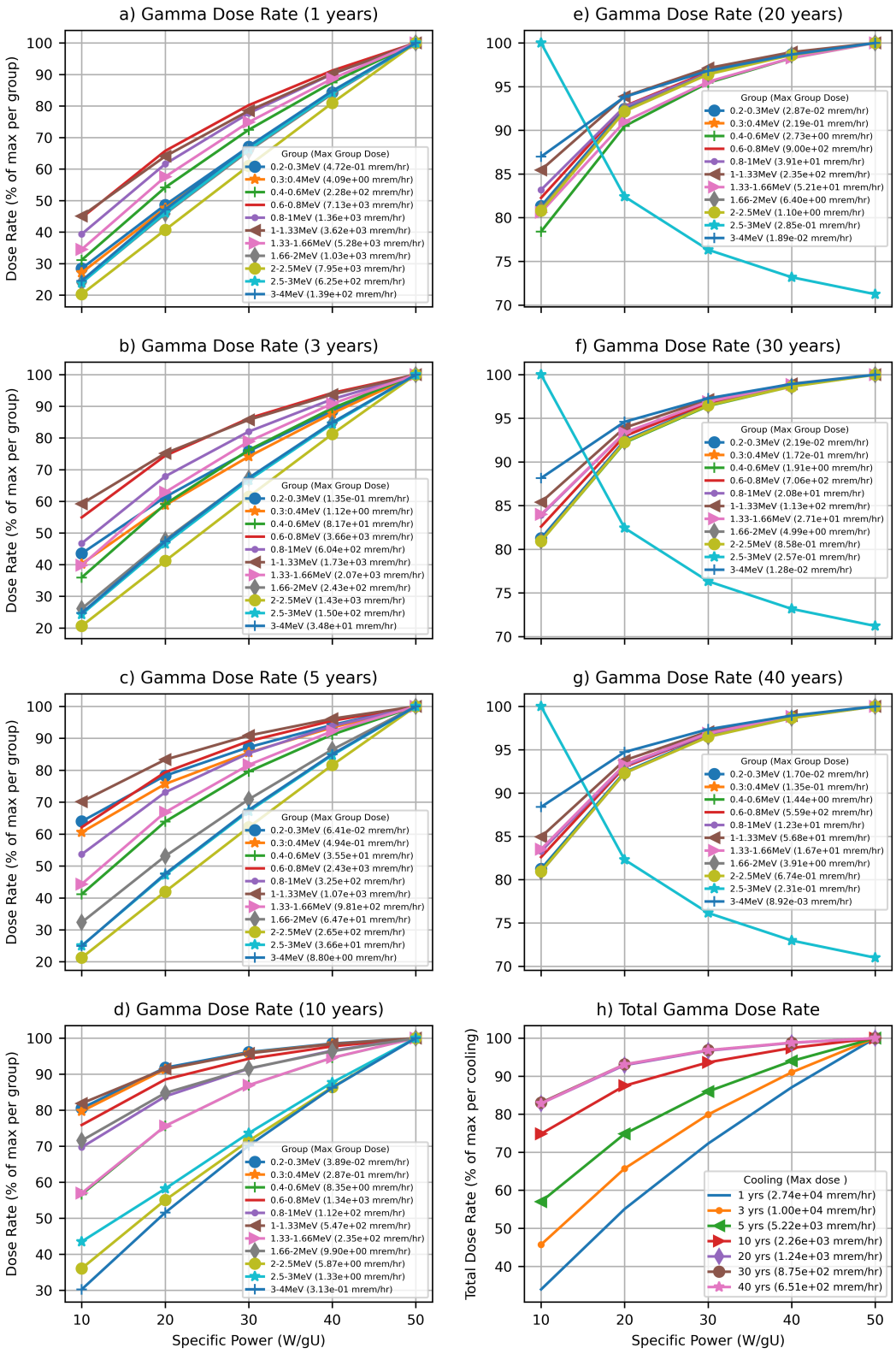

Figure 6. Gamma dose rate as a function of specific power.

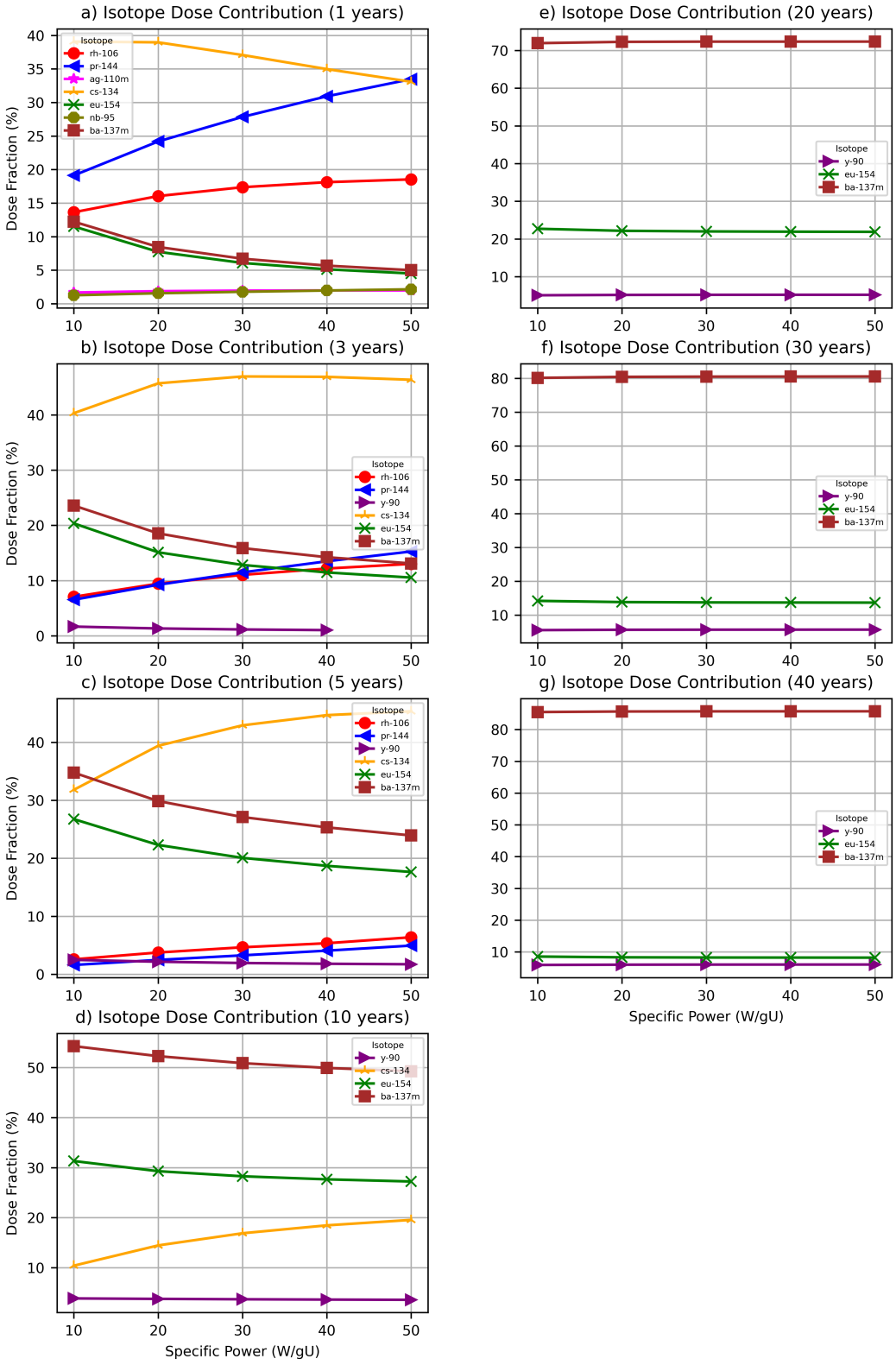

Figure 7. Radionuclide fractional contributions to gamma dose rate as a function of specific power.

4.1.1.2 Neutron Radiation and Secondary Gamma Radiation

In Figure 8(h), the total neutron radiation source terms are plotted as a function of specific power for selected cooling times. In this figure, the maximum total source strength over the entire range of evaluated specific power is found for each cooling time. The results with the given cooling time are then normalized by the corresponding maximum value as shown in the plot legend. The total strength of the neutron source terms increases with increasing specific power. However, the impact on neutron source terms is less pronounced than that observed for gamma source terms. Furthermore, as opposed to gamma source terms, the effect of specific power on neutron source terms does not significantly decrease with cooling time. At short cooling times, the difference in source terms between the lowest and highest specific power is approximately 11%. After 30–40 years of cooling, the difference remains mostly unchanged, at approximately 12%.

Figure 8(a–f) shows the neutron source strength for each energy group. The graphs show that the energy groups follow a trend similar to that of the total source term: increasing with increasing specific power. No significant changes in source term energy spectra are indicated by these results over the 40 years of cooling time. Contributions above 1% to neutron source terms from individual nuclides are shown in Figure 9. ^{244}Cm ($T_{1/2}$=18.1 years) is the dominating neutron source throughout the 40 years period. ^{242}Cm ($T_{1/2}$=0.45 years) is an important neutron emitter only for short cooling time (< 3 years), contributing between 8% to 10% of the total source strength at the one-year cooling time. Contribution from ^{246}Cm ($T_{1/2}$=4,760 years) increases with increasing cooling time, up to approximately 5%. After 30 years of cooling, contribution to neutron source from ^{238}Pu increases above 1%. The concentration of transuranic nuclides in irradiated fuel, including curium nuclides, increases with increasing specific power [23]. As shown in Figure 8(a–f), the curves beyond one-year of cooling, representing the variation of total and group-wise neutron source intensities as a function of specific power, overlap because all these neutron sources predominantly originate from ^{244}Cm spontaneous fission, and alpha decay with subsequent (alpha, n) reaction. The curve for the one-year cooling shown in Figure 8(h) has a slightly different increase rate than the curves for longer cooling times because the neutron source term for the one-year cooling time includes contributions from both ^{244}Cm and ^{242}Cm.

A dose rate calculation was performed using the simple shielded assembly model described in Section 3.5. The external neutron dose rate values plotted in Figure 10 exhibit an increasing trend with increasing specific power, which is consistent with the trend observed for the neutron source terms. It is important to point out that the purpose of using the simplified shielding model is to examine the trends of the dose rates against various parameters rather than to get the actual value of a specific cask design. For this purpose, a simplified cask model is sufficient.

Since the secondary gamma dose rates are associated with the neutron source terms, the trends are similar. For completeness, these results are provided in Figure A-1.

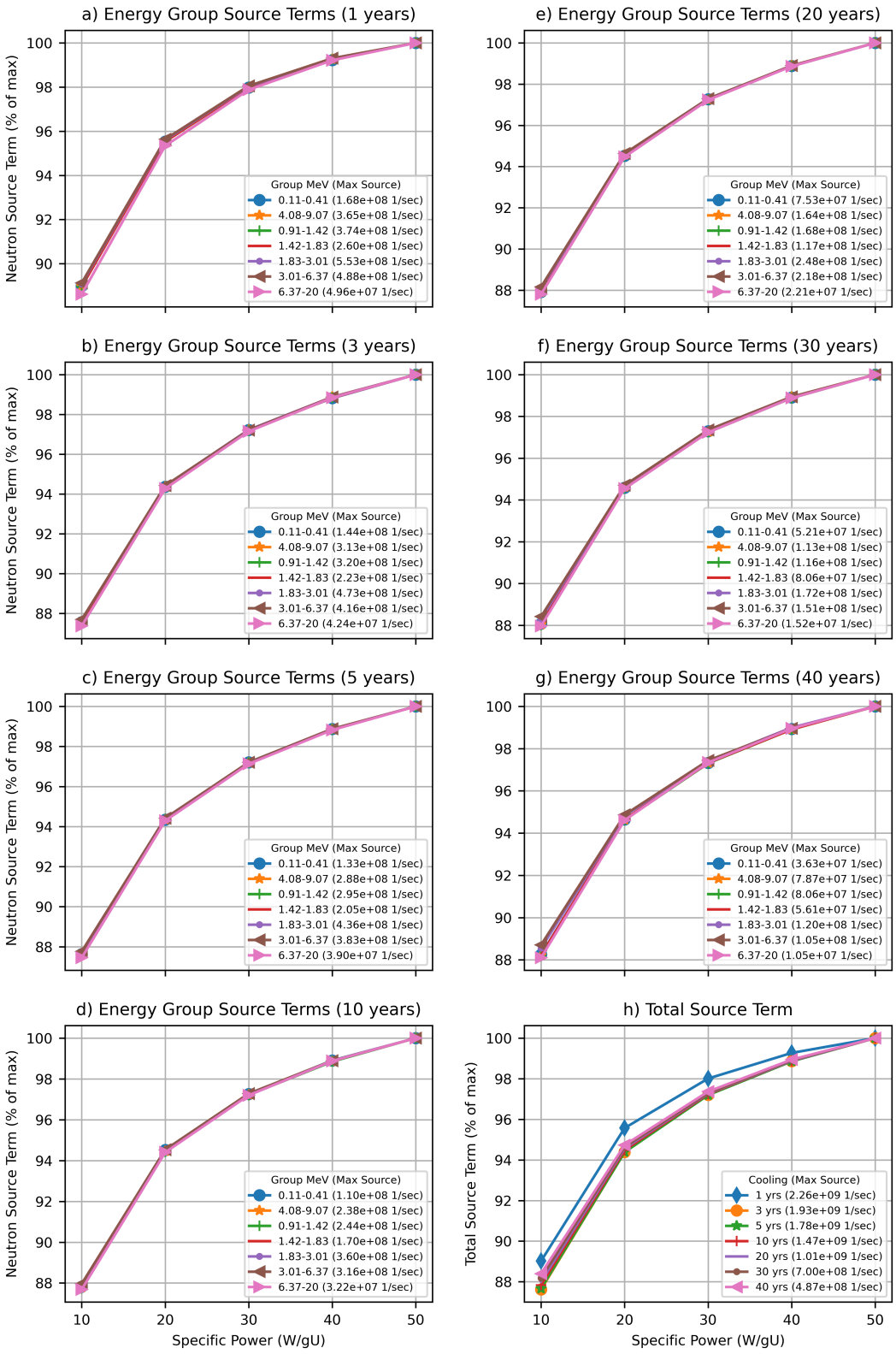

Figure 8. Neutron source terms as a function of specific power.

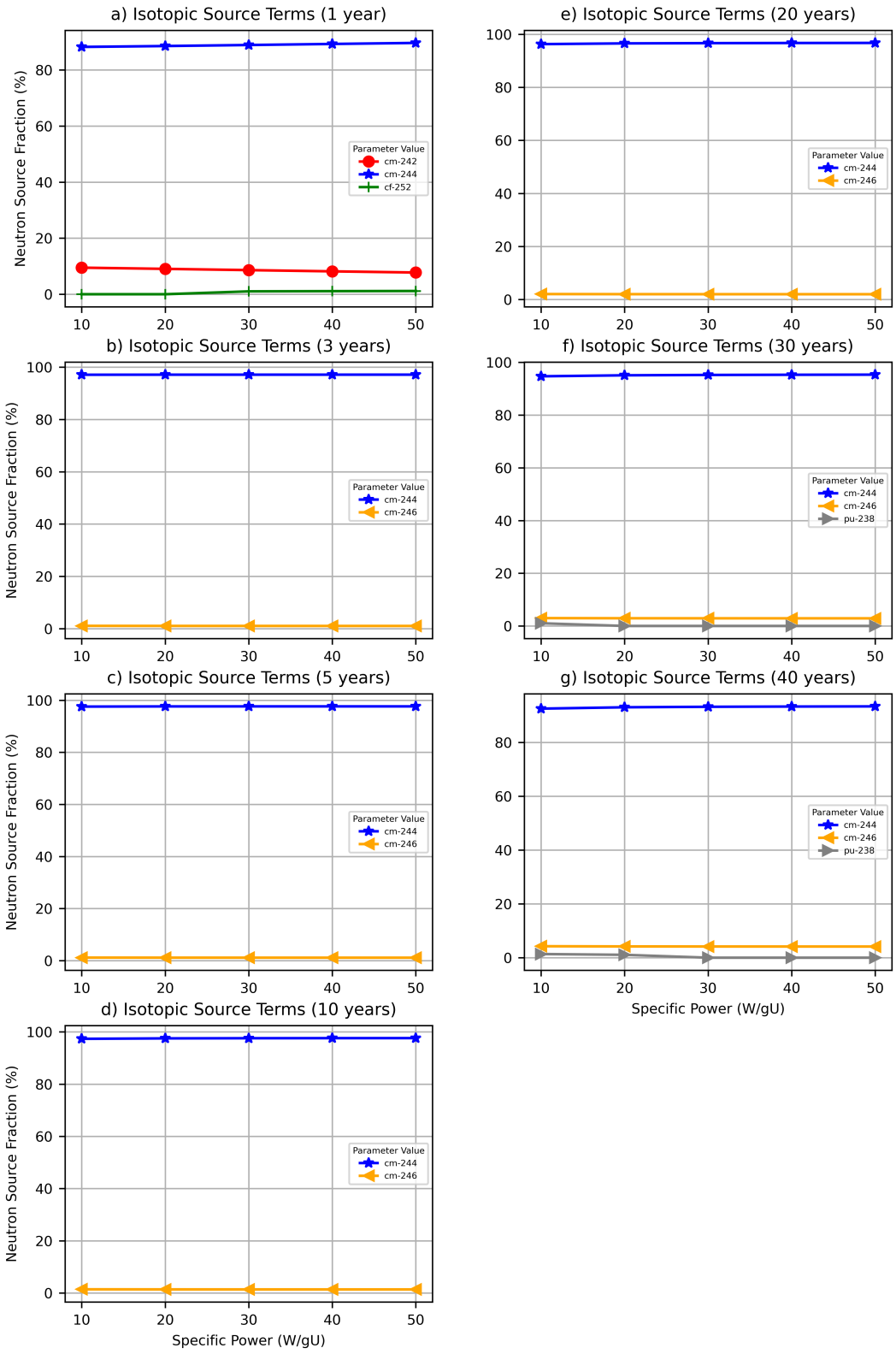

Figure 9. Radionuclide fractional contributions to total neutron source as a function of specific power.

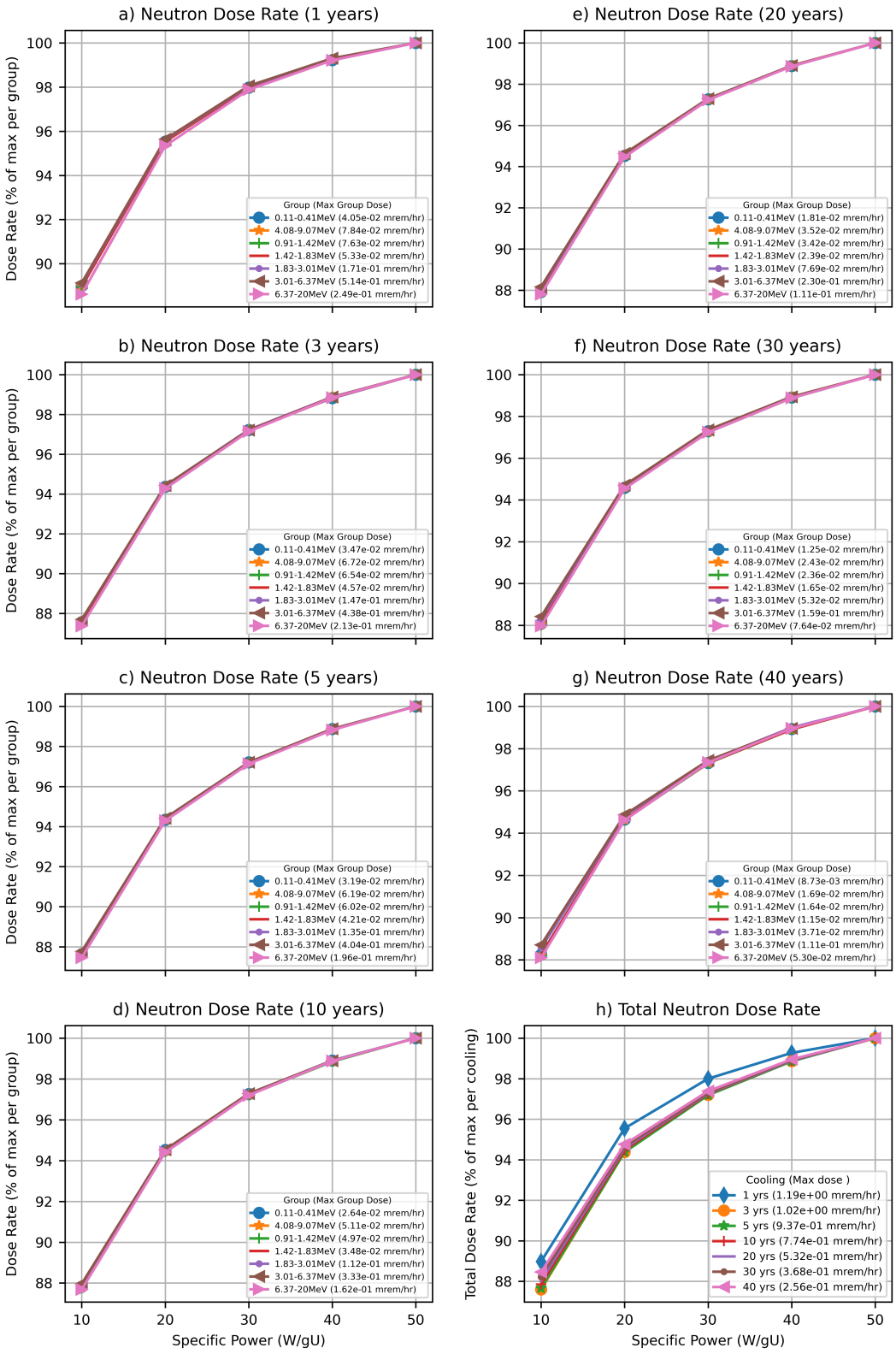

Figure 10. Neutron dose rate as a function of specific power.

4.1.1.3 Cobalt Activation Source Terms

The ^{60}Co ($T_{1/2}$=5.27 y) activity is evaluated by irradiating 1 g of ^{59}Co impurity in the active fuel region. The normalized ^{60}Co activity is plotted as a function of specific power in Figure 11. Similar to other source term plots, the ^{60}Co activity is normalized by the maximum ^{60}Co activity within the range of the evaluated variable and given cooling time. The maximum ^{60}Co activities per gram of ^{59}Co per MTU at various cooling times are provided in the legend of Figure 11. The curves in this figure overlap because ^{60}Co activity change as a function of specific power is the same for all cooling times. The ^{60}Co activity significantly increases as specific power increases primarily because the neutron flux increases with increasing specific power.

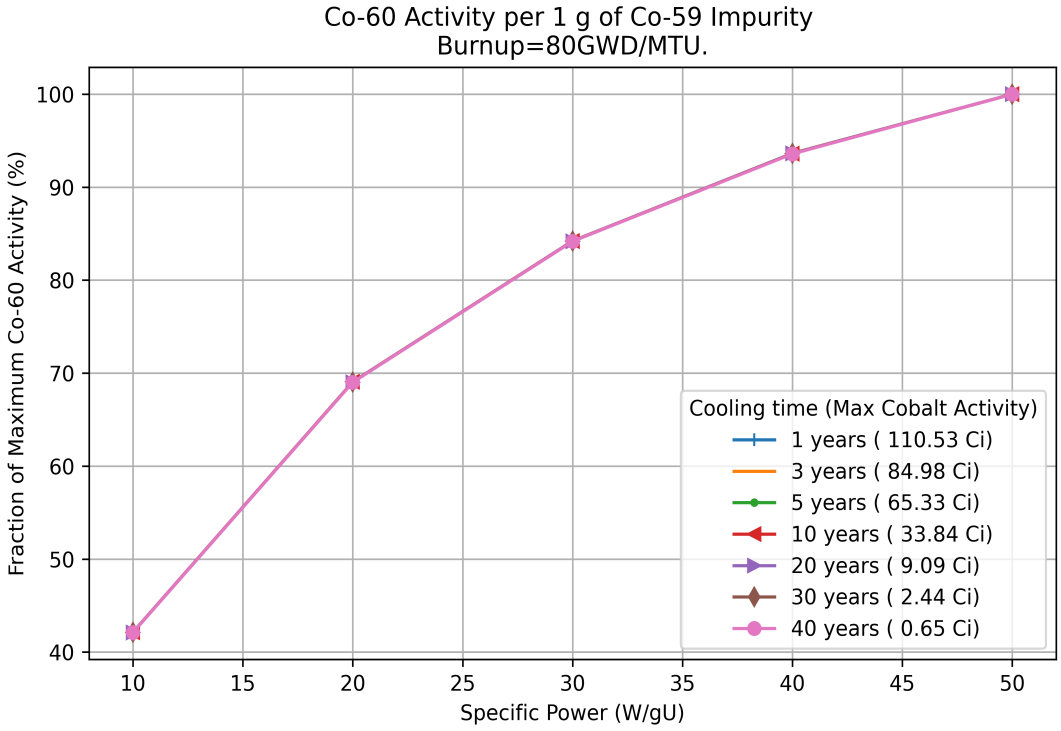

Figure 11. ^{60}Co activity as a function of specific power.

4.1.2 Initial Enrichment

This section analyzes trends of the radiation source terms as a function of initial fuel enrichment of a PWR fuel assembly with an average assembly burnup of 80 GWd/MTU. An increase of the fuel initial enrichment causes an increase of the ^{235}U absorption rate, a decrease of the absorption rates of other nuclides, a reduction of the thermal neutron flux [14], and neutron spectrum hardening. Fuel with higher enrichment will need lower neutron flux to achieve the same power density compared with fuel with lower enrichment.

4.1.2.1 Primary Gamma Radiation

In Figure 12(h), the total gamma radiation source terms are plotted as a function of assembly enrichment and cooling time. In this plot, the maximum total source strength over the entire range of evaluated enrichment values is found for each cooling time. The results for that cooling time are then normalized by that maximum value. The figure shows that the total strength of the gamma source term decreases with increasing enrichment for shorter cooling times (<10 years), whereas it increases with enrichment for longer cooling times (>10 years). Furthermore, the sensitivity of the total gamma source strength to the fuel initial enrichment decreases as cooling time increases. At short cooling times, the difference in source term between the lowest and highest specific power is approximately 17–28%. After 20 years of cooling, this difference diminishes to less than 7%.

Figure 12 (a–g) shows the trends of variation as a function of fuel enrichment of the gamma radiation sources within energy groups in the range of 0.2 MeV to 4 MeV. The maximum source strength over the entire range of evaluated initial enrichments was found for each energy group source terms, and the results within the energy group were then normalized by this maximum source terms value and plotted to illustrate the trend of variation with fuel enrichment. The normalized results show that the per energy group source terms generally follow a similar trend to the total source term: a decreasing trend with increasing enrichment for shorter cooling times (<10 years) and an increasing trend with increasing enrichment for longer cooling times (>10 years). The results in Figure 12 show a decreasing contribution to total dose rates from photons with energies below 0.4 MeV and above 3 MeV.

A dose rate calculation was performed using the simple shielded assembly model described in Section 3.5 to determine the trend of dose rate variation as a function of fuel enrichment. The gamma dose rates are plotted in Figure 13. The evaluation confirms the similar trends of the source terms as described above, in which the external dose rate decreases with increasing enrichment up to 5 years cooling, then there is a transition at about 10 years; and with further cooling time, the dose rates start to increase as enrichment increases. A further analysis with the contributing isotopes in the spent fuel as discussed below provide some insights on the observed behavior of the gamma source terms and corresponding dose rates. As shown in Figure 14, in the early discharge times (short cooling times), the dose rates are dominated by gamma radiation from the decay of the following fission products: ^{134}Cs ($T_{1/2}$=2.0652 years), ^{144}Ce ($T_{1/2}$=284.89 days)/^{144}Pr ($T_{1/2}$=17.29 min), ^{137}Cs ($T_{1/2}$=30.1 years)/^{137m}Ba ($T_{1/2}$=153 s), ^{106}Ru ($T_{1/2}$=1.02 years)/^{106}Rh ($T_{1/2}$=2.18 h), and ^{154}Eu ($T_{1/2}$=8.593 years). After 10 years of cooling, ^{137}Cs/^{137m}Ba, ^{154}Eu, and ^{90}Sr ($T_{1/2}$=28.78 years)/^{90}Y ($T_{1/2}$=64 h) are the most contributing radionuclides.

The trends observed in Figure 12(a–g) for the group-wise gamma source terms are further explained based on the accumulation and reduction resulting from neutron absorption and decay of the radionuclides during fuel irradiation and cooling time as presented in Table 7 and the effects of fuel enrichment variation on neutron flux and energy spectrum described at the beginning of Section 4.1.2.

Prompt gamma radiation from ^{244}Cm spontaneous fission contributes to the 3 – 4 MeV energy range. The decreasing trend observed from the 3 – 4 MeV energy range for all cooling times is consistent with a

decrease in ^{244}Cm concentration with increasing fuel enrichment for a given fuel burnup. A reduction of minor actinides with atomic number higher than ^{239}Pu occurs as the fuel initial enrichment increases [14].

The dominant gamma emitters for the energy range 2 – 3 MeV are ^{144}Ce/^{144}Pr and ^{106}Ru/^{106}Rh at cooling times less than 5 years, and ^{90}Sr/^{90}Y at longer cooling times. The concentration of ^{144}Ce in irradiated fuel increases with increasing fuel enrichment because its cumulative fission yield from ^{235}U is higher than that from ^{239}Pu. Further, ^{239}Pu concentration is lower with higher ^{235}U enrichment. In addition to its contribution to the energy group 0.4 – 0.6 MeV, ^{106}Ru/^{106}Rh is also a contributor to the gamma energy in the range of 1.66 – 4 MeV for cooling times less than 5 years. However, the concentration of ^{106}Ru in irradiated fuel decreases with increasing fuel enrichment because the fission yield of ^{106}Ru from ^{239}Pu is ~ 10 times higher than that from ^{235}U. These opposite trends between ^{144}Ce and ^{106}Ru produce the trends observed for the energy range 2.5 – 3 MeV up to 10 years of cooling: an ascending trend below 3 years of cooling and a descending trend from 5 to 10 years of cooling, depending on the dominant contributing radionuclide at each cooling time. Bremsstrahlung radiation associated with ^{90}Sr/^{90}Y beta decay is another contribution to the energy range 2 – 2.5 MeV. In fact, the maximum energy of the beta particles from ^{90}Y decay of 2.28 MeV produces bremsstrahlung radiation in almost all energy groups below this energy. The cumulative fission yield of ^{90}Sr from ^{235}U is more than twice as much as that from ^{239}Pu, which determines its increasing trend with increasing enrichment. Therefore, gamma sources in energy range 2 – 2.5 MeV exhibits an ascending trend for cooling times longer than 10 years.

The energy range 0.8 – 1.66 MeV is dominated by the gamma radiation from ^{134}Cs, ^{154}Eu, and ^{90}Sr/^{90}Y decay. ^{134}Cs is a self-shielded fission product [21] primarily produced by ^{133}Cs thermal capture reaction and the cumulative fission yields of ^{133}Cs from ^{235}U, ^{239}Pu, and ^{241}Pu are similar. ^{134}Cs concentration decreases as fuel enrichment increases because the thermal flux decreases with increasing fuel enrichment at constant fuel burnup. ^{154}Eu is another self-shielded fission product, primarily produced by ^{153}Eu thermal capture reaction. However, the fission yield of ^{153}Eu from ^{239}Pu is more than twice as much as the fission yield of ^{153}Eu from ^{235}U, which explains the increasing trend of ^{154}Eu contributions with increasing fuel enrichment.

The gamma radiation in energy range 0.6 – 0.8 MeV contains sources from ^{134}Cs, ^{154}Eu, and ^{137}Cs/^{137m}Ba decay, with ^{134}Cs being the dominant contributor for shorter cooling times. The cumulative fission yields of ^{137}Cs from ^{235}U, ^{239}Pu, and ^{241}Pu fissions are relatively similar. Therefore, ^{137}Cs production rate does not exhibit significant sensitivity to fuel enrichment at constant power density. As previously described, ^{134}Cs exhibits a decreasing trend with increasing enrichment while ^{154}Eu exhibits an increasing trend with increasing enrichment at constant burnup. This explains the decreasing trend at cooling times shorter than 10 years and the slightly increasing trend at longer cooling times observed for the energy range 0.6 – 0.8 MeV as a function of fuel enrichment.

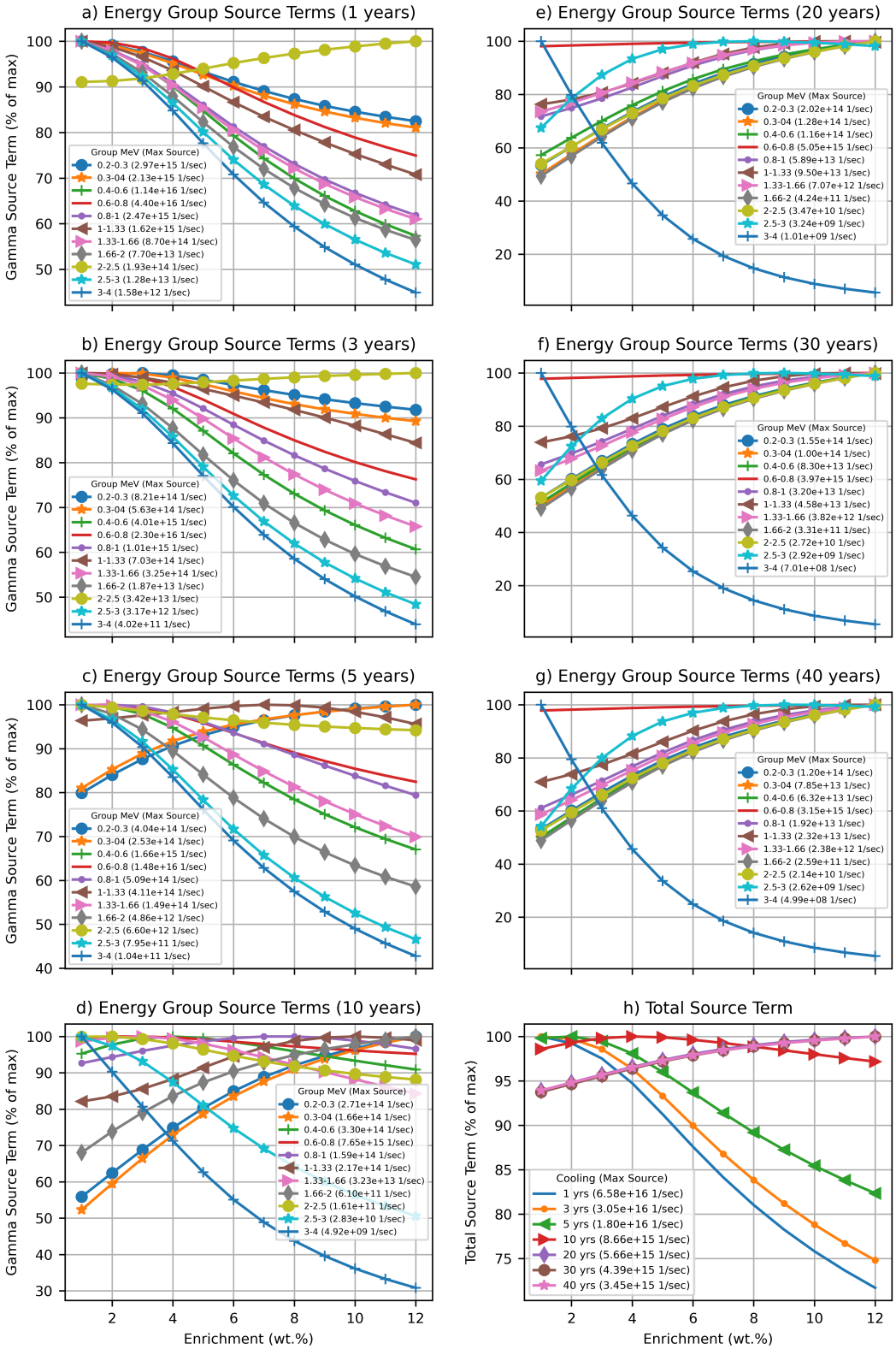

Figure 12. Gamma source terms as a function of initial enrichment.

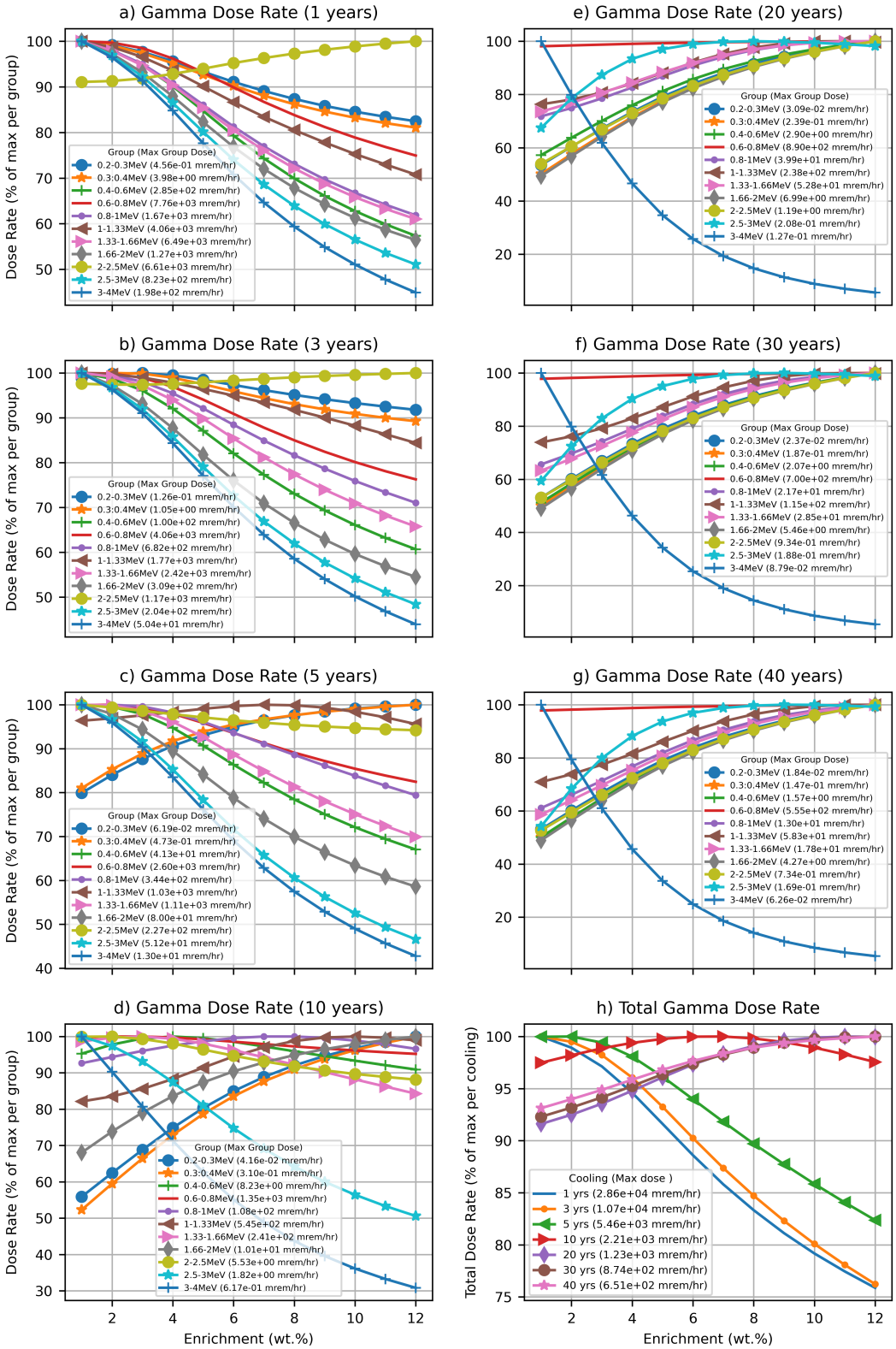

Figure 13. Gamma dose rates as a function of initial enrichment.

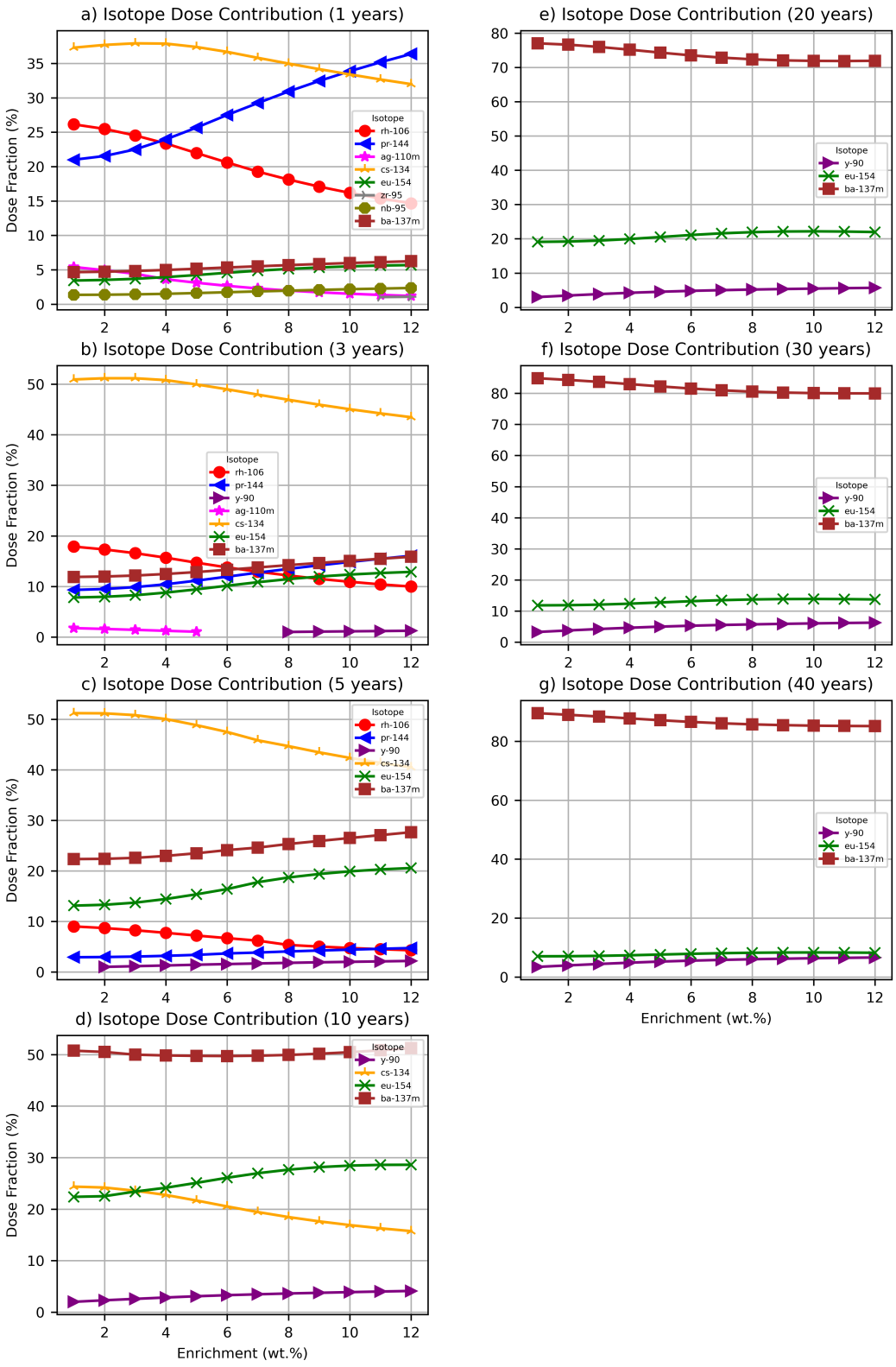

Figure 14. Radionuclide fractional contributions to gamma dose rate as a function of enrichment.

4.1.2.2 Neutron Radiation and Secondary Gamma Radiation

An increase of the fuel initial enrichment causes an increase of the ^{235}U absorption rate and a reduction of the thermal flux [14]. The net effect is a reduction of minor transuranic actinides as the fuel initial enrichment increases. In Figure 15(h), the total neutron radiation source terms are plotted as a function of initial enrichment for the 80-GWd/MTU average assembly burnup and selected cooling times. In this plot, the maximum total source strength over the whole range of evaluated initial enrichments is found for each cooling time. The results for that cooling time are then normalized by that maximum value. From this figure, it can be observed that the total strength of the neutron source terms decreases with increasing initial enrichment.

Figure 15(a–g) shows the neutron source strength for each energy group. The results show that all energy groups follow a trend similar to that of the total source term: decreasing with increasing initial enrichment. No significant changes in source terms spectra are indicated by these results over the 40 years of cooling time. Contributions above 1% to neutron source terms from individual isotopes is shown in Figure 16. From Figure 16, it can be observed that contributions to source terms from ^{244}Cm ($T_{1/2}$=18.1 years), ^{242}Cm ($T_{1/2}$=0.45 years), and ^{246}Cm ($T_{1/2}$=4,760 years) decrease over time. ^{244}Cm ($T_{1/2}$=18.1 years) is the dominating source throughout the 40 years period. Since the source terms are dominated by ^{244}Cm, therefore the total source and group-wise source terms in Figure 15(a–g) follow the same trend. At lower enrichments and shorter cooling times, contribution from ^{252}Cf may increase up to 50% of the source. Since ^{252}Cf has a half-life of 2.645 year, the source will quickly decay to a small contributor. After 30 years of cooling, contributions to neutron source from ^{238}Pu and ^{240}Pu increase above 1%.

For the same fuel burnup, fuel with low enrichment contains greater quantities of transuranic nuclides, including ^{246}Cm ($T_{1/2}$=4,760 years) and ^{252}Cf ($T_{1/2}$=2.645 years), than fuel with higher enrichment.

A dose rate calculation was performed using the simple shielded assembly model as described in Section 3.5. The neutron dose rates are plotted in Figure 17. The evaluation confirms the similar trends of the source terms, where external dose rates decrease with increasing initial enrichment. Since trends in the secondary gamma dose rates are linked to neutron source terms, the trends are similar. For completeness, these results are provided in Figure A-2.

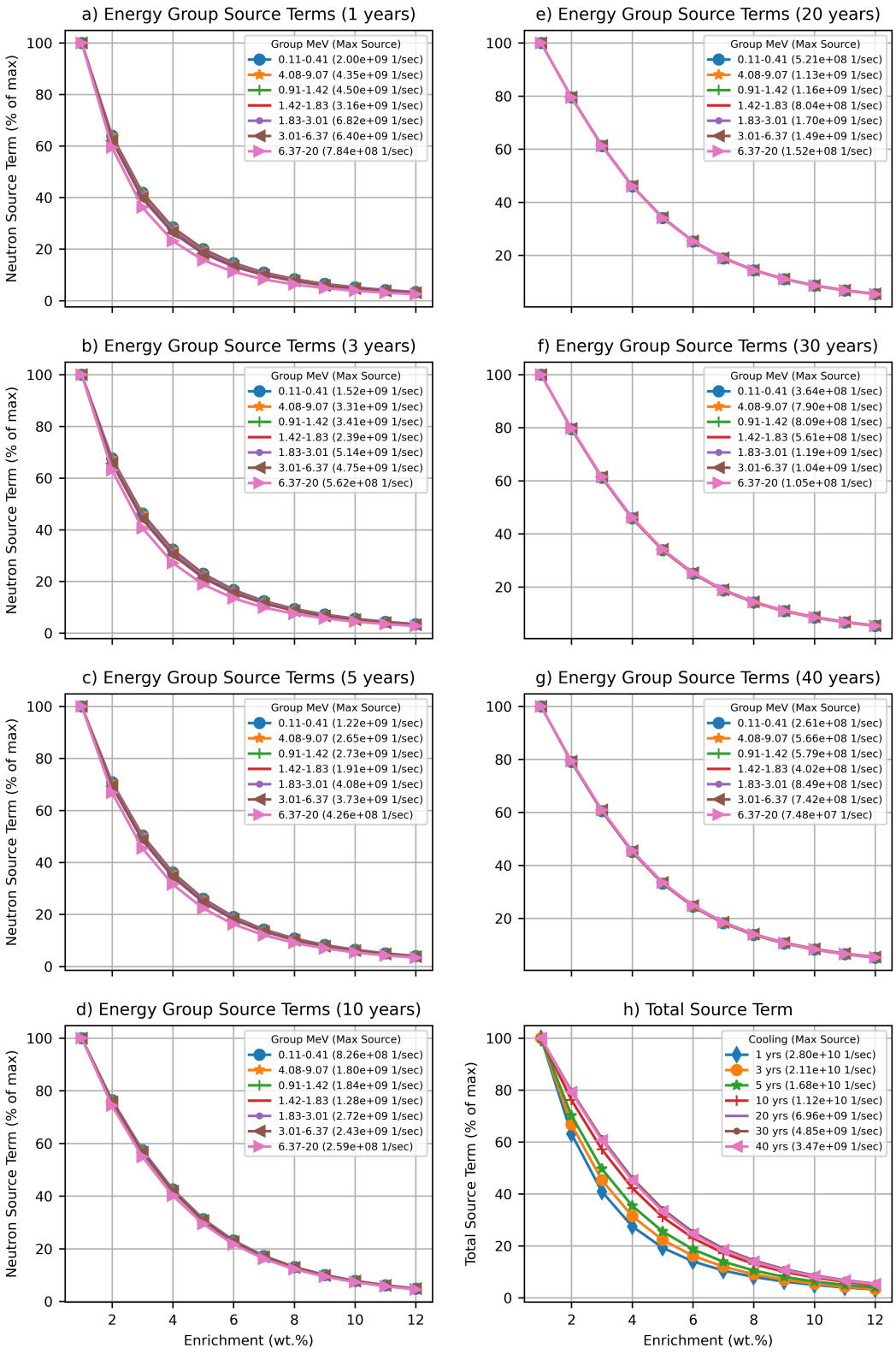

Figure 15. Neutron source terms as a function of enrichment.

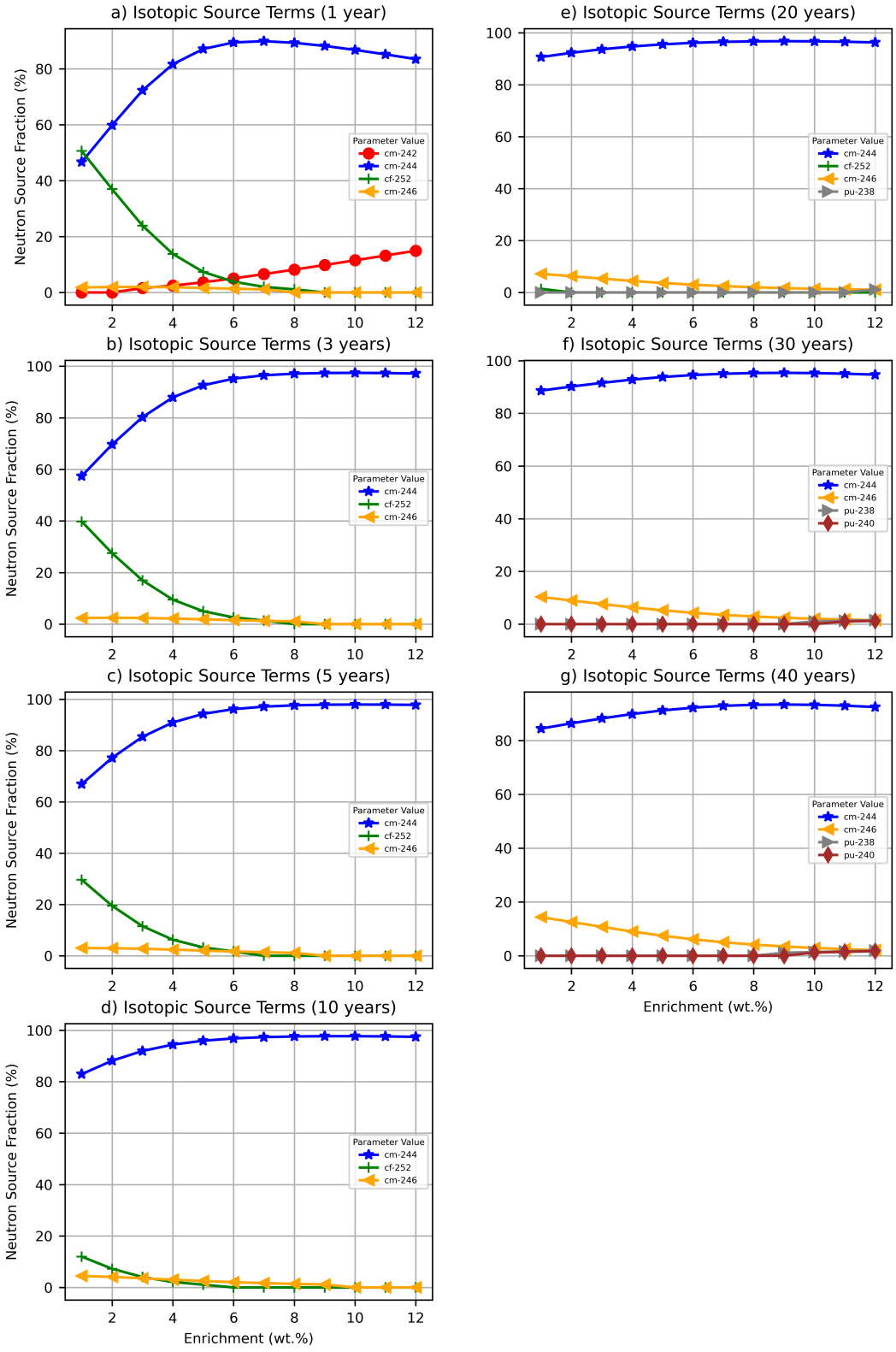

Figure 16. Radionuclide fractional contributions to total neutron source as a function of enrichment.

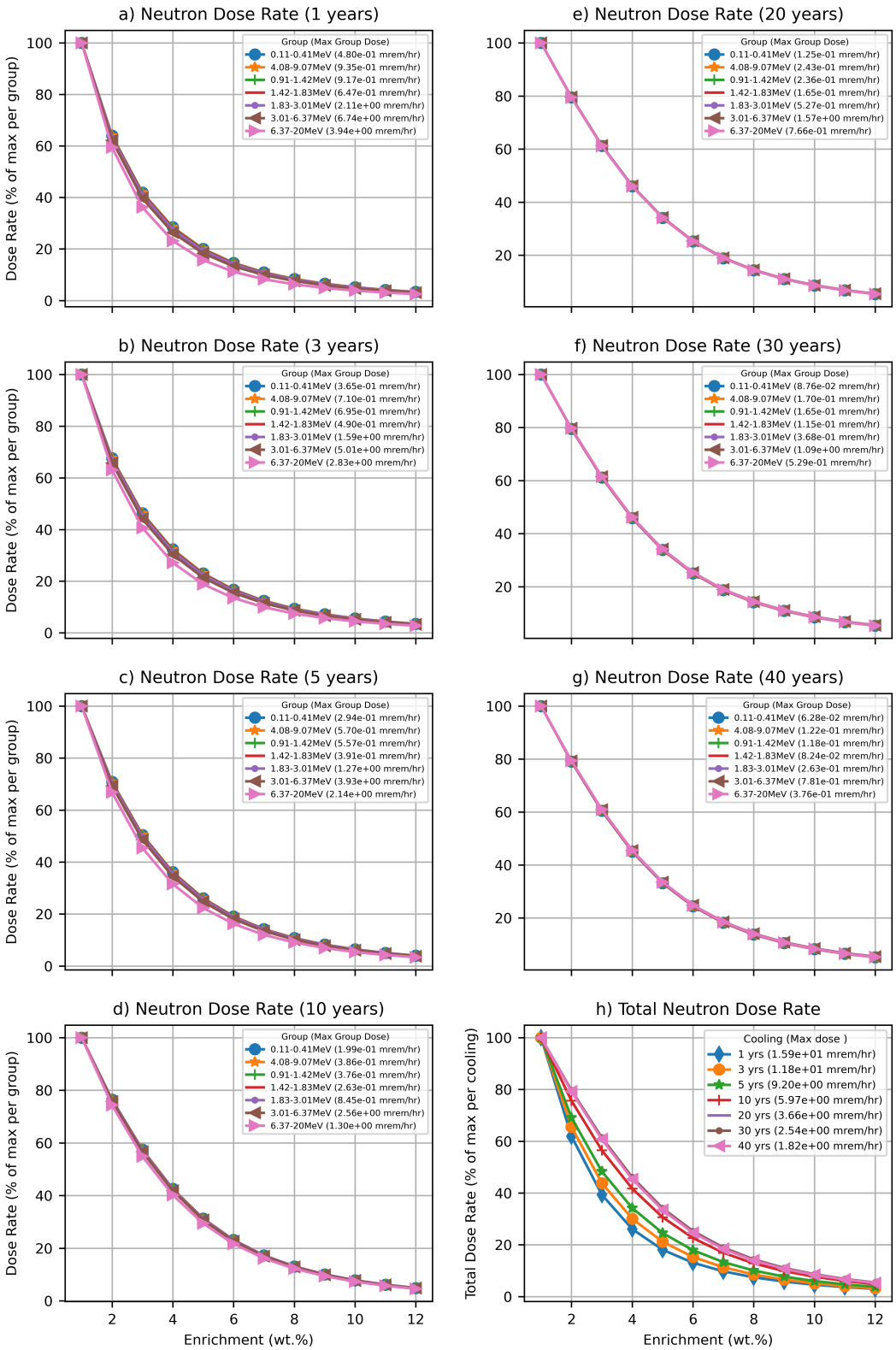

Figure 17. Neutron dose rates as a function of enrichment.

4.1.2.3 Cobalt Activation Source Terms

Activated fuel hardware and activated NFH loaded in a cask can contribute significantly to the cask dose rates, depending on the cooling time. One of the main contributions is from activation of the ^{59}Co impurities in hardware materials during their irradiation in the reactors. The trend in cobalt activity is evaluated in this analysis. The ^{60}Co ($T_{1/2}$ = 5.27 y) activity is evaluated by irradiating 1 g of ^{59}Co impurity in the active fuel region. For ^{59}Co impurities other than 1 gram, the ^{60}Co activity can be simply scaled up by multiplying the activity of 1 gram by the actual amount of impurity in the fuel hardware and NFH.

Normalized ^{60}Co activity is plotted as a function of initial fuel enrichment in Figure 18. Similar to other source terms plots, the ^{60}Co activity is normalized by the maximum ^{60}Co activity within the range of evaluated variable and given cooling time for gaining better intuitive understanding of the impact of the various irradiation parameters. The maximum ^{60}Co activities per gram of ^{59}Co per MTU at various cooling times are provided in the legend of Figure 18. The cobalt source terms decrease with increasing initial enrichment and with increasing cooling time. This result is consistent with the basic nuclear physics in that fuel with higher enrichment will need lower neutron flux to achieve the same power density; low flux will produce lower ^{60}Co content.

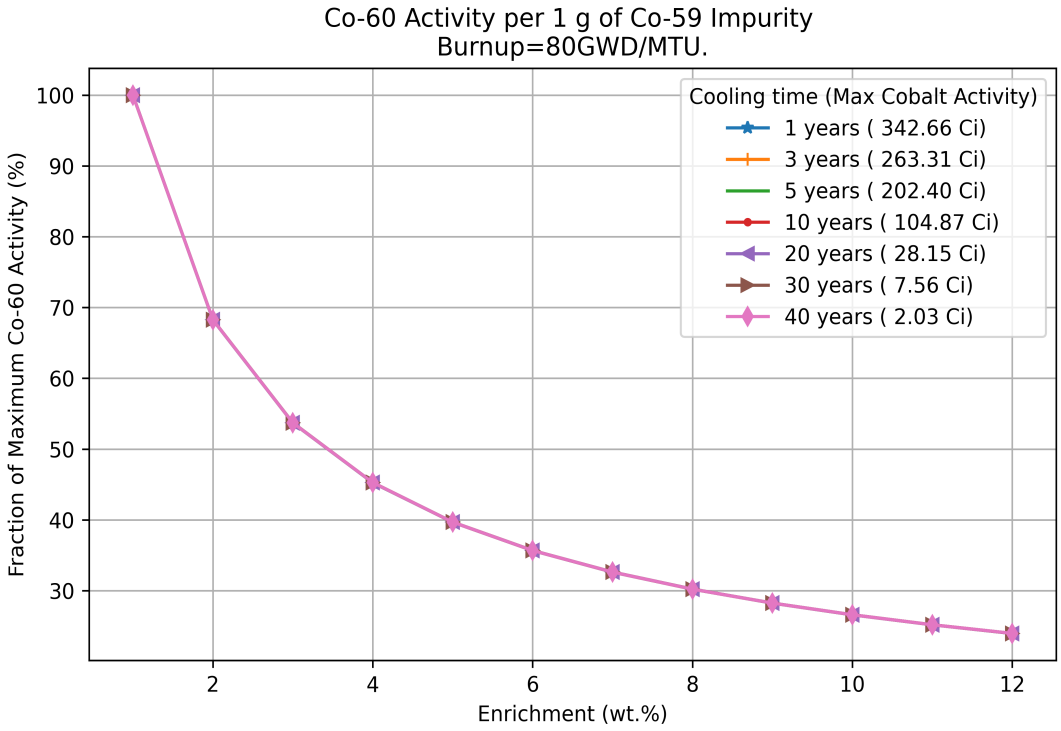

Figure 18. ^{60}Co activity as a function of initial enrichment.

4.1.3 Fuel Density

This section analyzes trends of variation with fuel density for the radiation source terms of a PWR fuel assembly with an average assembly burnup of 80 GWd/MTU. Fuel density affects ^{238}U resonance self-shielding. By increasing fuel density, fewer actinides will be produced. In this parametric study, fuel mass is maintained constant, and the varying pellet radius is limited by the inner radius of the fuel cladding. Therefore, the range of fuel density in this parametric study is from 10.0 to 10.75 g/cm^3.

4.1.3.1 Primary Gamma Radiation

Fuel density is another factor that may affect the gamma source from the fuel. In Figure 19(h), the total gamma radiation source terms are plotted as a function of fuel density at selected cooling times. In this plot, the maximum total source strength over the whole range of evaluated fuel density values is found for each cooling time. The results for that cooling time are then normalized by that maximum value. The maximum source strength value is shown in the plot legend. It is shown that the total strength of the gamma source term slightly decreases with increasing fuel density. The changes in total source strength of primary gamma radiation as a result of fuel density varying from 10.0 to 10.75 g/cm^3 is less than 0.2 % over 40 years of cooling, i.e., the fuel density has negligible effects on the primary gamma source from the fuel. Figure 19(a–g) shows the trends of variation with fuel density of the gamma radiation sources within energy groups in the range of 0.2 MeV to 4 MeV.

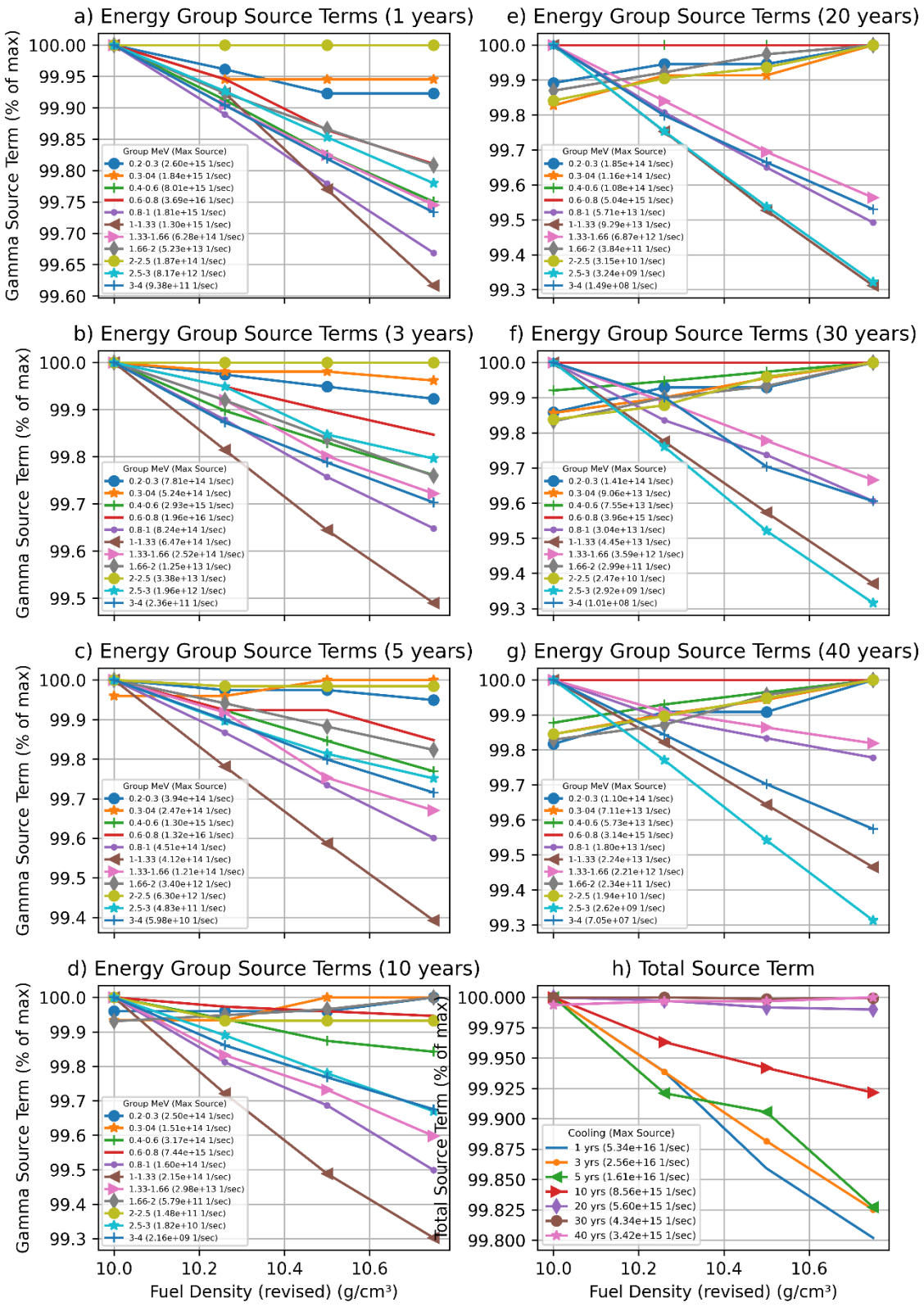

Figure 19. Gamma source terms as a function of fuel density.

4.1.3.2 Neutron Radiation and Secondary Gamma Radiation

In Figure 20(h), the total neutron radiation source terms are plotted as a function of fuel density and cooling times. In this plot, the maximum total source strength over the entire range of evaluated fuel density is shown for each cooling time. The results for that cooling time are then normalized by the maximum value. The total strength of the neutron source term slightly decreases with increasing fuel density at constant fuel mass. The change in total neutron strength due to fuel density variation from 10.00 to 10.75 g/cm^3 is less than 0.5 % over 40 years of cooling, i.e., the fuel density has negligible effects on the neutron source from the fuel. Figure 20(a–g) shows the trends of variation with fuel density of the neutron sources within energy groups in the range of 0.11 to 20 MeV.

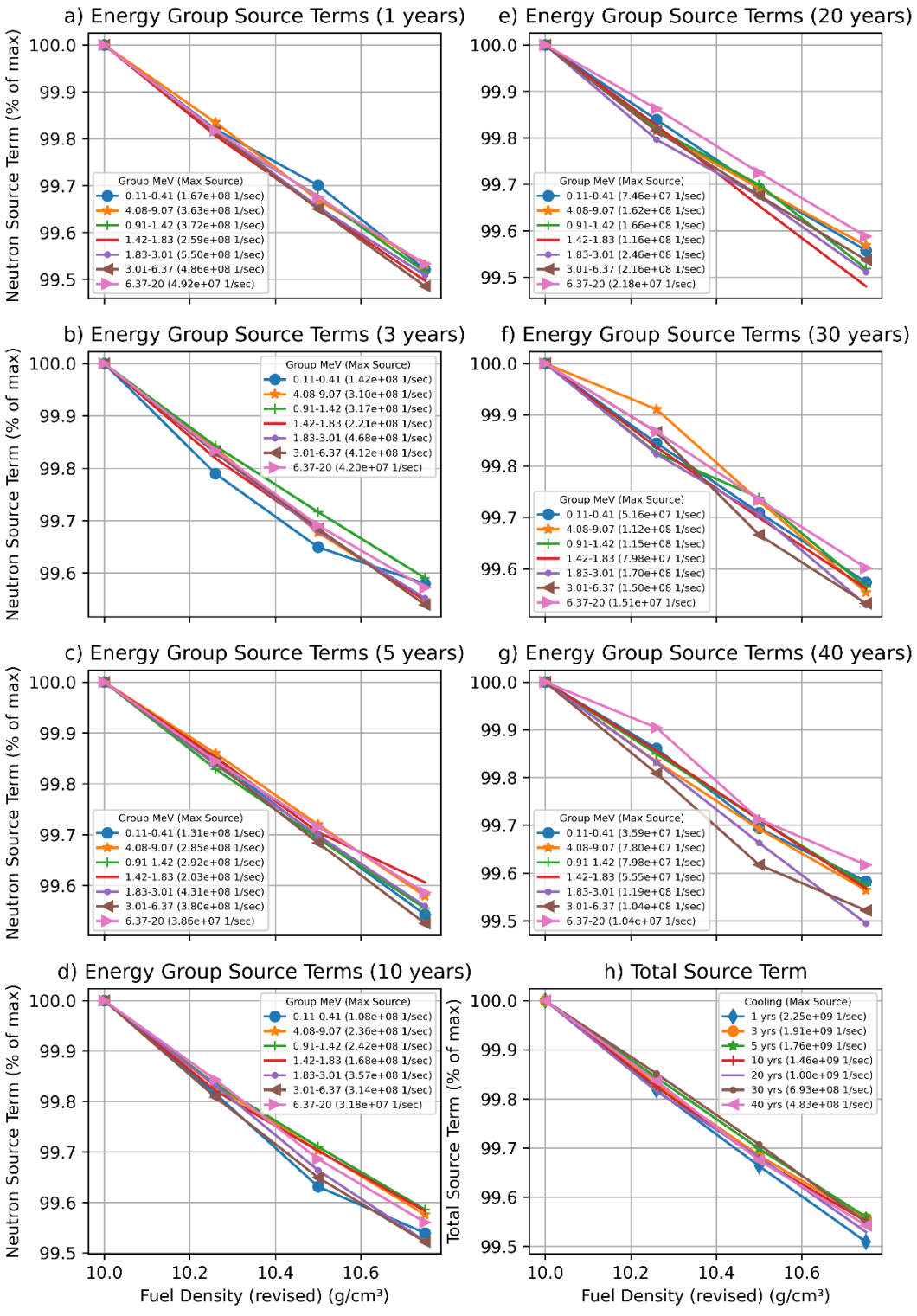

Figure 20. Neutron source terms as a function of fuel density.

4.1.4 Fuel Temperature

This section analyzes trends of variation with fuel temperature for the radiation source terms of a PWR fuel assembly with an average assembly burnup of 80 GWd/MTU. Fuel temperature increase has a broadening effect of the resonance capture cross section of fertile nuclides (e.g., ^{238}U and ^{240}Pu), which increases the probability of neutrons with energies near the resonance to be captured in the fuel pellet. Therefore, this effect is accompanied by slightly higher concentrations of transuranic nuclides compared to lower fuel temperature values as well as hardening of neutron energy spectrum.

4.1.4.1 Primary Gamma Source

In Figure 21(h), the total gamma source terms are plotted as a function of fuel temperature and cooling times. In this figure, the maximum total source strength over the entire range of evaluated fuel temperature values is shown for each cooling time. In order to help understand the impact of fuel temperature on the primary gamma source terms of the fuel, the results for that cooling time are normalized to the maximum value. The plots show that the total strength of the gamma source terms remains mostly unchanged with fuel temperature.

Figure 21(a–g) shows the trends of variation with fuel temperature of the gamma radiation sources within energy groups in the range of 0.2 MeV to 4 MeV. In this plot, the maximum source strength over the entire range of evaluated fuel temperatures is found for each energy group source terms, and the results within the energy group are then normalized by this maximum source terms value. This maximum source terms value is shown in the plot legend. The results show that the per energy group source terms vary within approximately 6%. The results in Figure 22 show a negligible contribution to total dose rates from photons with energies below 0.4 MeV and above 3 MeV.

As a confirmation, a dose rate calculation was performed using the simple shielded assembly model described in Section 3.5. The gamma dose rates are plotted in Figure 22. The evaluation confirms the similar trends of the source terms described above: the external dose rates remain mostly unchanged with fuel temperature.

A further breakdown of the dose rates according to contribution from individual isotopes is shown in Figure 23. Similar to the above discussion, the dose rates are dominated by ^{144}Ce/^{144}Pr, ^{137}Cs/^{137m}Ba, ^{106}Ru/^{106}Rh, and ^{154}Eu at the early cooling times. After 10 years of cooling, ^{154}Eu, ^{137}Cs/^{137m}Ba, and ^{90}Sr/^{90}Y are the most contributing isotopes. Only ^{144}Ce and ^{90}Sr production rates decrease with increasing fuel temperature because their cumulative fission yields from ^{235}U are greater than those from ^{239}Pu. The production rates of the other gamma emitters exhibit an increasing trend due to increased ^{239}Pu production as fuel temperature increases. Fuel temperature appears to have some limited effect on total gamma source strength, dose rate, and radionuclide fractional contributions to dose rates.

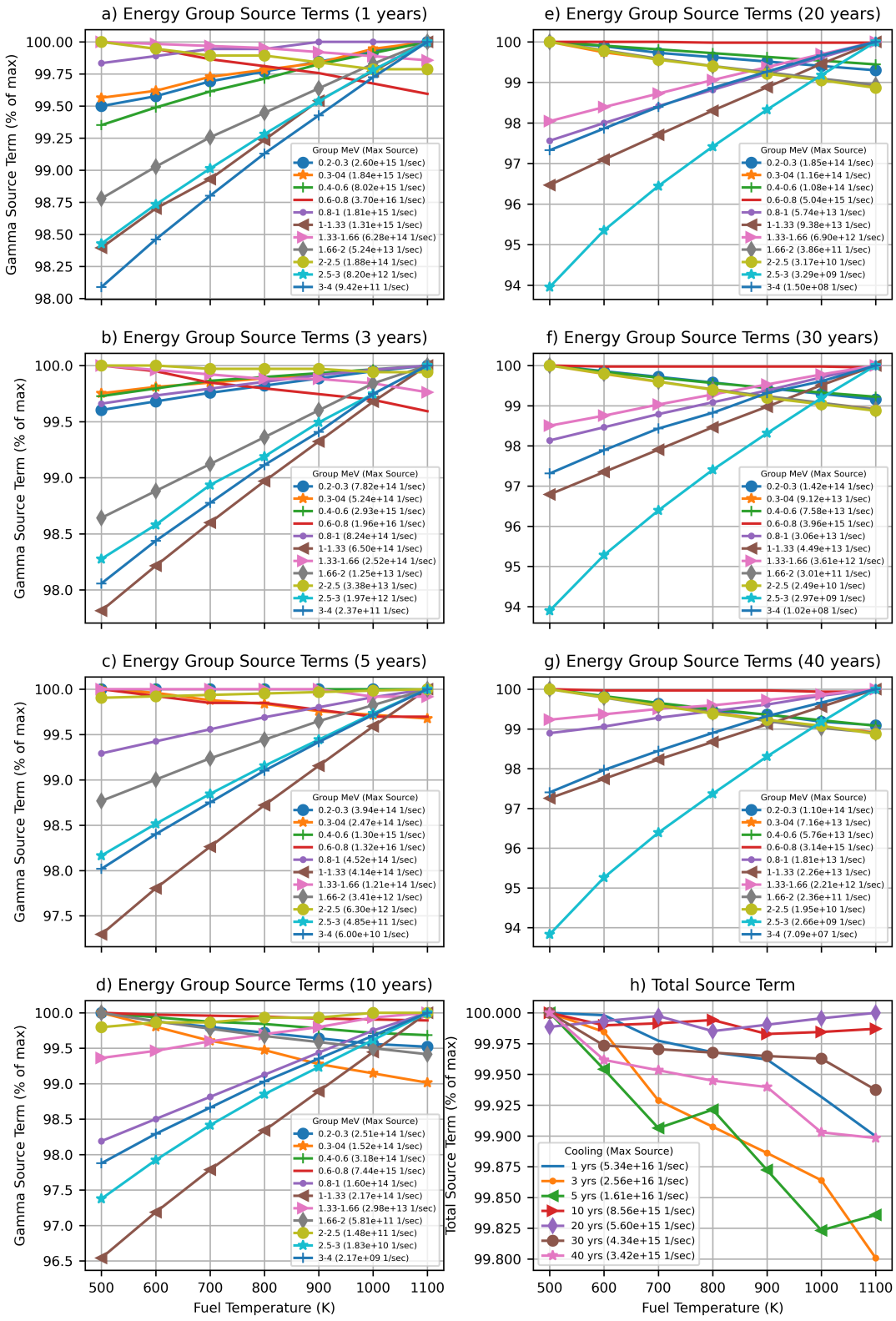

Figure 21. Gamma source terms as a function of fuel temperature.

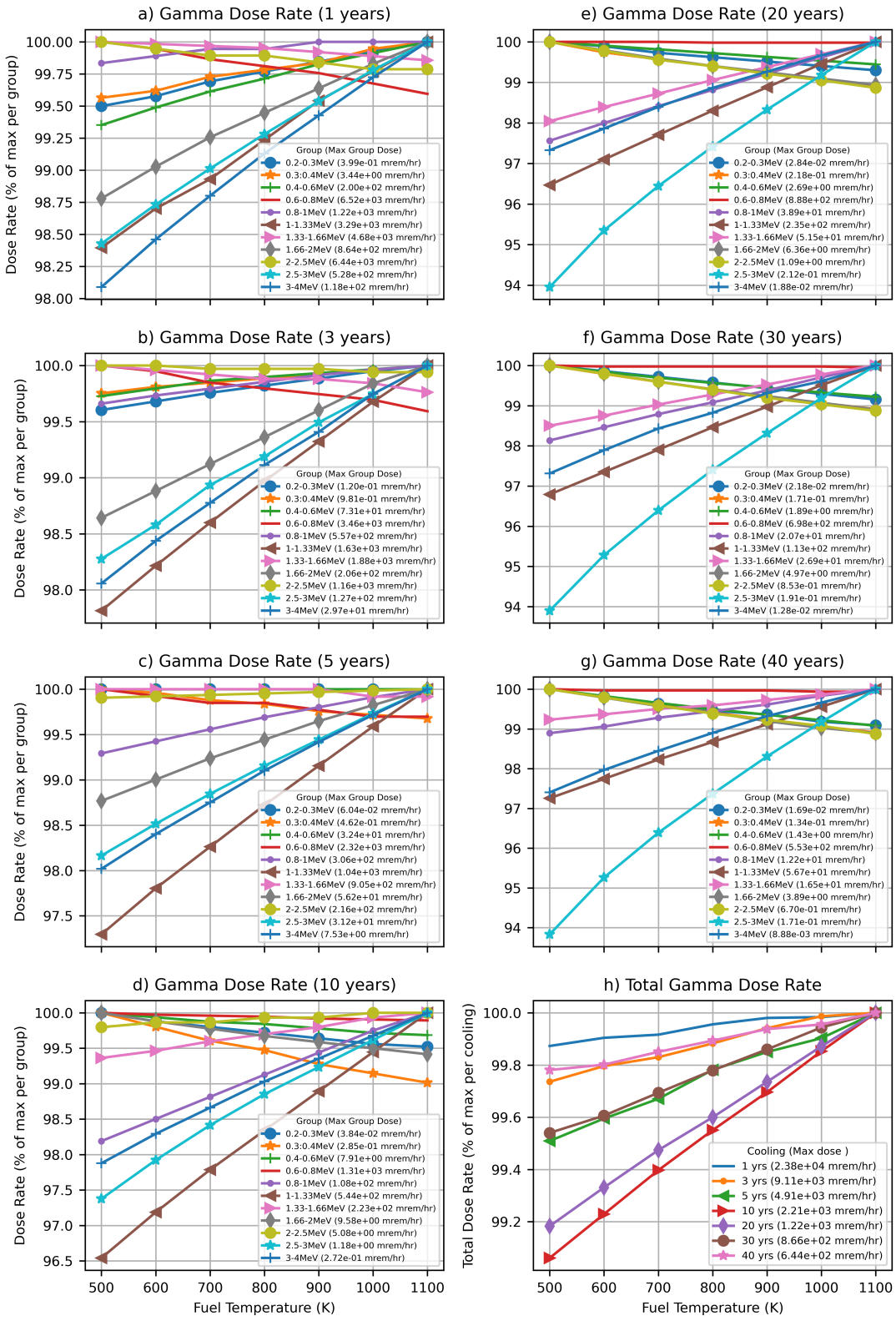

Figure 22. Gamma dose rate as a function of fuel temperature.

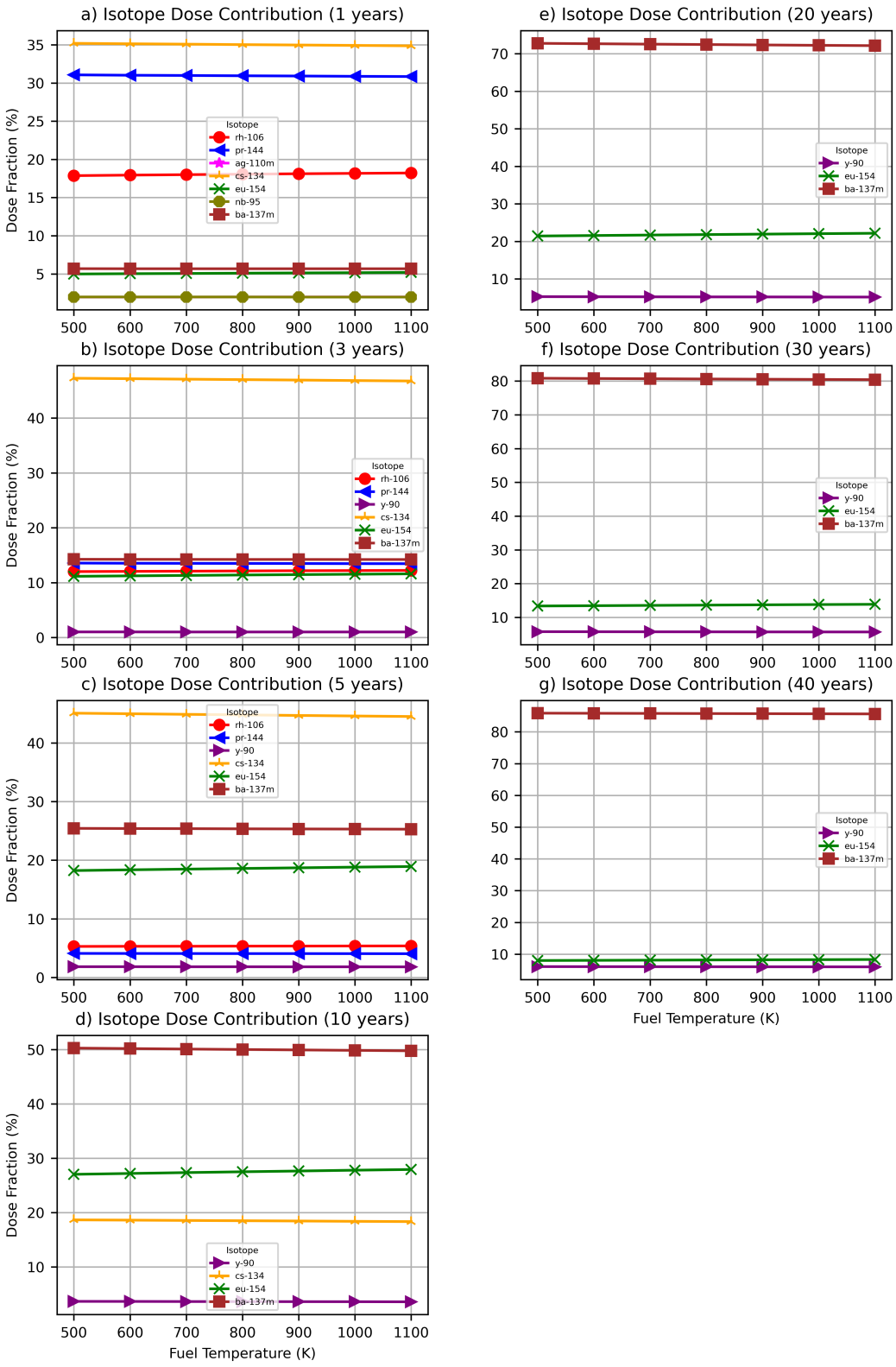

Figure 23. Radionuclide fractional contributions to gamma dose rate as a function of fuel temperature.

4.1.4.2 Neutron Radiation and Secondary Gamma Radiation

In Figure 24(h), the total neutron radiation source terms are plotted as a function of fuel temperature and cooling times. In this plot, the maximum total source strength over the whole range of evaluated fuel temperature values is found for a selected cooling time. The results for that cooling time are then normalized by that maximum value. The results show that the total strength of the neutron source term is increasing with increasing fuel temperature. The increase is approximately 2.5% from fuel temperature of 500 K to 1,100 K. Figure 29(h) also shows that at high end temperature (1,100 K) the differences in neutron source terms between different cooling times is negligible.

Figure 24(a–g) shows the neutron strength values for defined energy groups. The results show that the source strength for all energy groups as a function of fuel temperature follow a similar trend to that of the total source term: slightly increasing with fuel temperature. No significant changes in source term spectra are indicated by these results over the 40 years of cooling time. Contributions above 1% to neutron source term from individual isotopes is shown in Figure 25. As discussed above, the main contributors to neutron dose rates are ^{242}Cm, ^{244}Cm, ^{246}Cm and ^{252}Cf, where ^{244}Cm always contributes over 90% of the source. For each cooling time, the fractional neutron source contributions of the main neutron emitters are not affected by changes in fuel temperature.

A dose rate calculation was performed using the simple shielded assembly model described in Section 3.5. The neutron dose rates are plotted in Figure 26. The evaluation confirms the similar trends of the source terms.

Neutron source terms give rise to secondary gamma dose rates. Since trends in the secondary gamma dose rates are linked to neutron source terms, the trends are similar. For completeness, these results are provided in Figure A-3.

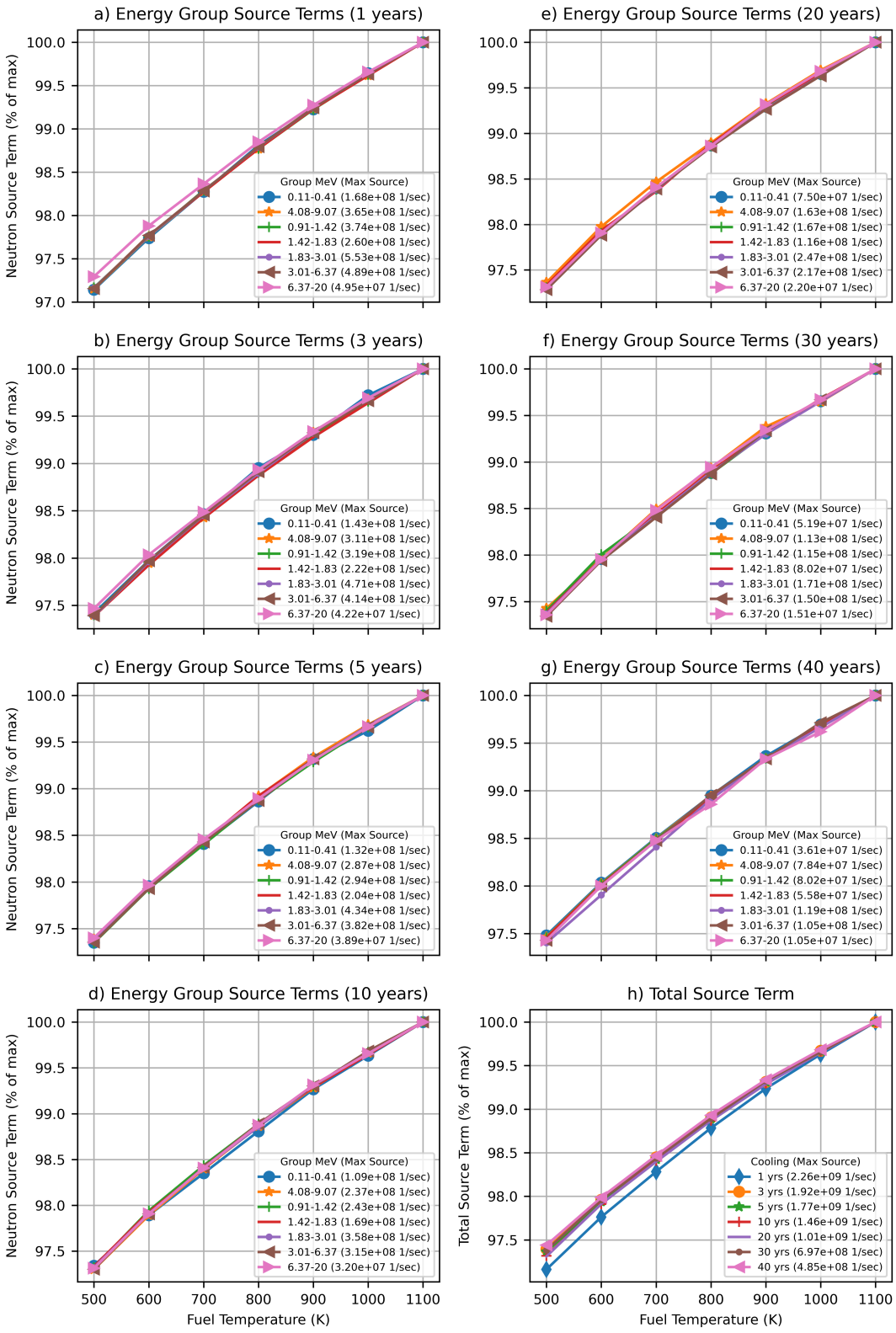

Figure 24. Neutron source terms as a function of fuel temperature.

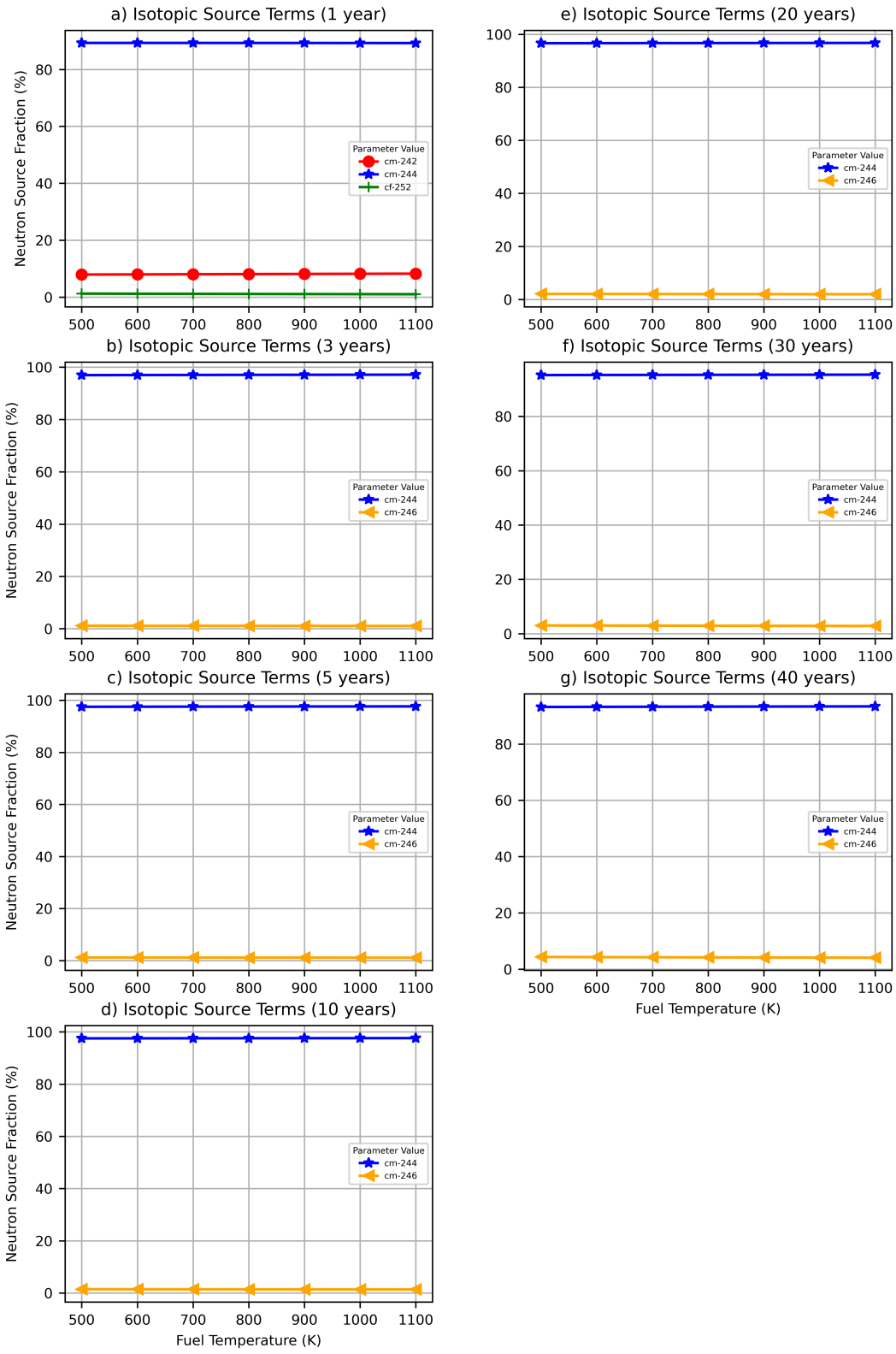

Figure 25. Radionuclide fractional contributions to total neutron source as a function of fuel temperature.

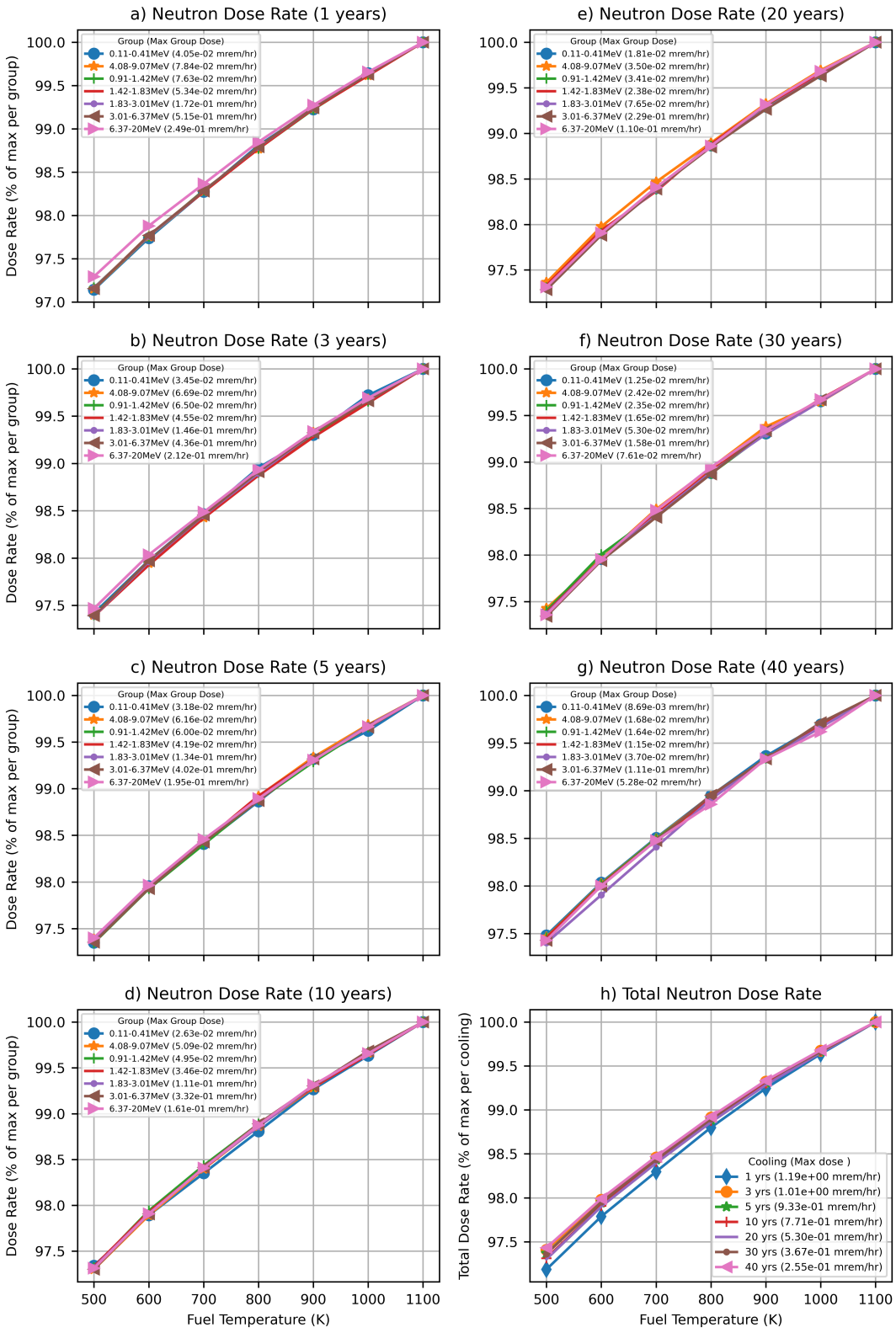

Figure 26. Neutron dose rate as a function of fuel temperature.

4.1.4.3 Cobalt Activation Source Terms

Activation of fuel hardware and NFH can contribute significantly to the cask dose rates, depending on exposure and cooling time. The dominating contribution is from activated ^{59}Co impurities in the fuel hardware and NFH. Therefore, the trend in cobalt activity was evaluated in this sensitivity analysis. The ^{60}Co ($T_{1/2}$ = 5.27 y) activity is evaluated by irradiating 1 g of ^{59}Co impurity in the active fuel region. Similar to other source terms plots, the ^{60}Co activity is normalized by the maximum ^{60}Co activity within the range of evaluated variable and given cooling time. The ^{60}Co activity is then plotted as a function of fuel temperature in Figure 27. The maximum ^{60}Co activities per gram of ^{59}Co per MTU are provided in the legend of Figure 27 for selected cooling times. The effect of fuel temperature variation during depletion on cobalt source terms is negligible.

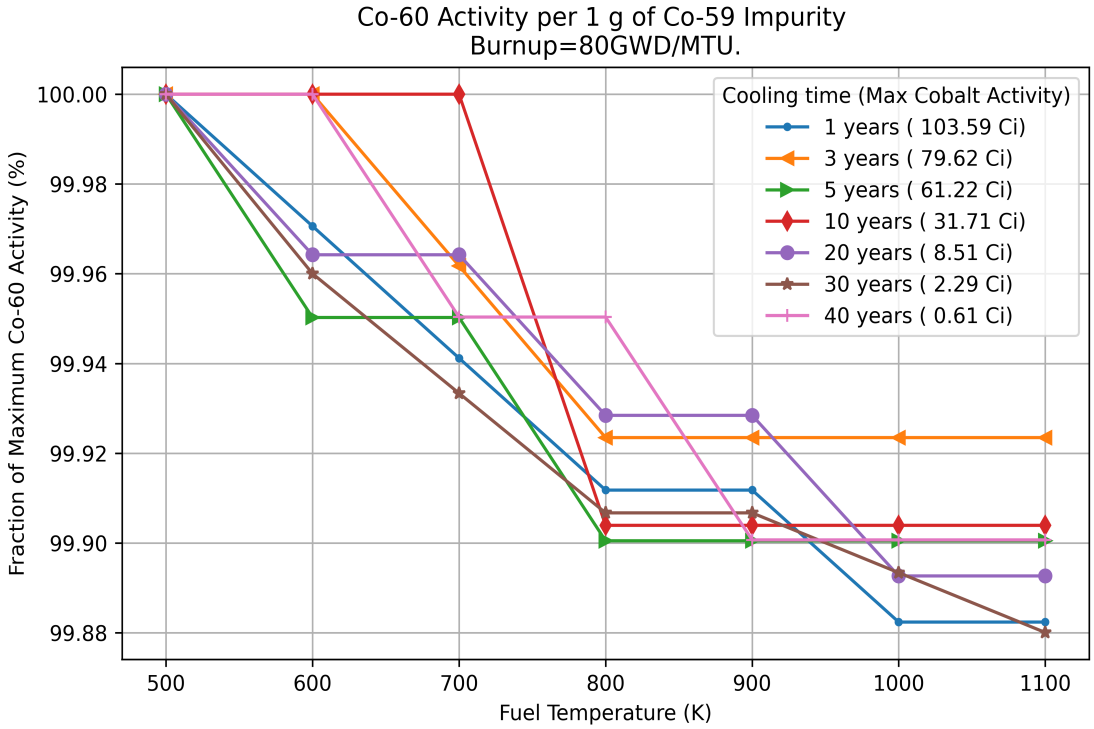

Figure 27. ^{60}Co activity as a function of fuel temperature.

4.1.5 Moderator Density

By increasing moderator density, the thermal flux is increased, the thermal absorption reactions are increased, and the resonance absorption reactions are decreased causing lower ^{239}Pu and transplutonium nuclide production rates.

4.1.5.1 Primary Gamma Radiation

In Figure 28(h), the total gamma radiation source terms are plotted as a function of moderator density and cooling times. In this plot, the maximum total source strength over the entire range of evaluated moderator density values is shown for each cooling time. The results for that cooling time are then normalized by that maximum value. It is shown that the total strength of the gamma source terms decreases with increasing moderator density for shorter cooling times; this effect largely disappears after about 10 years of cooling time.

Figure 28(a–g) shows the trends of variation with moderator density of the gamma radiation sources within energy groups in the range of 0.2 MeV to 4 MeV. In this plot, the maximum source strength over the entire range of evaluated moderator densities is found for each energy group, and the results within the energy group are then normalized by this maximum value. The results show that the per energy group source terms decrease with increasing moderator density for short cooling times; for longer cooling times, the source strength from dominating energy groups starts to decrease. The results in Figure 29 show negligible contributions to total dose rates from photons with energies below 0.4 MeV and above 3 MeV.

For confirmation analysis, a dose rate calculation was performed using the simple shielded assembly model described in Section 3.5. The gamma dose rates are plotted in Figure 29. The evaluation confirms the similar trends of the source terms described above, i.e., dose rates outside the cask decrease with increasing moderator density.

A further breakdown of dose rates according to contributions from individual isotopes is shown in Figure 30. For the shorter cooling times, the dose rates are dominated by gamma emissions from ^{134}Cs ($T_{1/2}$=2.0652 years), ^{144}Ce ($T_{1/2}$=284.89 days)/^{144}Pr ($T_{1/2}$=17.29 min), ^{137}Cs ($T_{1/2}$=30.1 years)/^{137m}Ba ($T_{1/2}$=153 s), ^{106}Ru ($T_{1/2}$=1.02 years)/^{106}Rh ($T_{1/2}$=2.18 h), and ^{154}Eu ($T_{1/2}$=8.593 years). After 10 years of cooling, ^{137}Cs/^{137m}Ba, ^{154}Eu, and ^{134}Cs remain the most contributing isotopes. The ^{137}Cs/^{137m}Ba fractional contribution to dose rate increases with increasing moderator density, whereas the fractional contribution of ^{154}Eu trends in an opposite direction.

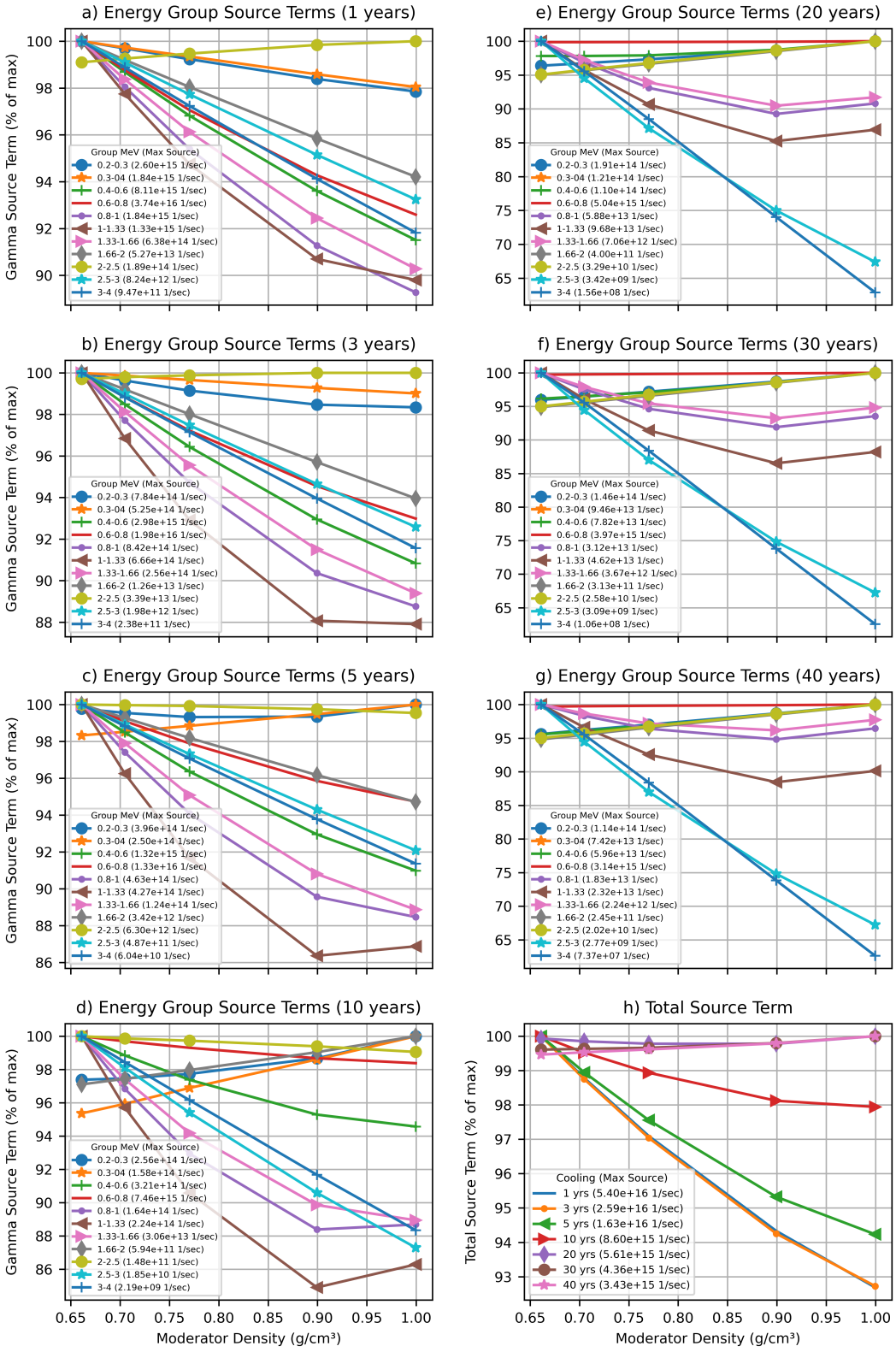

Figure 28. Gamma source terms as a function of moderator density.

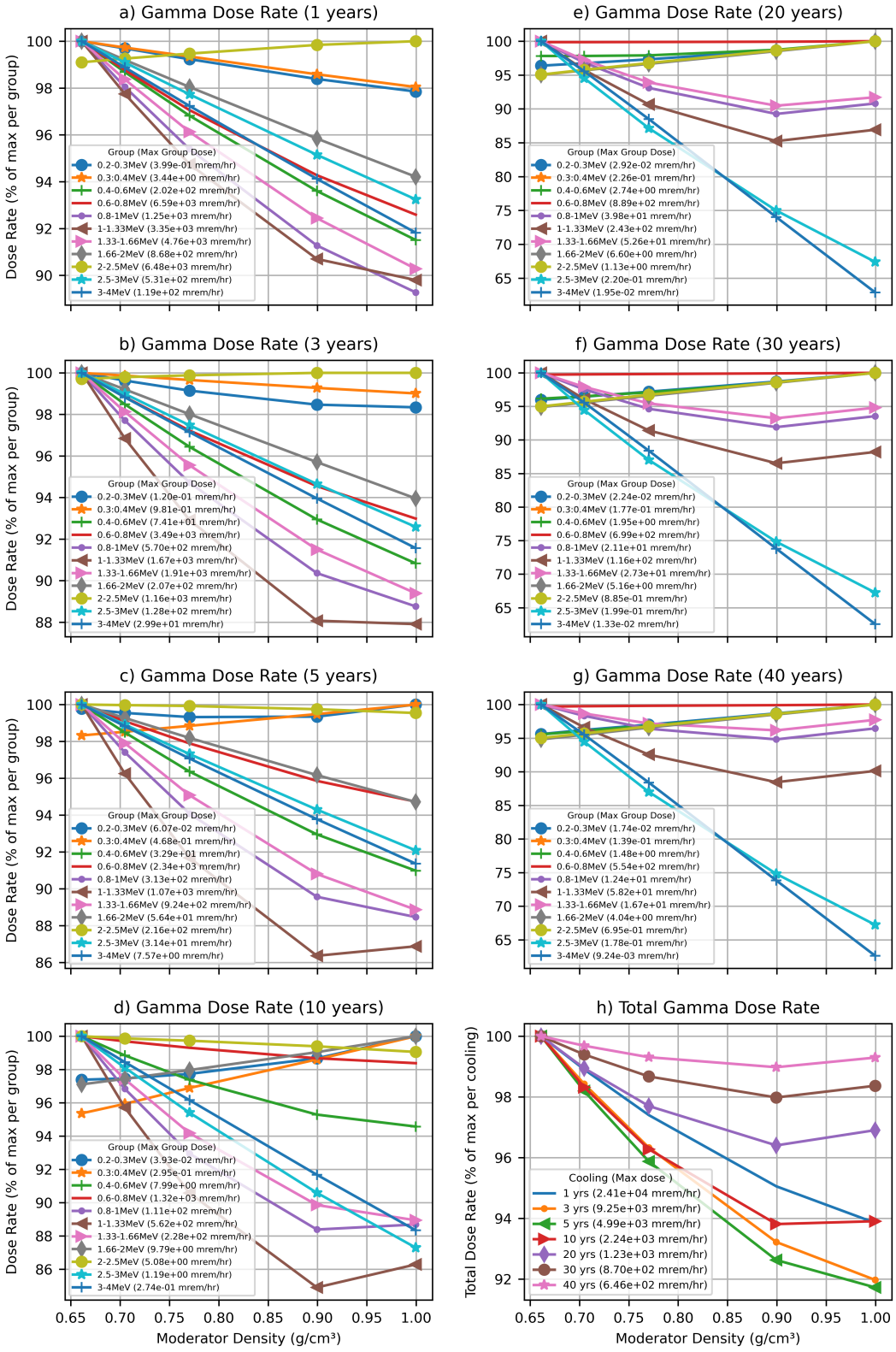

Figure 29. Gamma dose rate as a function of moderator density.

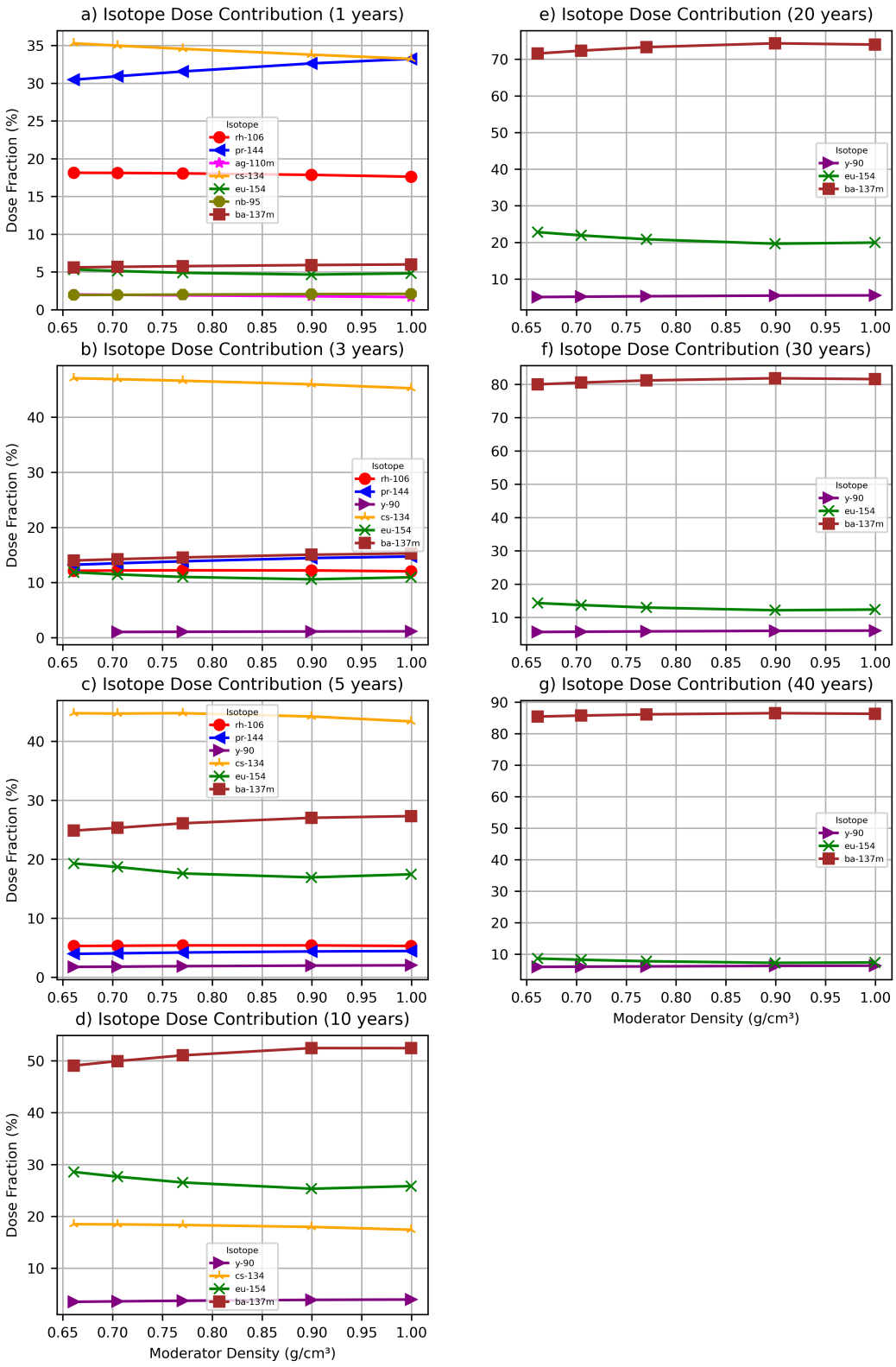

Figure 30. Radionuclide fractional contributions to gamma dose rate as a function of moderator density.

4.1.5.2 Neutron Radiation and Secondary Gamma Radiation

In Figure 31(h), the total neutron radiation source terms are plotted as a function of moderator density and cooling times. In this plot, the maximum total source strength over the entire range of evaluated moderator densities is found for the selected cooling times. The results for that cooling time are then normalized by that maximum value. It is shown that the total strength of the neutron source terms decreases with increasing moderator density.

Figure 31(a–g) shows neutron strength values for the selected energy groups. The results show that the energy groups follow a similar trend to that of the total source term: decreasing with increasing moderator density. No significant changes in source terms spectra are indicated by these results over the 40 years of cooling time. Contributions above 1% to neutron source terms from individual isotopes are shown in Figure 32. As discussed above, the main contributors to neutron dose rates are ^{242}Cm, ^{244}Cm, ^{246}Cm and ^{252}Cf, where ^{244}Cm always contributes over 90% of the source. The fractional contribution of the contributing nuclides to the total source term is not sensitive to fuel density variations. The neutron source strength decreases with increasing moderator density because the resonance capture cross section of fertile nuclides (e.g., ^{238}U and ^{240}Pu) decrease as moderator density increases. Therefore, neutron emitter production rate decreases as moderator density increases.

A dose rate calculation was performed using the simple shielded assembly model described in Section 3.5. The neutron dose rates are plotted in Figure 33. The trend of normalized dose rate curves is identical to the trend of the curves for the normalized source terms.

Neutron source terms give rise to secondary gamma dose rates through interactions with fuel and structural materials. Since trends in the secondary gamma dose rates are directly linked to neutron source terms, for the same fuel load and cask design the trends are similar. For completeness, these results are provided in Figure A-4.

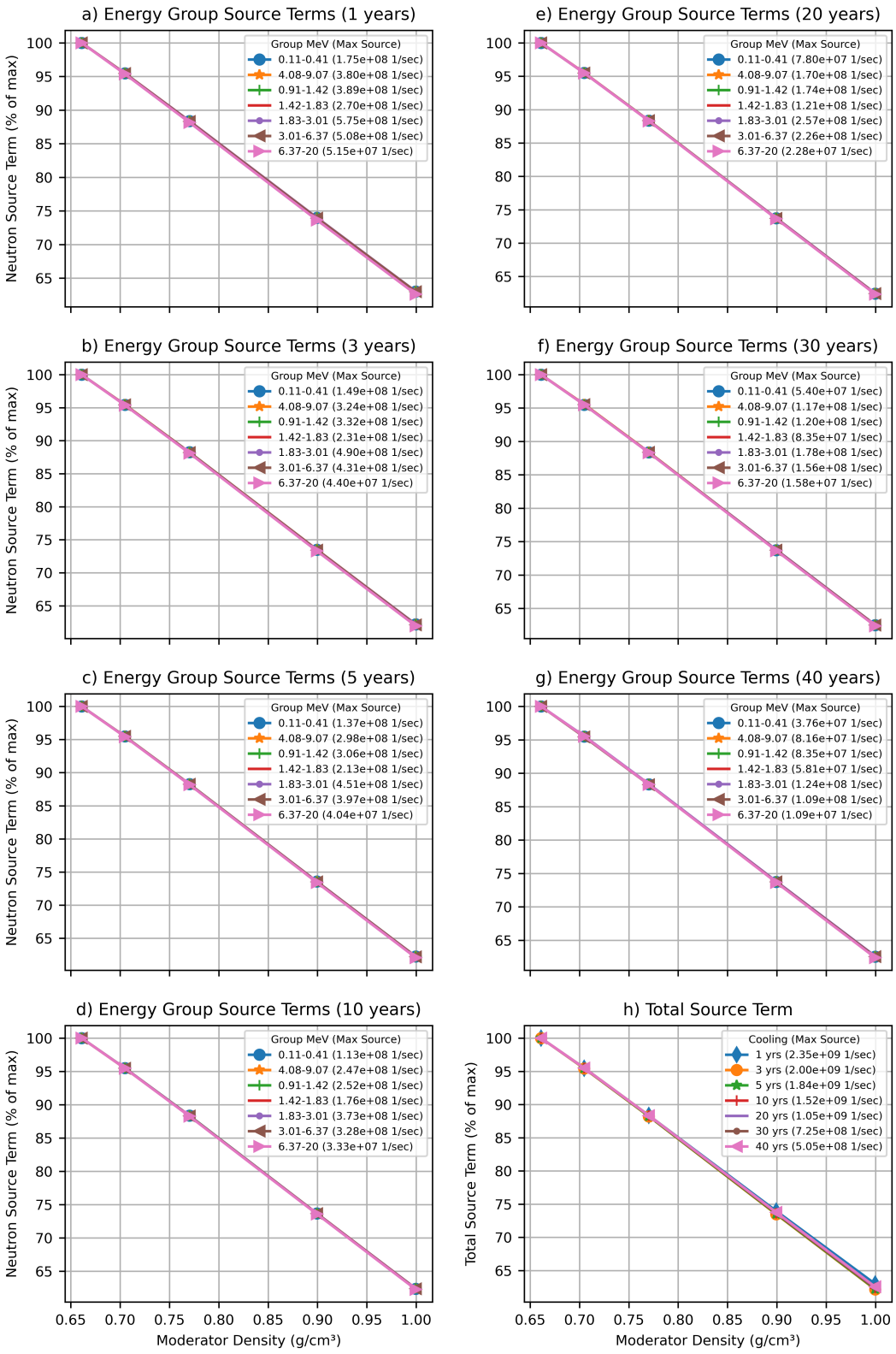

Figure 31. Neutron source terms as a function of moderator density.

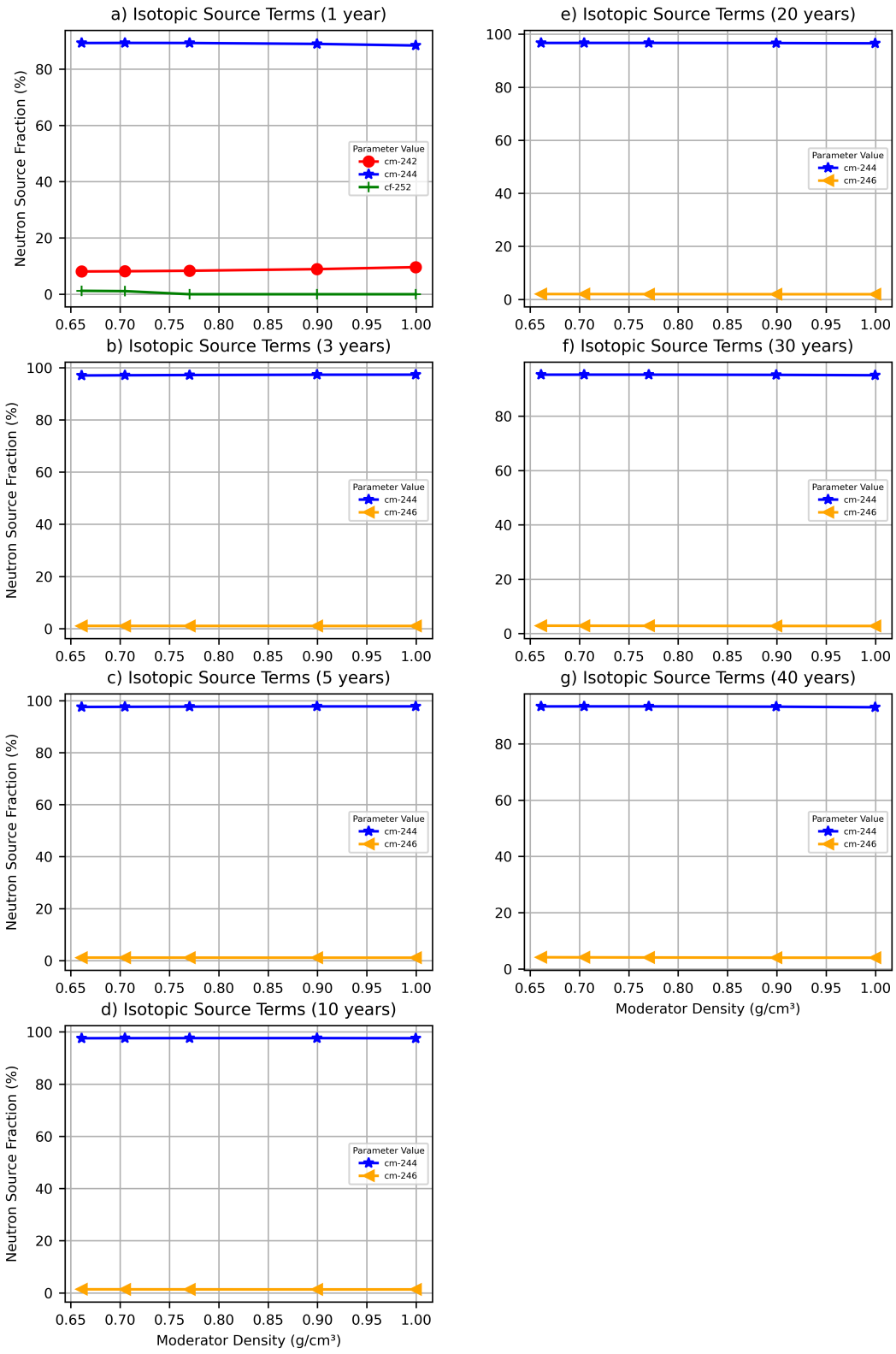

Figure 32. Radionuclide fractional contributions to total neutron source as a function of moderator density.

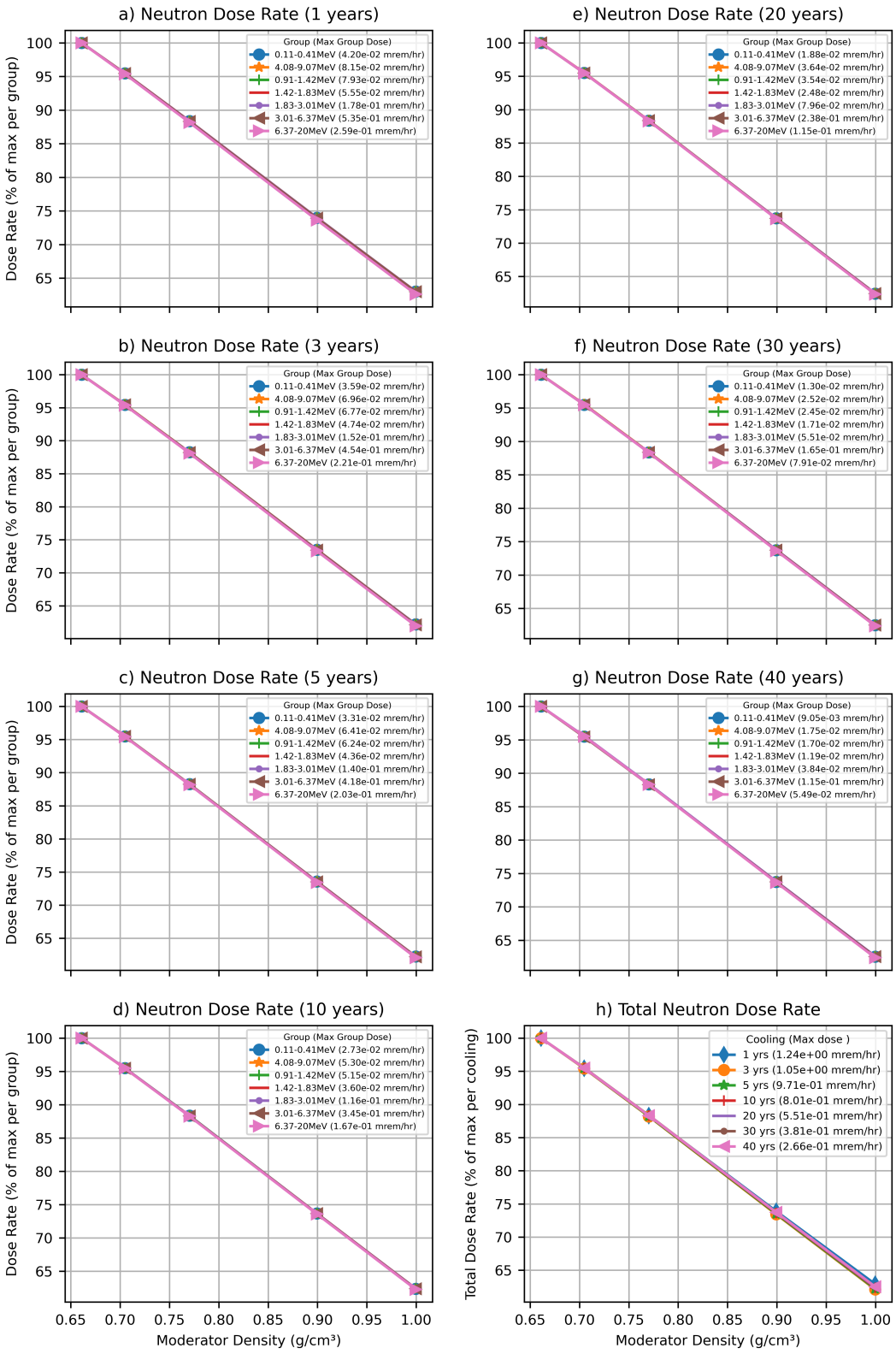

Figure 33. Neutron dose rate as a function of moderator density.

4.1.5.3 Cobalt Activation Source Terms vs Moderator Density

Activation of fuel hardware and NFH can contribute significantly to the cask dose rates, depending on exposure and fuel cooling time. One of the main contributions is from activated cobalt impurities. Therefore, the trend in cobalt activity is evaluated in this sensitivity analysis. The ^{60}Co ($T_{1/2}$ = 5.27 y) activity is evaluated for one gram of ^{60}Co impurity irradiated in the active fuel region. The actual ^{60}Co level can be easily scaled to the specific ^{59}Co impurity for specific fuel design or NFH designs. Similar to other source terms plots, the ^{60}Co activity is normalized by the maximum ^{60}Co activity within the range of evaluated variable and given cooling time. The ^{60}Co activities are then plotted as a function of moderator density in Figure 34. The maximum ^{60}Co activities per gram of ^{59}Co per MTU are provided as a function of cooling time in the legend of Figure 34. The cobalt source terms decrease with increasing moderator density during depletion. This is consistent with the cross-section data from ENDF/B-VIII for ^{59}Co neutron capture reaction. ^{60}Co has a large cross section with the neutrons in the thermal and epithermal energy range. Neutron energy spectrum softening increases the ^{235}U absorption rate and decreases the absorption rates of other nuclides.

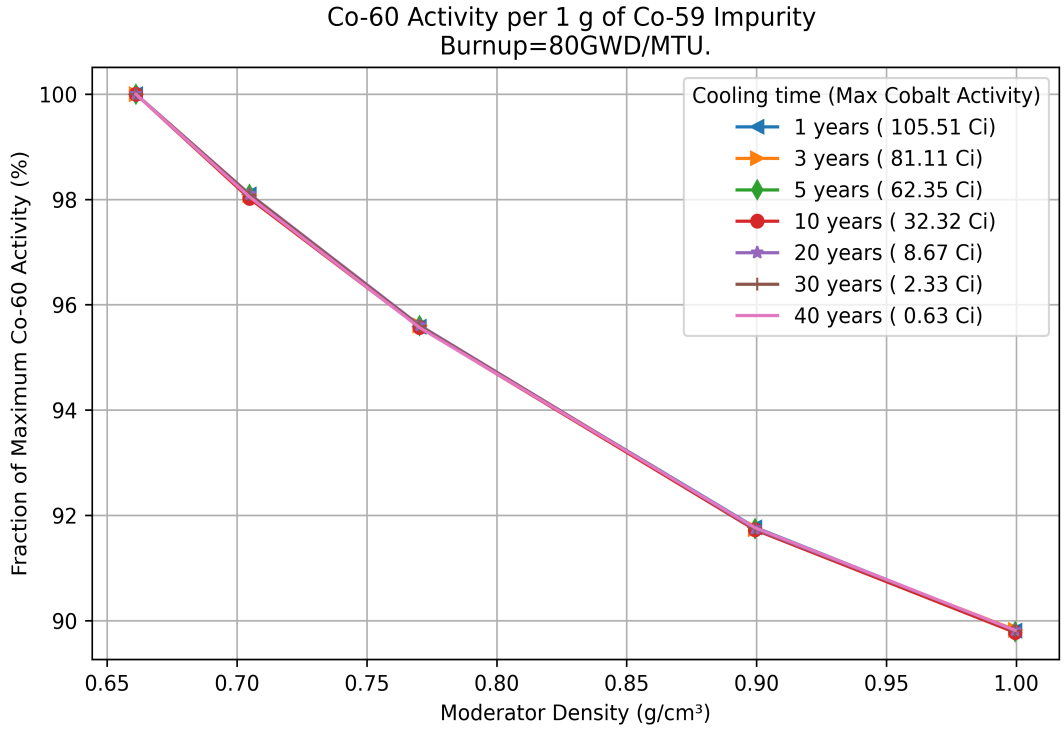

Figure 34. ^{60}Co activity as a function of moderator density.

4.1.6 Average Soluble Boron Concentration for PWR fuel

This section analyzes trends of variation with average soluble boron concentration for the radiation source terms of a PWR fuel assembly with an average assembly burnup of 80 GWd/MTU. Neutron absorption by boron diluted in PWR coolant results in hardening of the neutron energy spectrum, increased resonance captures in fertile nuclides (e.g., ^{238}U and ^{240}Pu), and increased production of transuranic nuclides.

The range of cycle-average soluble boron concentration analyzed in this parametric study, 0 – 1,700 ppm, and the results of the parametric study will need to be validated as more relevant technical information on soluble boron requirements for increased enrichment and higher burnup fuel becomes available.

4.1.6.1 Primary Gamma Radiation

In Figure 35(h), the total gamma radiation source terms are plotted as a function of cycle-average soluble boron concentration in coolant at selected cooling times. In this plot, the maximum total source strength over the entire range of evaluated boron concentration is found for each cooling time. The results for that cooling time are then normalized by the maximum value. It is shown that the total strength of the gamma source terms remains mostly unchanged with boron content varying by 2% in short cooling times, while after 10 years of cooling this effect is largely diminished.

Figure 35(a–g) shows the trends of variation with average soluble boron content of the gamma radiation sources within energy groups in the range of 0.2 MeV to 4 MeV. In this plot, the maximum source strength over the selected range of evaluated soluble boron concentration is found for source terms in each energy group, and the results within the energy group are then normalized by this maximum source terms value. The results show that the per energy group source terms vary within 10%. The results in Figure 36 show a negligible contribution to total dose rates from photons with energies below 0.4 MeV and above 3 MeV.

A dose rate calculation was performed using the simple shielded assembly model described in Section 3.5. The gamma dose rates are plotted in Figure 36. The evaluation confirms that the dose rates increase with soluble boron concentration for fuel with short cooling time and that this effect decreases for longer cooling time.

A further breakdown of dose rates according to contribution from individual radionuclides is shown in Figure 37. For the early cooling times, the dose rates are dominated by gamma emissions from ^{144}Ce ($T_{1/2}$=284.89 days)/^{144}Pr ($T_{1/2}$=17.29 min), ^{137}Cs ($T_{1/2}$=30.1 years)/ ^{137m}Ba ($T_{1/2}$=153 s), ^{106}Ru ($T_{1/2}$=1.02 years)/^{106}Rh ($T_{1/2}$=2.18 h), ^{134}Cs ($T_{1/2}$=2.0652 years), and ^{154}Eu ($T_{1/2}$=8.593 years). After 10 years of cooling, ^{137}Cs/^{137m}Ba, ^{154}Eu, ^{134}Cs, and ^{90}Sr ($T_{1/2}$=28.78 years)/^{90}Y ($T_{1/2}$=64 h) remain the most contributing isotopes. Only ^{144}Ce and ^{90}Sr production rates decrease with increasing average soluble boron concentration because their cumulative fission yields from ^{235}U are greater than those from ^{239}Pu. The production rates of the other gamma emitters exhibit an increasing trend due to increased ^{239}Pu production as average soluble boron concentration increases.

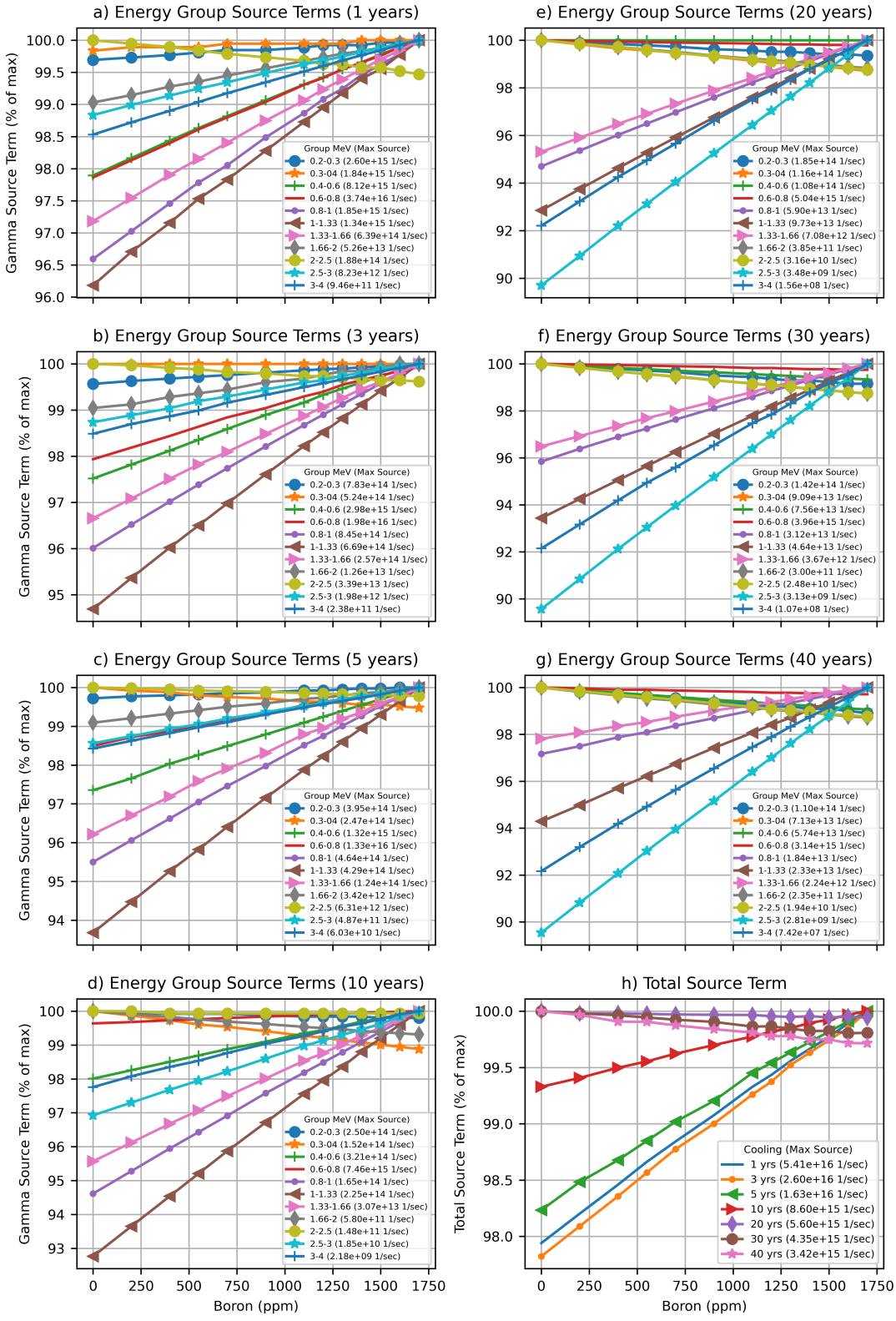

Figure 35. Gamma source terms as a function of average soluble boron content.

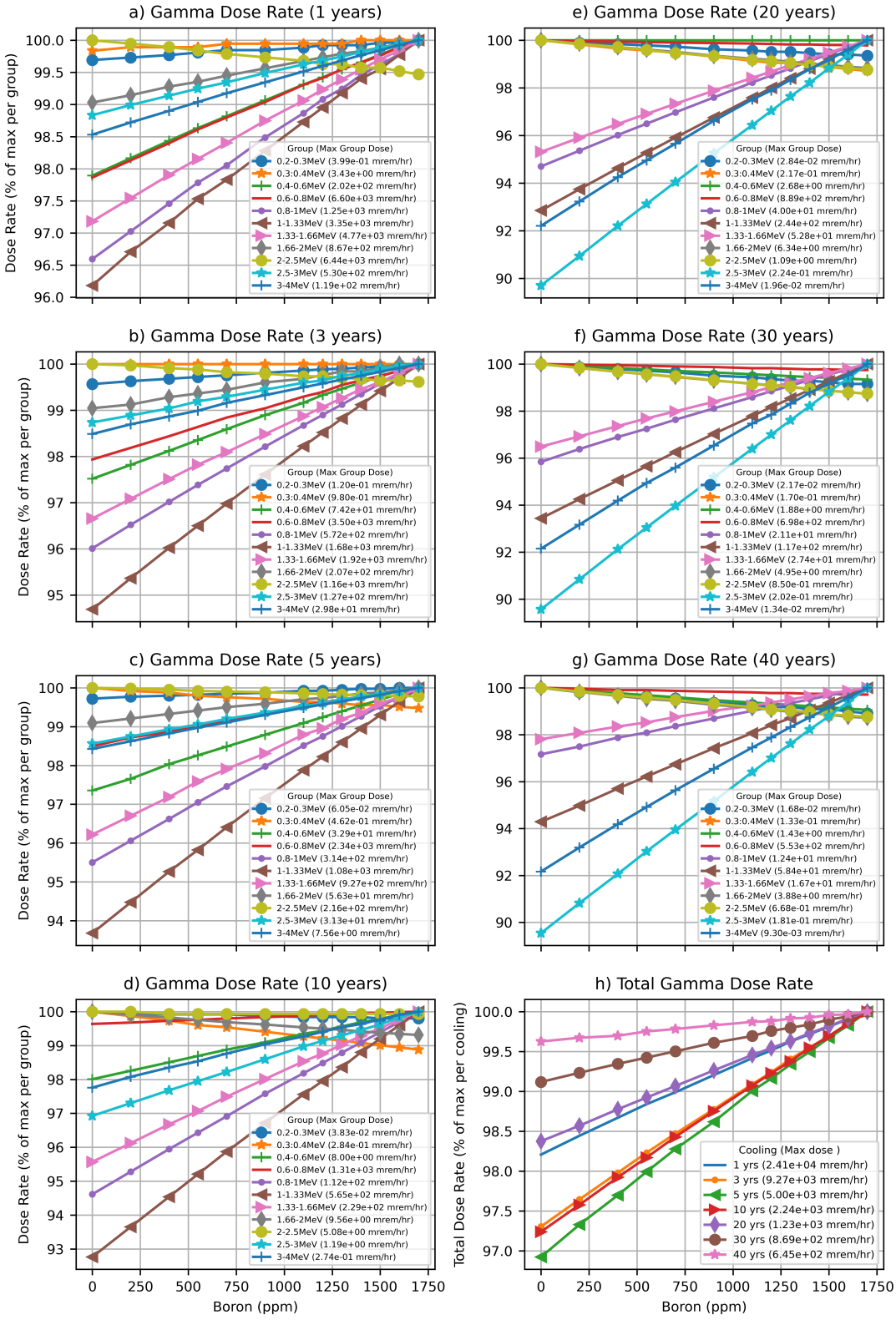

Figure 36. Gamma dose rate as a function of average soluble boron content.

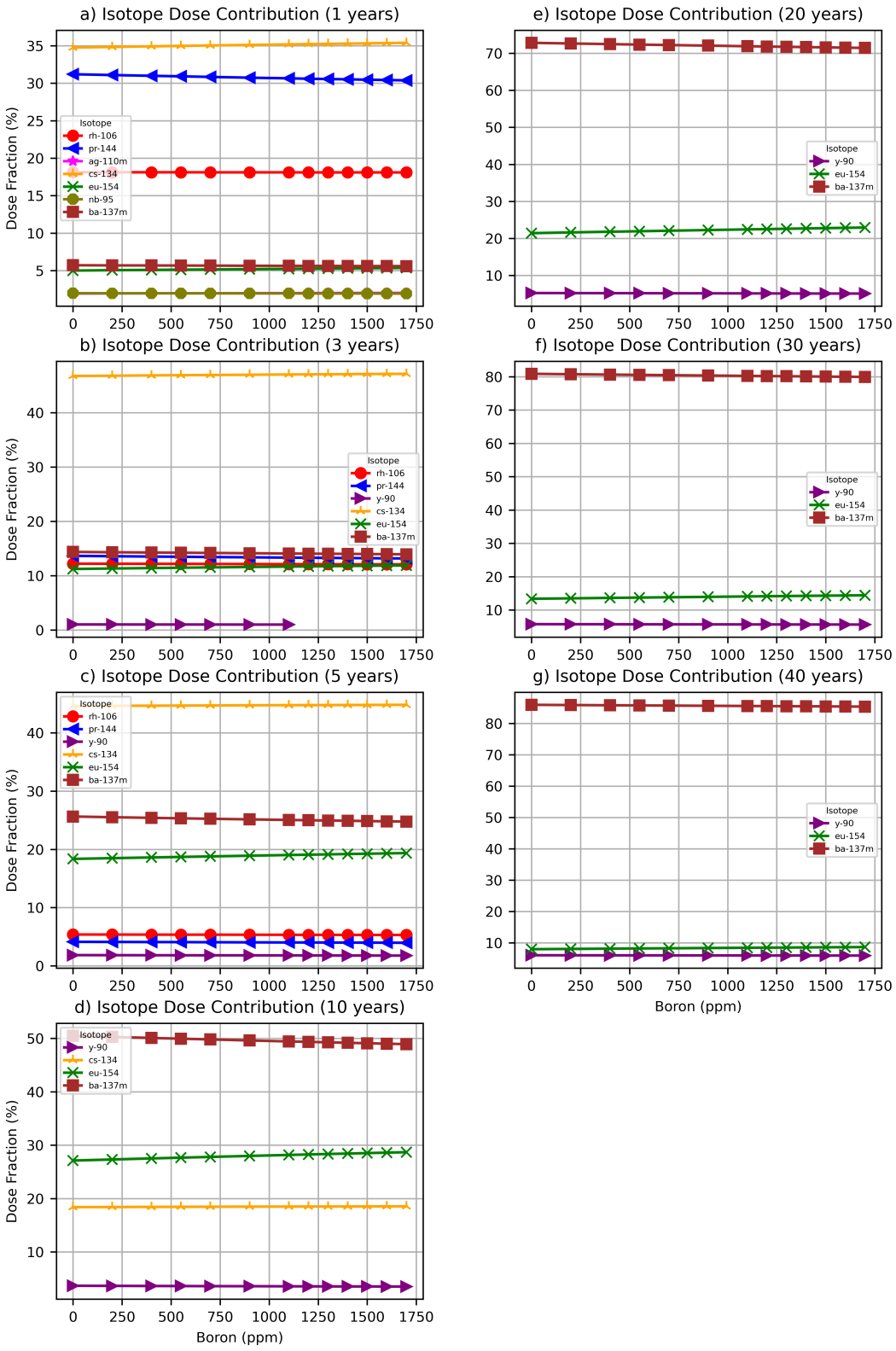

Figure 37. Radionuclide fractional contributions to gamma dose rate as a function of average soluble boron content.

4.1.6.2 Neutron Radiation and Secondary Gamma Radiation

In Figure 38(h), the total neutron radiation source terms are plotted as a function of average soluble boron concentration in the coolant and cooling times. In this plot, the maximum total source strength over the entire range of evaluated boron concentrations is found for each cooling time. The results for that cooling time are then normalized by that maximum value. It is shown that the total strength of the neutron source terms increases with increasing average soluble boron concentration. This phenomenon can be explained as the increased soluble boron cause hardening of the neutron spectrum in the reactor and hence more production of actinides.

Figure 38(a–g) shows the trends of neutron source strength for neutron energy groups. The results show that the energy groups follow a trend similar to that of the total source term: increasing with increased soluble boron concentration. No significant changes in source terms spectra are indicated by these results over the 40 years of cooling time. Contributions above 1% to neutron source terms from individual isotopes is shown in Figure 32. As discussed above, the main contributors to neutron dose rates are isotopes of ^{242}Cm, ^{244}Cm, ^{246}Cm, and ^{252}Cf, where ^{244}Cm contributes over 90% of the source throughout the range of the analyzed cooling time, 1 to 40 years, ^{242}Cm has a contribution of approximately 8 % at 1 year after fuel discharge only because of its short half-life of 0.45 years, ^{252}Cf has a minor contribution for the 1 year cooling time, and ^{246}Cm has a minor contribution for cooling times greater than 1 year.

A dose rate calculation was performed using the simple shielded assembly model described in Section 3.5. The neutron dose rates are plotted in Figure 40 for selected cooling times. The evaluation show that neutron dose rate and neutron source terms have identical trends of variation with average soluble concentration, as expected.

Neutrons will produce secondary gammas through interactions with the package/cask materials. Since trends in the secondary gamma dose rates are directly linked to neutron source terms, the trends are similar. For completeness, these results are provided in Figure A-5.

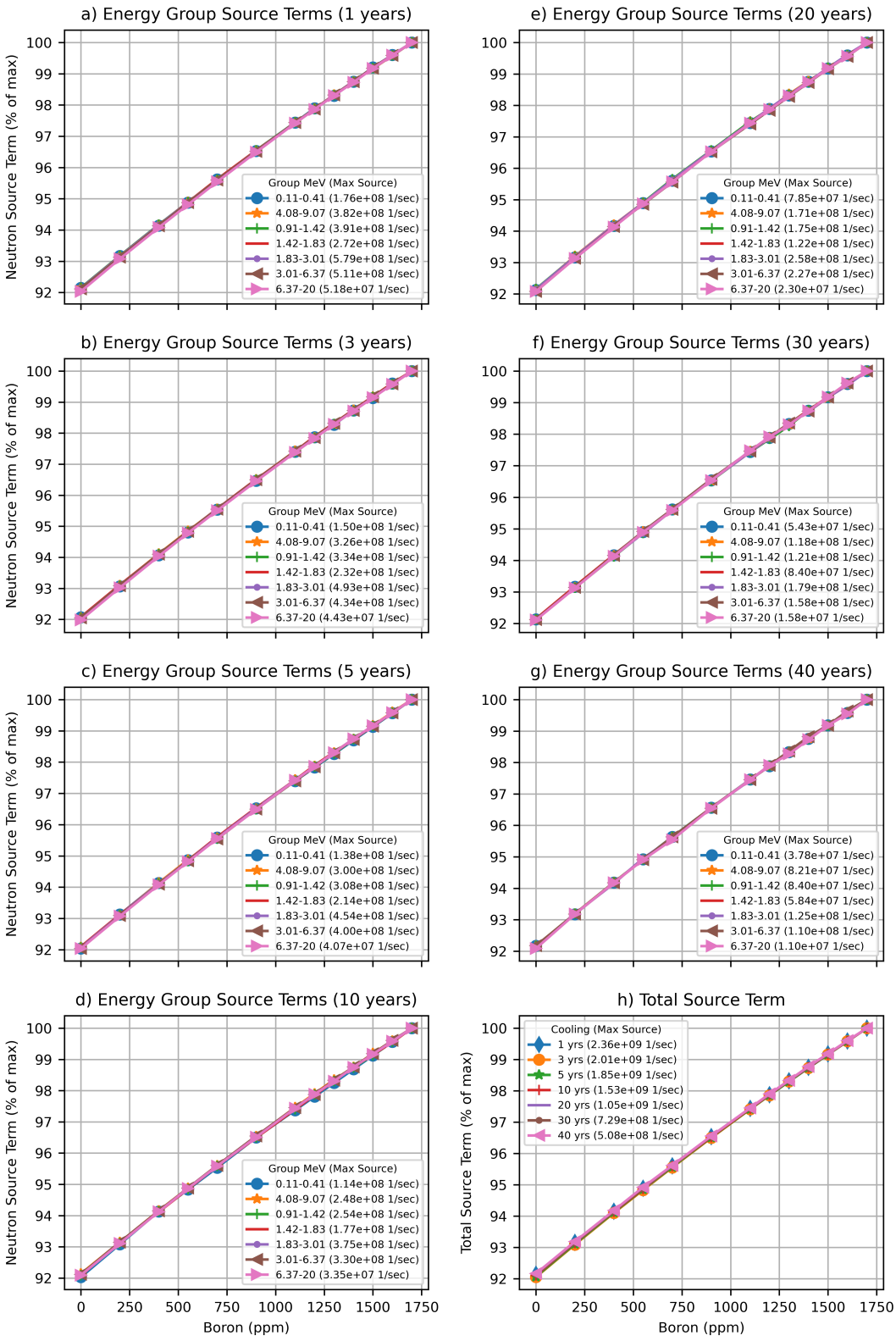

Figure 38. Neutron source terms as a function of average soluble boron content.

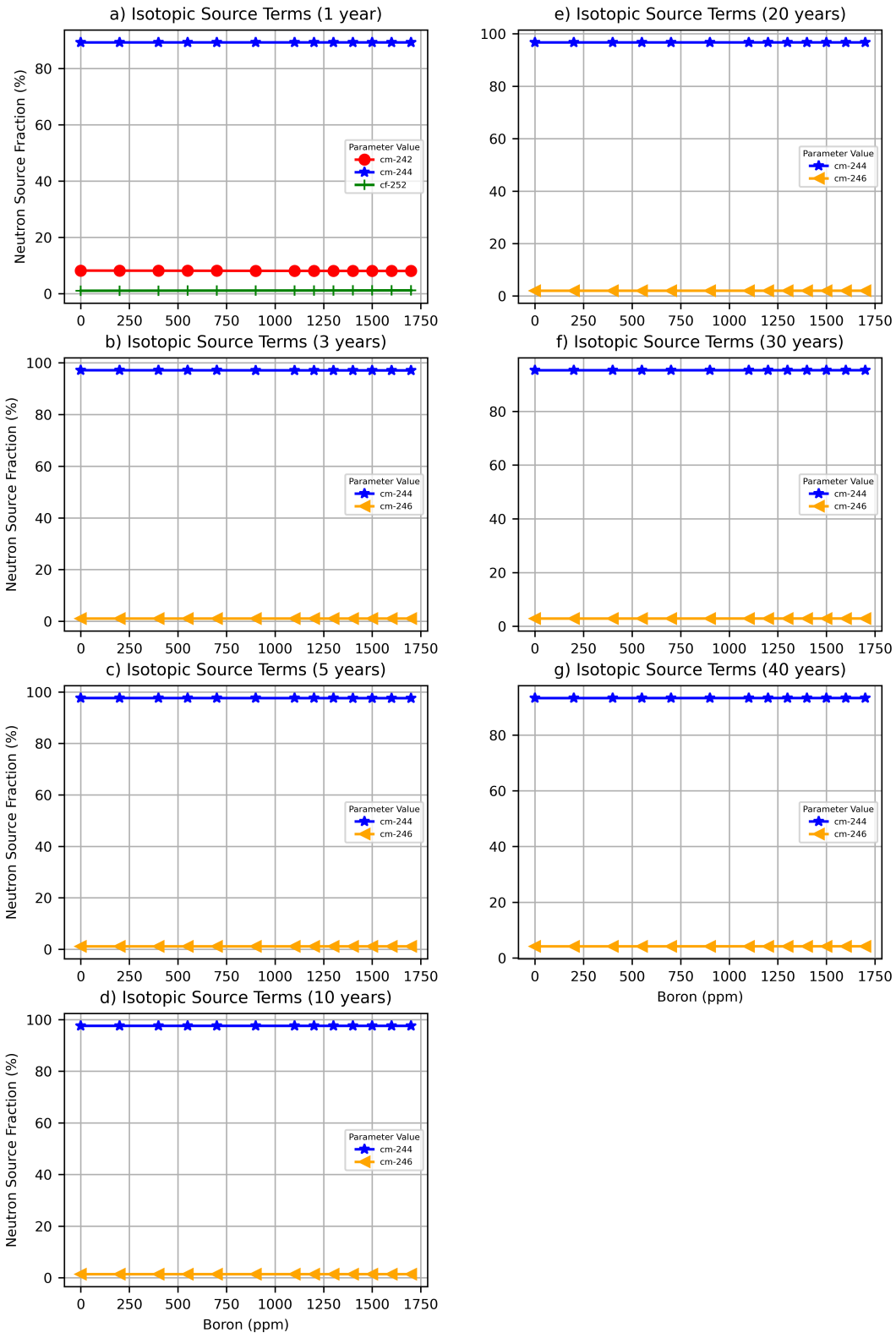

Figure 39. Radionuclide fractional contributions to total neutron source as a function of average soluble boron content.

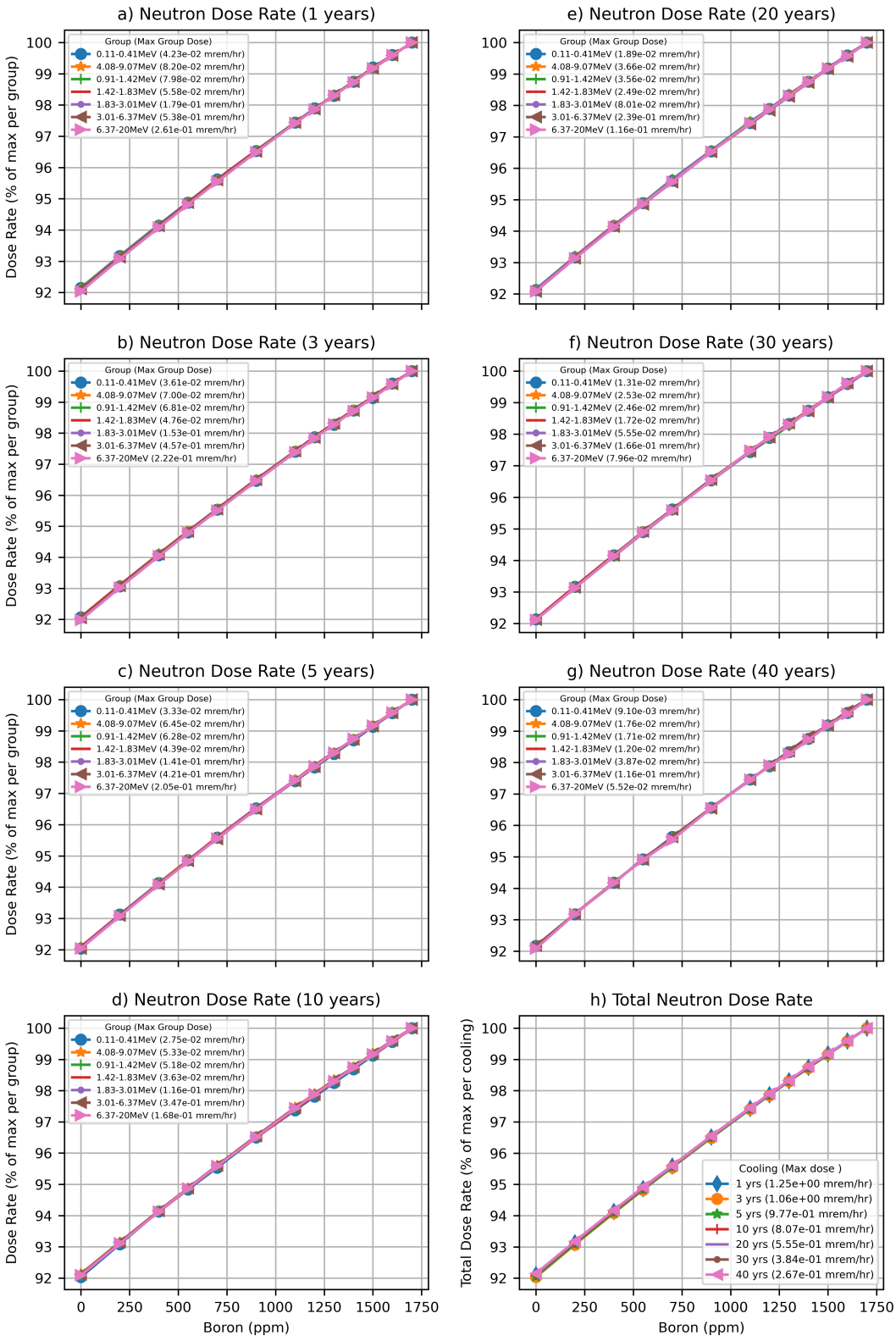

Figure 40. Neutron dose rate as a function of average soluble boron content.

4.1.6.3 Effect of Soluble Boron Concentration on Cobalt Activation Source Terms

Activation of fuel hardware and NFH can contribute significantly to the cask dose rates depending on exposure and cooling time. One of the main contributions to gamma radiation from PWR fuel cask is activated cobalt impurities. The trend in cobalt activity as a function of soluble boron in PWR is also evaluated in this study. The ^{60}Co ($T_{1/2}$ = 5.27 y) activity is evaluated by including one gram of ^{59}Co impurity in the active fuel region. The ^{60}Co activity is then plotted as a function of average soluble boron concentration in Figure 41. Similar to other source terms plots, the activities are normalized by the maximum ^{60}Co activity within the range of evaluated variables and given cooling time. The maximum ^{60}Co activities per gram of ^{59}Co per MTU at various cooling times are provided in the legend of Figure 41. The cobalt source terms slightly increase with increasing soluble boron content during depletion.

The low-energy cross sections of ^{59}Co follow a 1/v behavior; however, a large capture resonance at approximately 100 keV dominates ^{59}Co neutron capture. The depression in the thermal neutron flux and the neutron spectrum hardening that occur with increasing average soluble boron concentration cause an increasing trend of the ^{60}Co production with increasing average soluble boron concentration, as shown in the graph.

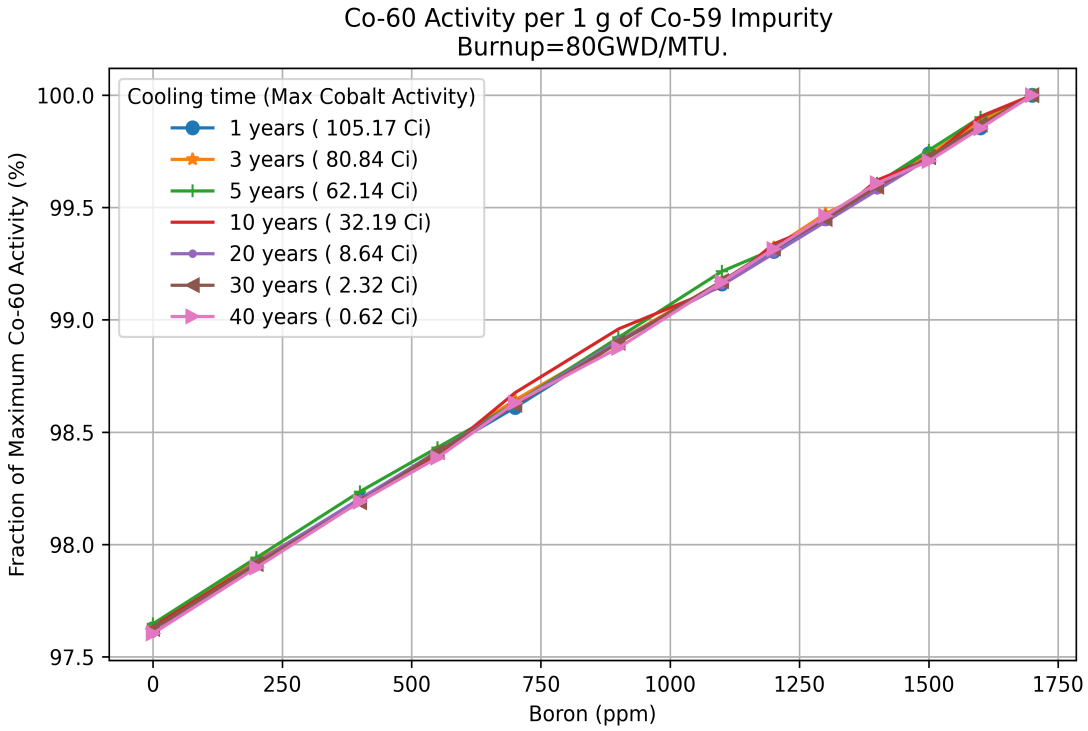

Figure 41. ^{60}Co activity as a function of soluble boron content.

4.2 BWR ASSEMBLY STUDY

The parametric study on the BWR fuel assembly in this section is limited to the fuel primary gamma and neutron source terms. A BWR SNF assembly may be stored with its fuel channel. However, the typical material for the fuel channel is Zircaloy-2 which has a negligible activation source compared with the SNF primary gamma and/or neutron sources. The main neutron activation product in Zircaloy is ^{93}Zr, a long-lived beta emitter with a low beta particle energy. Beta particles and associated bremsstrahlung radiation emitted by the fuel channel are absorbed by the internal structural material of the cask; therefore, no further evaluation is required concerning the impact of the beta radiation on the dose rates outside the cask.

The trends of variation of the BWR source terms with the evaluated depletion parameters are similar to those observed for the PWR source terms because the same physical phenomena cause these trends. An explanation of these trends is provided in Section 4.1 and is not repeated in this section.

Additional sensitivity studies are provided in Section 6.5, which analyzes the effects of a control blade insertion on BWR radiation sources when the fuel is irradiated in the reactor. Section 6.7 provides analyses for the effects of part-length rods on BWR radiation source terms.

4.2.1 Specific Power

4.2.1.1 Primary Gamma Radiation

In Figure 42(h), the total gamma radiation source terms are plotted as a function of specific power and cooling time. In this plot, the maximum total source strength over the selected range of specific powers is found for each cooling time. The results are then normalized by that maximum value. The results show that the total strength of the gamma source terms increases with increased specific power. Furthermore, the effect of specific power on source term decreases with increased cooling time. At short cooling times, the difference in source terms between the lowest and highest specific power is approximately 60 to 80%. After 20 years of cooling, this difference decreases to about 40%.

Figure 42(a–g) shows the trends of variation with specific power of the gamma radiation sources within energy groups in the range of 0.2 MeV to 4 MeV. This figure shows variation of the normalized gamma source strength for each energy group as a function of specific power. The results show that the per energy group source terms follow a similar trend to that of the total source term: increasing with increasing specific power. However, the source terms for photons in energy group 2–2.5 MeV shows an opposite trend with longer cooling times. However, this effect does not have a meaningfully impact on the overall dose from the cask. This is because the source strength for this group is approximately two orders of magnitude lower compared with the source terms from the dominating energy groups.

The results for BWR assembly are similar to that for the PWR fuel assembly analyzed above; therefore, the same conclusions apply and no dose rate calculations were perfomed for the BWR fuel.

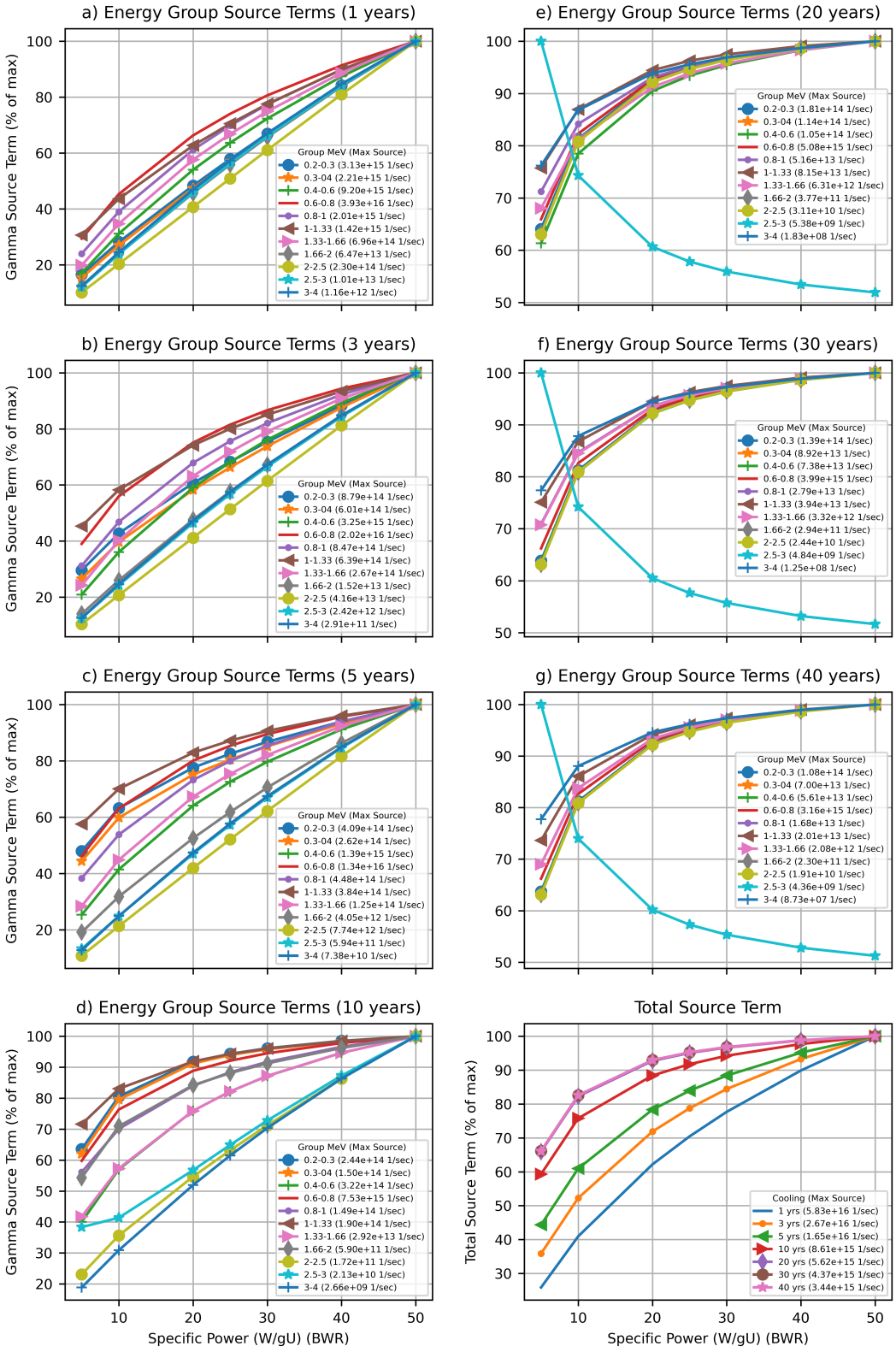

Figure 42. Gamma source terms as a function of specific power (BWR).

4.2.1.2 Neutron Radiation and Secondary Gamma Radiation

Figure 43(h) provides plots of the dependence of the total neutron radiation source terms as a function of specific power at selected cooling times. In this plot, the maximum total source strength over the entire range of evaluated specific powers is shown for each cooling time. The results for that cooling time are then normalized by that maximum value. The total strength of the neutron source terms increases with increasing specific power. However, impact on neutron source terms is less pronounced than what was observed for gamma dose rates. In addition, it is also observed that the effect of specific power on source terms is not significantly diminishing with cooling time. At short cooling times, the difference in source terms between the lowest and highest specific power is approximately 25%. After 30–40 years of cooling, this difference does not change appreciably.

Figure 43(a–f) shows the trend of variation with specific power for neutron sources within energy groups. The results show that the energy group follow a similar trend to that of the total source term: increasing with increasing specific power. No significant changes in source terms spectra are indicated by these results over the 40 years of cooling time.

The results for BWR assembly are similar to that analyzed above for PWR fuel; therefore, the same conclusions apply and no secondary gamma analysis or shielding calculations were repeated for the BWR case.

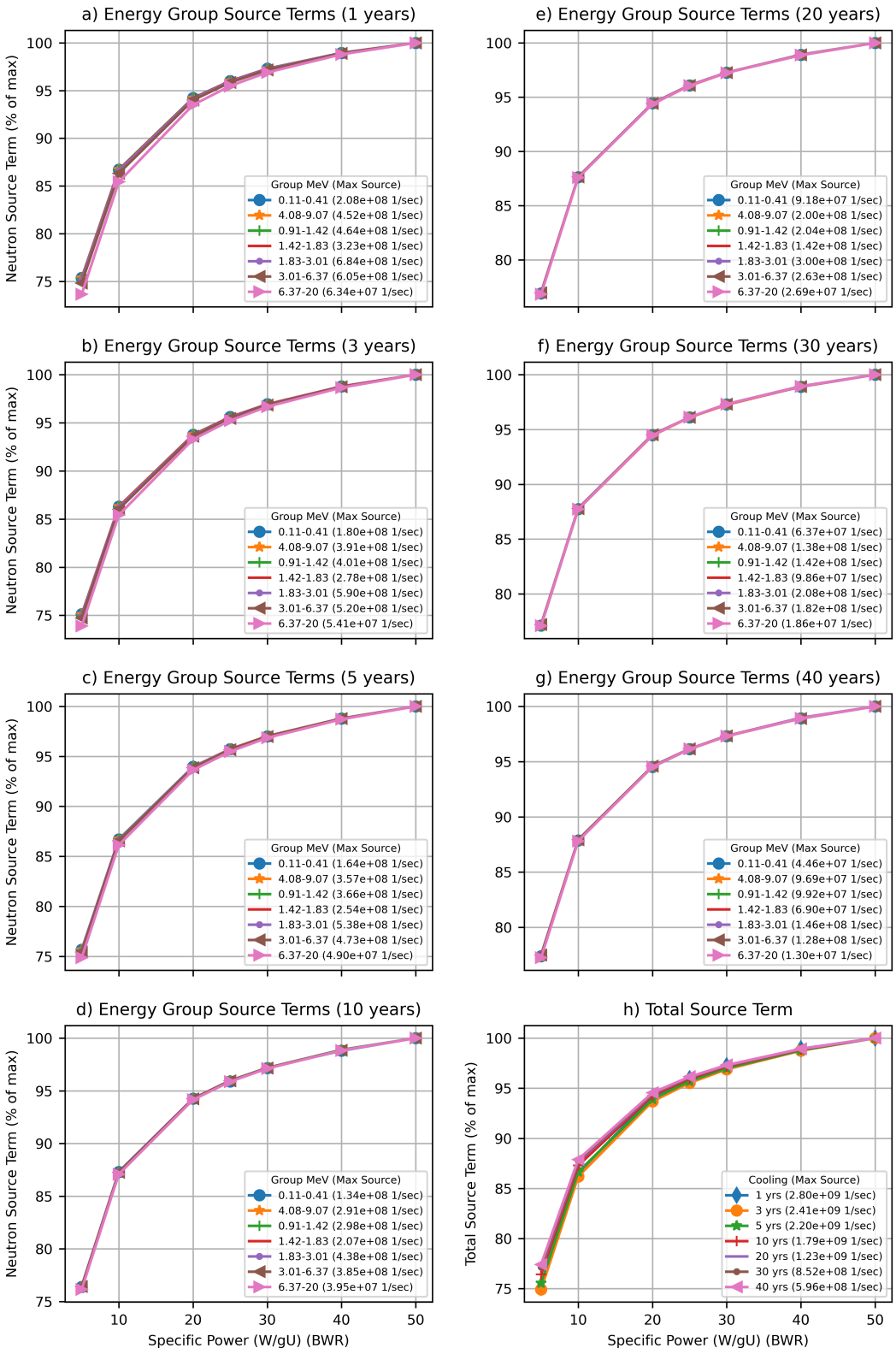

Figure 43. Neutron source terms as a function of specific power (BWR).

4.2.2 Initial Enrichment

4.2.2.1 Primary Gamma Radiation

In Figure 44(h), the total gamma radiation source terms are plotted as a function of initial assembly average enrichment at selected cooling times. The enrichment axial distribution is assumed uniform. For each cooling time, the maximum total source strength over the selected range of evaluated enrichment values is found and the results for each initial enrichment value are normalized by that maximum value. The results show that the total strength of the gamma source terms decreases with increasing enrichment for shorter cooling times (<10 years), whereas it increases with enrichment for longer cooling times (>10 years). Furthermore, the gamma source terms are less sensitive to fuel initial enrichment variations at longer cooling times. At short cooling times, the difference in source terms between the lowest and highest specific power is approximately 12–20%. After 20 years of cooling, this difference diminishes to less than 7%. The trends of variation observed for the BWR gamma source terms are similar to those provided and explained in Section 4.1.2.1 for PWR fuel.

Figure 44(a–g) shows the trends of variation with fuel initial enrichment of the gamma radiation sources within energy groups in the range of 0.2 MeV to 4 MeV. In this plot, the maximum source strength over the selected range of evaluated initial enrichments is found for each energy group of the fuel gamma source terms, and the results for each energy group are then normalized by this maximum source terms value. The results show that the per energy group source terms follow the similar trend as that of the total source term: decreasing with increasing enrichment for shorter cooling times (<10 years) and increasing with enrichment for longer cooling times (>10 years). However, at longer cooling times ($\geq$10 years), the source terms for photons start to show an opposite trend. The results for BWR assembly are similar to PWR fuel analyzed above; therefore, the same conclusions apply and no shielding calculations were perfomed for the BWR case.

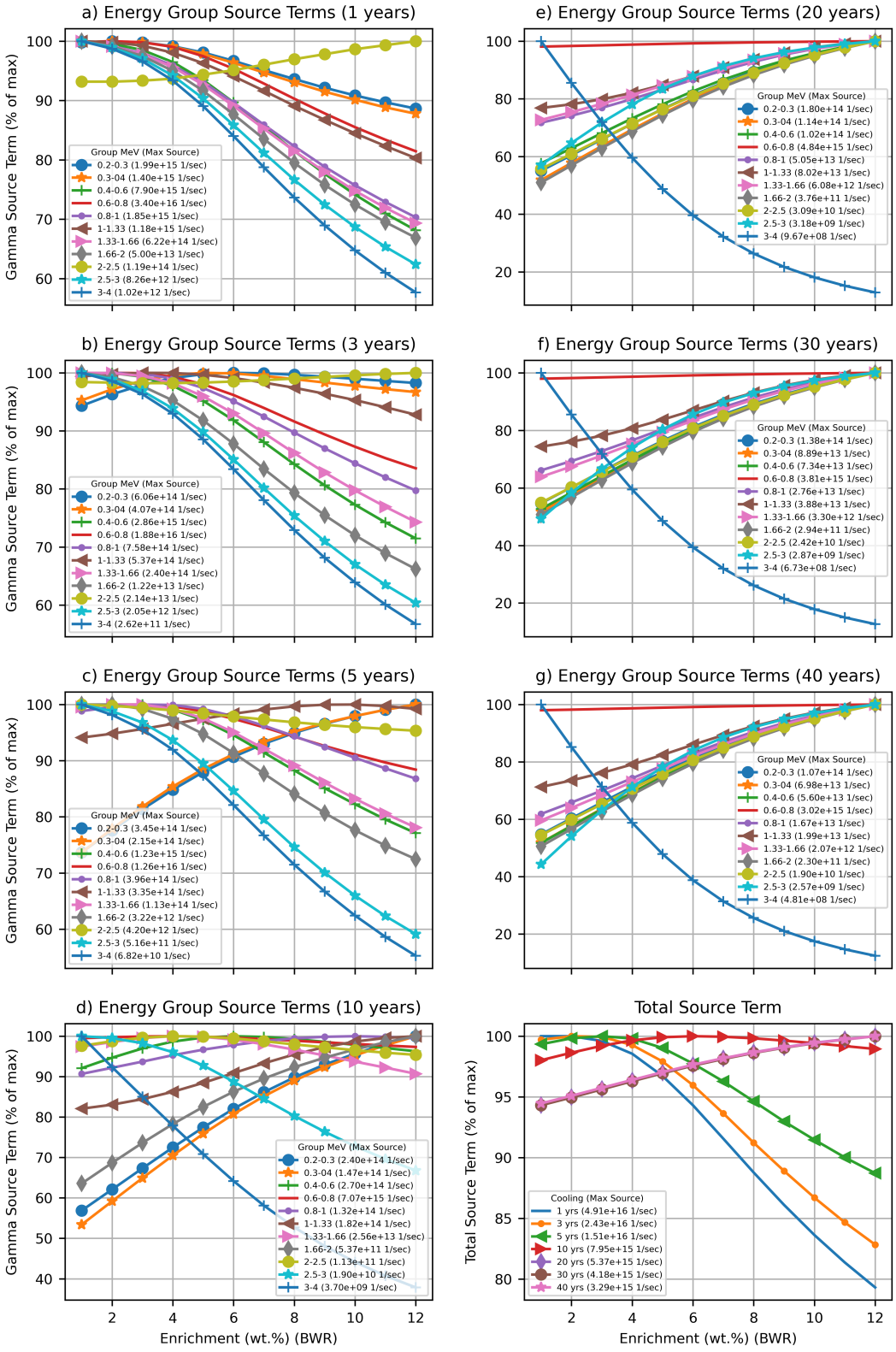

Figure 44. Gamma radiation as a function of initial enrichment (BWR).

4.2.2.2 Neutron Radiation and Secondary Gamma Radiation

In Figure 45(h), the total neutron radiation source terms are plotted as a function of initial assembly average enrichment at selected cooling times. In this plot, the maximum total source strength over the whole range of evaluated initial enrichments is shown for each cooling time. The results for that cooling time are then normalized by that maximum value. It is shown that the total strength of the neutron source terms decreases with increasing initial enrichment. The fundamental physics for this behavior is that a fuel higher enrichment will produce less actinides for the same burnup. By increasing fuel initial enrichment, the ^{235}U absorption rate is increased, the thermal neutron flux is decreased, and the absorption rates of other nuclides is decreased.

Figure 45(a–g) shows neutron radiation per starting neutron particles energy groups. The results show that the energy group follow a similar trend to that of the total source term: decreasing with increasing initial enrichment. No significant changes in source terms spectra are indicated by these results over the 40 years of cooling time.

The results for BWR assembly are similar to those of the PWR fuel analyzed above; therefore, the same conclusions apply and no secondary gamma analysis or shielding calculations were perfomed for the BWR case.

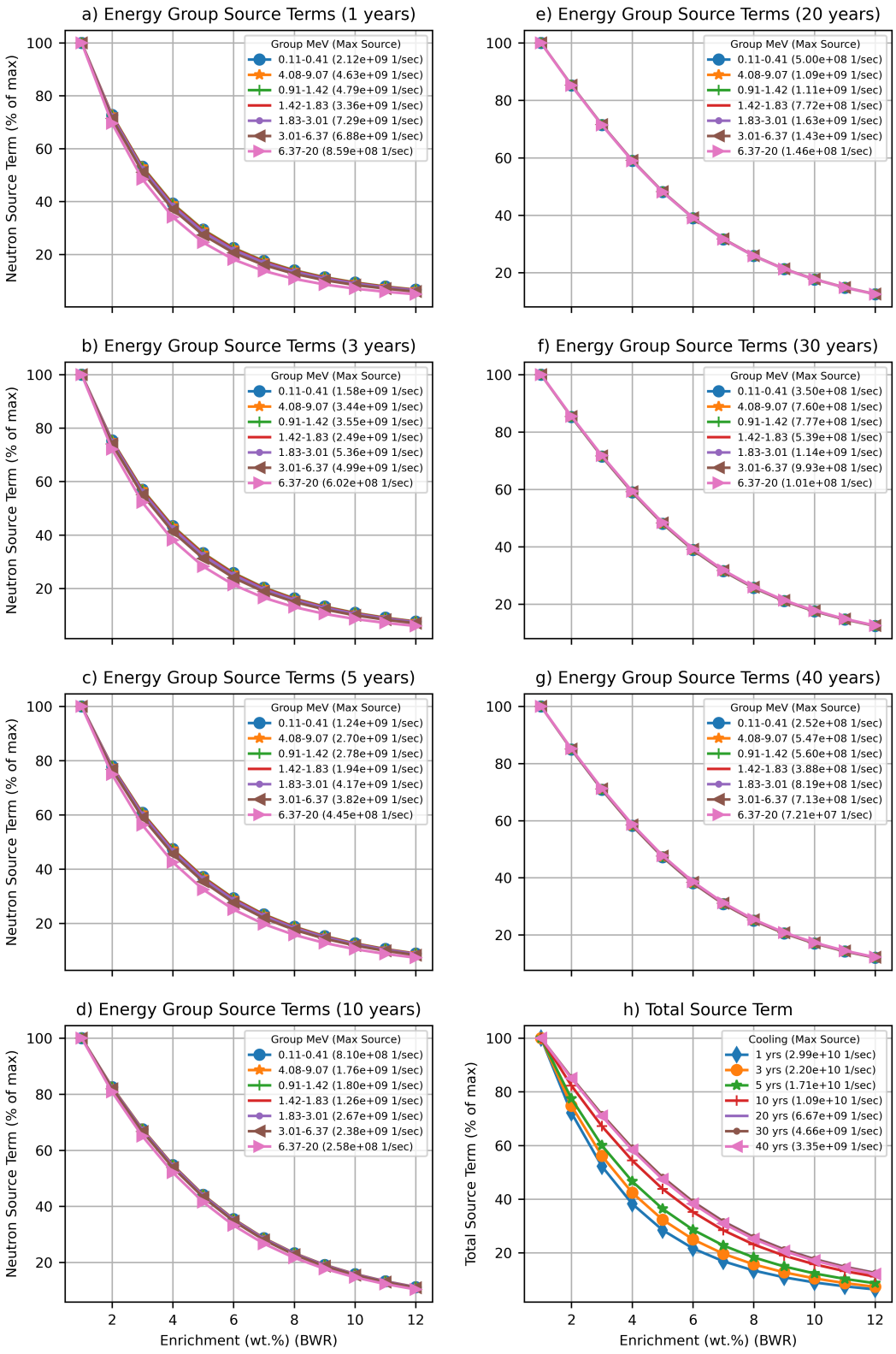

Figure 45. Neutron source terms as a function of enrichment (BWR).

4.2.3 Fuel Density

Fuel density affects ^{238}U resonance self-shielding. By increasing fuel density, fewer transuranic actinides will be produced. In this parametric study, fuel mass is maintained constant, and the varying pellet radius is limited by the inner radius of the fuel cladding. Therefore, the fuel density varies from 10.26 to 10.96 g/cm^3 in this parametric study.

4.2.3.1 Primary Gamma Radiation

In Figure 46(h), the total gamma radiation source terms are plotted as a function of fuel density at selected cooling times. In this plot, the maximum total source strength over the selected range of evaluated fuel density values is found for each cooling time. The results for that cooling time are then normalized by that maximum value. It is shown that the total strength of the gamma source terms slightly decreases with increasing fuel density at constant fuel mass. The changes in total primary gamma source due to fuel density variation from 10.26 to 10.96 g/cm^3 is less than 0.2 % over 40 years of cooling, i.e., negligible effects. Figure 46(a–g) shows the trends of variation with fuel density of the gamma radiation sources within energy groups in the range of 0.2 MeV to 4 MeV.

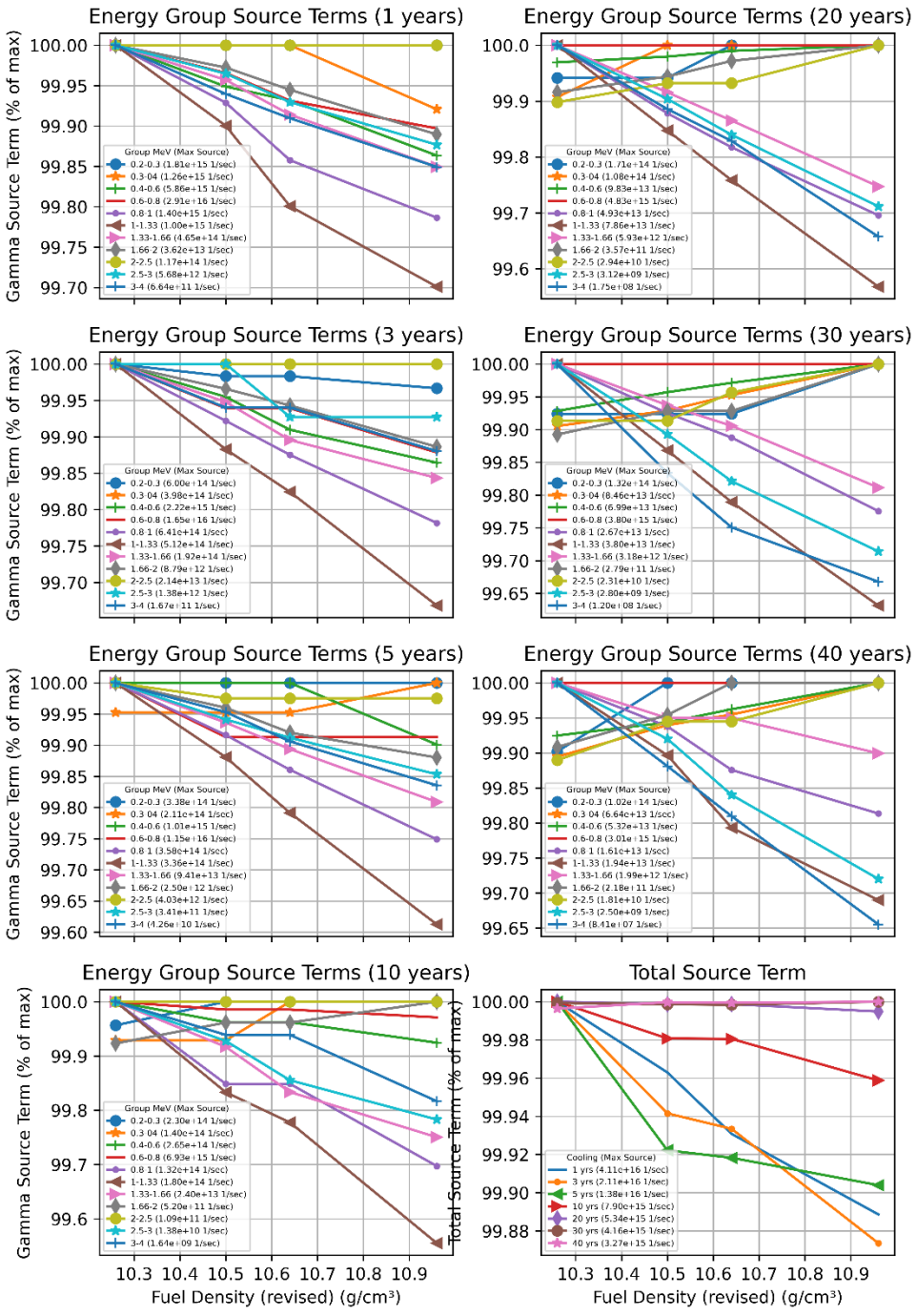

Figure 46. Gamma source terms as a function of fuel density (BWR).

4.2.3.2 Neutron Radiation and Secondary Gamma Radiation

In Figure 47(h), the total neutron radiation source terms from fuel are plotted as a function of fuel density at selected cooling times. In this plot, the maximum total source strength over the entire range of evaluated fuel densities is found for each cooling time. The results for that cooling time are then normalized by that maximum value. The total strength of the neutron source terms slightly decreases with increasing fuel density at constant fuel mass. The change in total neutron strength due to fuel density variation from 10.26 to 10.96 g/cm^3 is less than 0.4 % over 40 years of cooling, i.e., negligible effects.

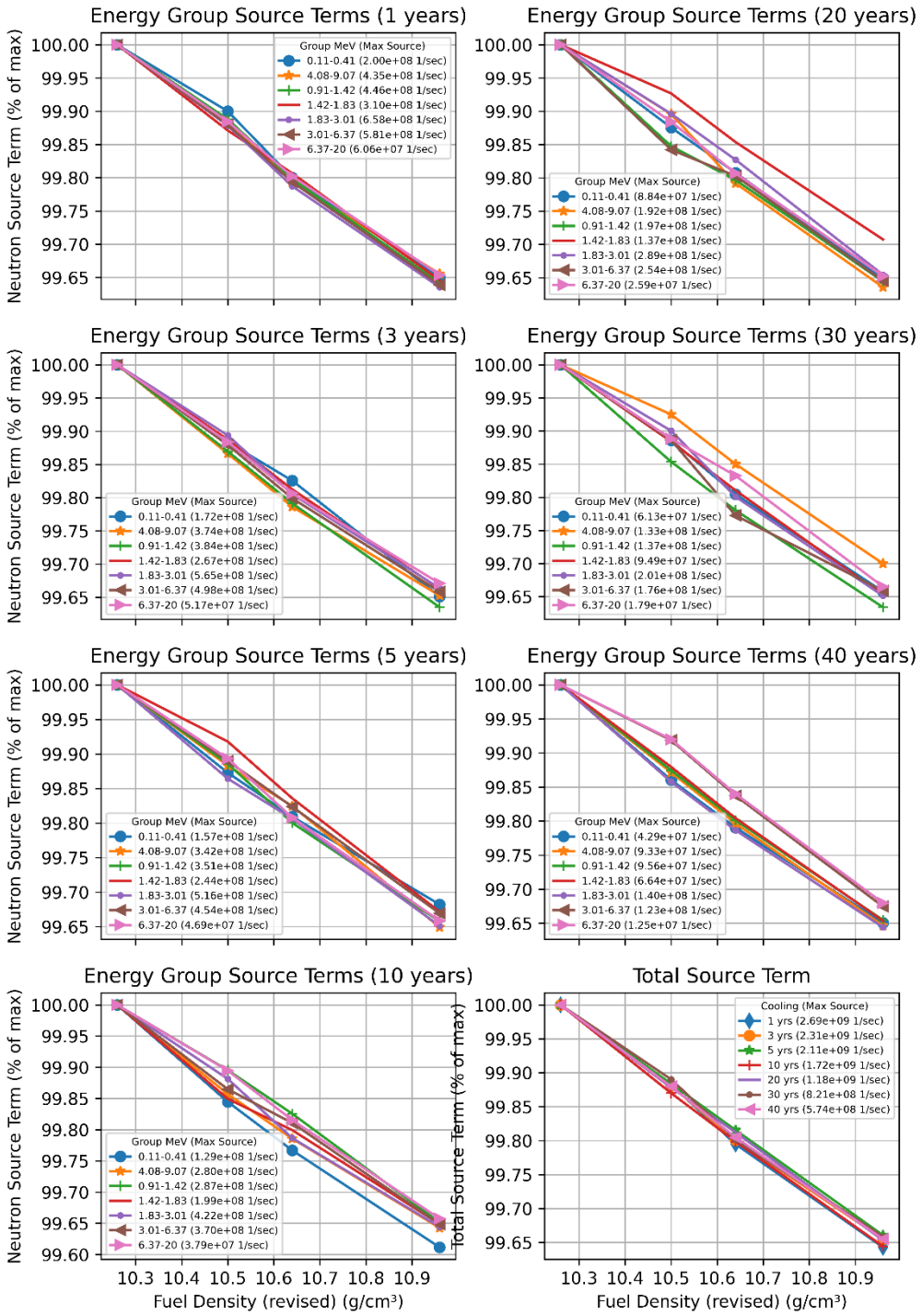

Figure 47. Neutron source terms as a function of fuel density (BWR).

4.2.4 Fuel Temperature

4.2.4.1 Primary Gamma Radiation

In Figure 48(h), the total gamma radiation source terms are plotted as a function of fuel temperature at selected cooling times. In this plot, the maximum total source strength over the entire range of evaluated fuel temperature values is found for each cooling time. The results for that cooling time are then normalized by that maximum value. The maximum value is shown in the plot legend. It is shown that the total strength of the gamma source terms remains mostly unchanged with fuel temperature. The change in total source strength is less than 1% over the range of evaluated temperatures.

Figure 48(a–g) shows the trends of variation with fuel temperature of the gamma sources within energy groups in the range of 0.2 MeV to 4 MeV. In this plot, the maximum source strength over the entire range of evaluated fuel temperatures is found for each energy group source terms, and the results within the energy group are then normalized by this maximum source terms value. This maximum source terms value is shown in the plot legend. The source terms with the highest strength are in the energy group 0.6-0.8 MeV. The effect of temperature on the source terms in the energy group 0.6-0.8 MeV is low. The change in source strength is less than 1% over the range of evaluated temperatures. This corresponds to change in the total source strength discussed above. Variation in source strength in other energy groups can be up to 6%, but photons in these energy groups contribute much less to the total source strength, therefore their effect on the total source strength is negligible.

The results for BWR assembly are similar to PWR fuel analyzed in Section 4.1.4.1; therefore, no shielding calculations were perfomed.

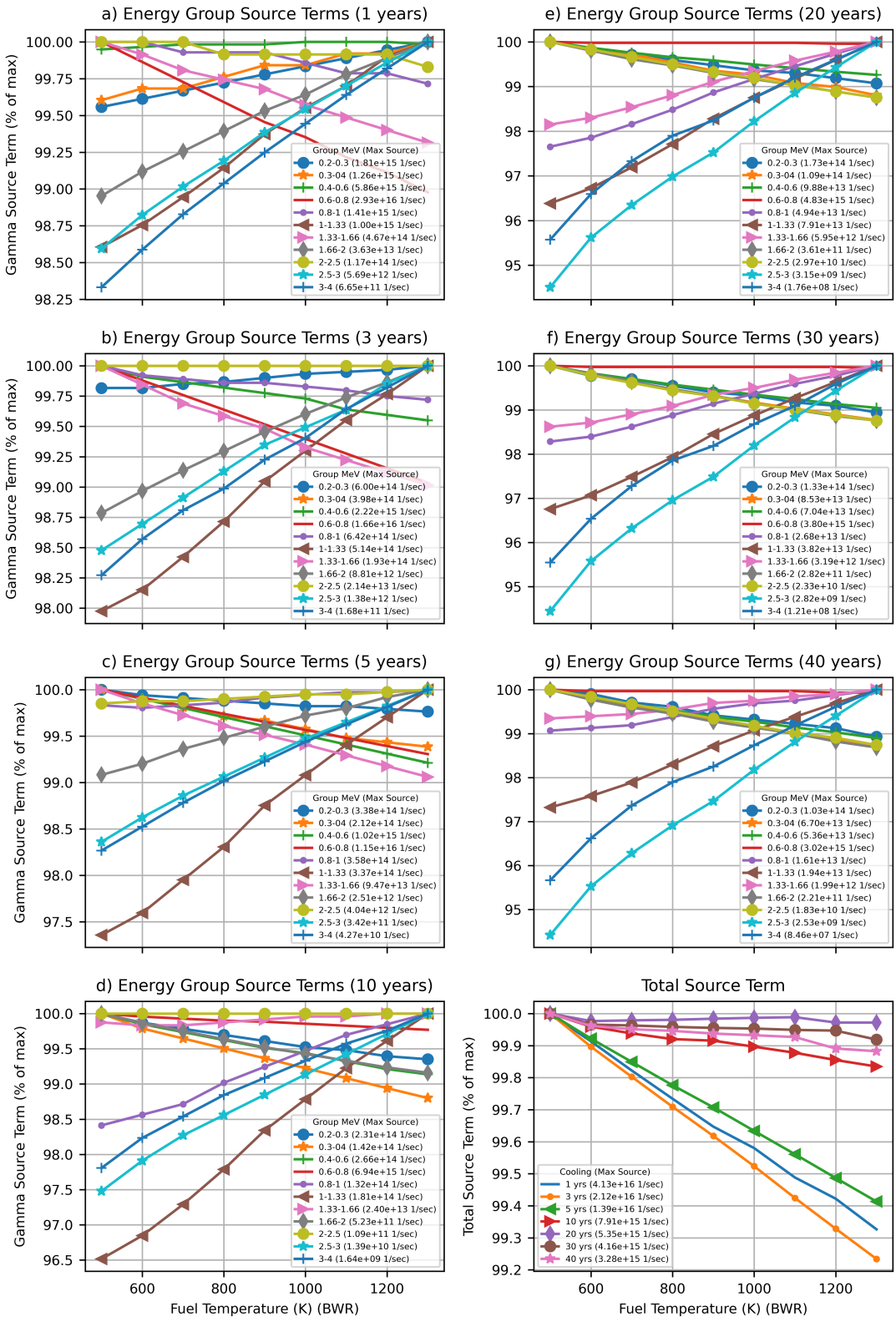

Figure 48. Gamma source terms as a function of fuel temperature (BWR).

4.2.4.2 Neutron Radiation and Secondary Gamma Radiation

In Figure 49(h), the total neutron radiation source terms are plotted as a function of fuel temperature and cooling times. In this plot, the maximum total source strength over the entire range of evaluated fuel temperatures is shown for each cooling time. The results for that cooling time are then normalized by that maximum value. The figures show that the total strength of the neutron source terms increases with increasing fuel temperature; the increase is approximately 4% from 500 K to approximately 1,300 K.

Figure 49(a–g) shows the trends of variation with fuel temperature of neutron radiation sources within energy groups. The results show that the energy groups follow a trend similar to that of the total source term: increasing with fuel temperature. No significant changes in source terms spectra are indicated by these results over the 40 years of cooling time.

The results for BWR assembly are similar to PWR fuel analyzed above; therefore, no neutron shielding calculations or secondary gamma analysis were perfomed.

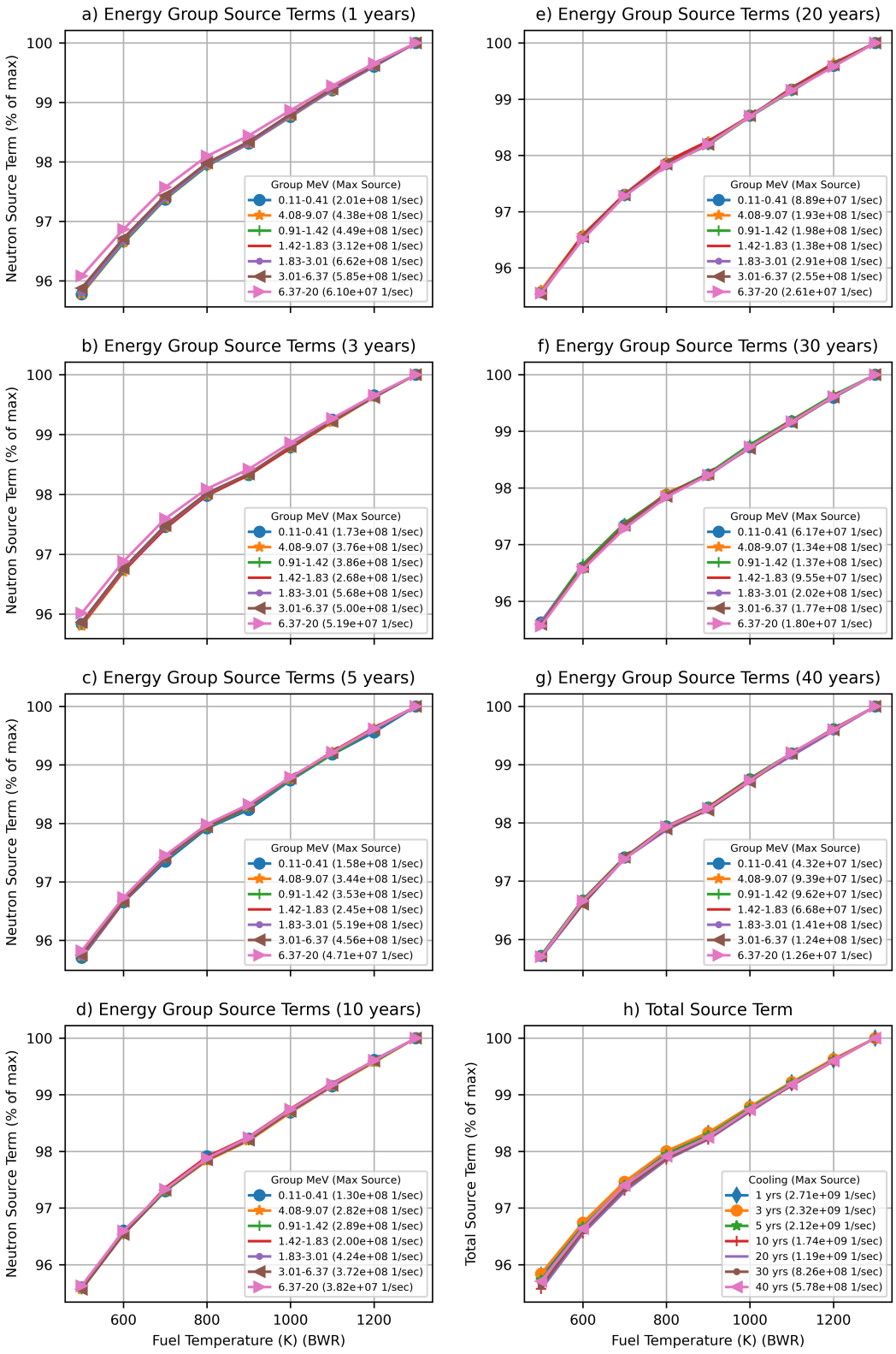

Figure 49. Neutron source terms as a function of fuel temperature (BWR).

4.2.5 Moderator Void Fraction

The effects of increased BWR moderator void fraction include increased resonance captures in fertile nuclides (e.g., ^{238}U and ^{240}Pu) and increased production of transuranic radionuclides because of the neutron energy spectrum hardening as a result of losing moderator.

4.2.5.1 Primary Gamma Radiation

In Figure 50(h), the total gamma radiation source terms are plotted as a function of moderator void fraction and cooling times. In this plot, the maximum total source strength over the entire range of evaluated moderator void fraction values is analyzed for each cooling time. The results for that cooling time are then normalized by that maximum value. The maximum value is shown in the plot legend. The total strength of the gamma source terms increases with moderator void fraction for shorter cooling times. After about 20 years cooling time, the total gamma source becomes much less sensitive to moderator void fraction variations because these source terms are dominated by gamma emissions from ^{137}Cs decay. The cumulative fission yields of ^{137}Cs from ^{235}U, ^{239}Pu, and ^{241}Pu fissions are relatively similar. Therefore, ^{137}Cs production rate does not exhibit significant sensitivity to moderator void fraction variations at constant power density.

Figure 50(a–g) shows the trends of variation with moderator void fraction of the gamma radiation sources within energy groups in the range of 0.2 MeV to 4 MeV for more precise results. In this plot, the maximum source strength over the whole range of evaluated moderator densities is found for the source terms in each energy group, and the results within the energy group are then normalized by this maximum source terms value.

The trends observed in Figure 50(a–g) for the group-wise gamma source terms are the result of the contributing gamma emitters to each energy group, their cumulative yields presented in Table 7, and the effects of moderator void fraction on the neutron energy spectrum and transuranic radionuclides described at the beginning of this section.

For short cooling times, the dose rates are dominated by gamma radiation from the decay of the following fission products: ^{134}Cs ($T_{1/2}$=2.0652 years), ^{144}Ce ($T_{1/2}$=284.89 days)/^{144}Pr ($T_{1/2}$=17.29 min), ^{137}Cs ($T_{1/2}$=30.1 years)/^{137m}Ba ($T_{1/2}$=153 s), ^{106}Ru ($T_{1/2}$=1.02 years)/^{106}Rh ($T_{1/2}$=2.18 h), and ^{154}Eu ($T_{1/2}$=8.593 years). After 10 years of cooling, $^{137}Cs/^{137m}Ba$, ^{154}Eu, and ^{90}Sr ($T_{1/2}$=28.78 years)/^{90}Y ($T_{1/2}$=64 h) are the most contributing radionuclides. Only ^{144}Ce and ^{90}Sr production rates decrease with increasing moderator void fraction because their cumulative fission yields from ^{235}U are greater than those from ^{239}Pu. The production rates of the other gamma emitters exhibit an increasing trend due to increased ^{239}Pu production as moderator void fraction increases.

As a confirmation, a simplified shielding calculation was performed using the shielded assembly model with a concrete shielding described in Section 3.5. The gamma dose rates are plotted in Figure 51. The evaluation confirms the similar trends of the source terms described above: external dose rates increase with moderator void fraction. A further breakdown of dose rates according to contribution from individual isotopes is shown in Figure 52.

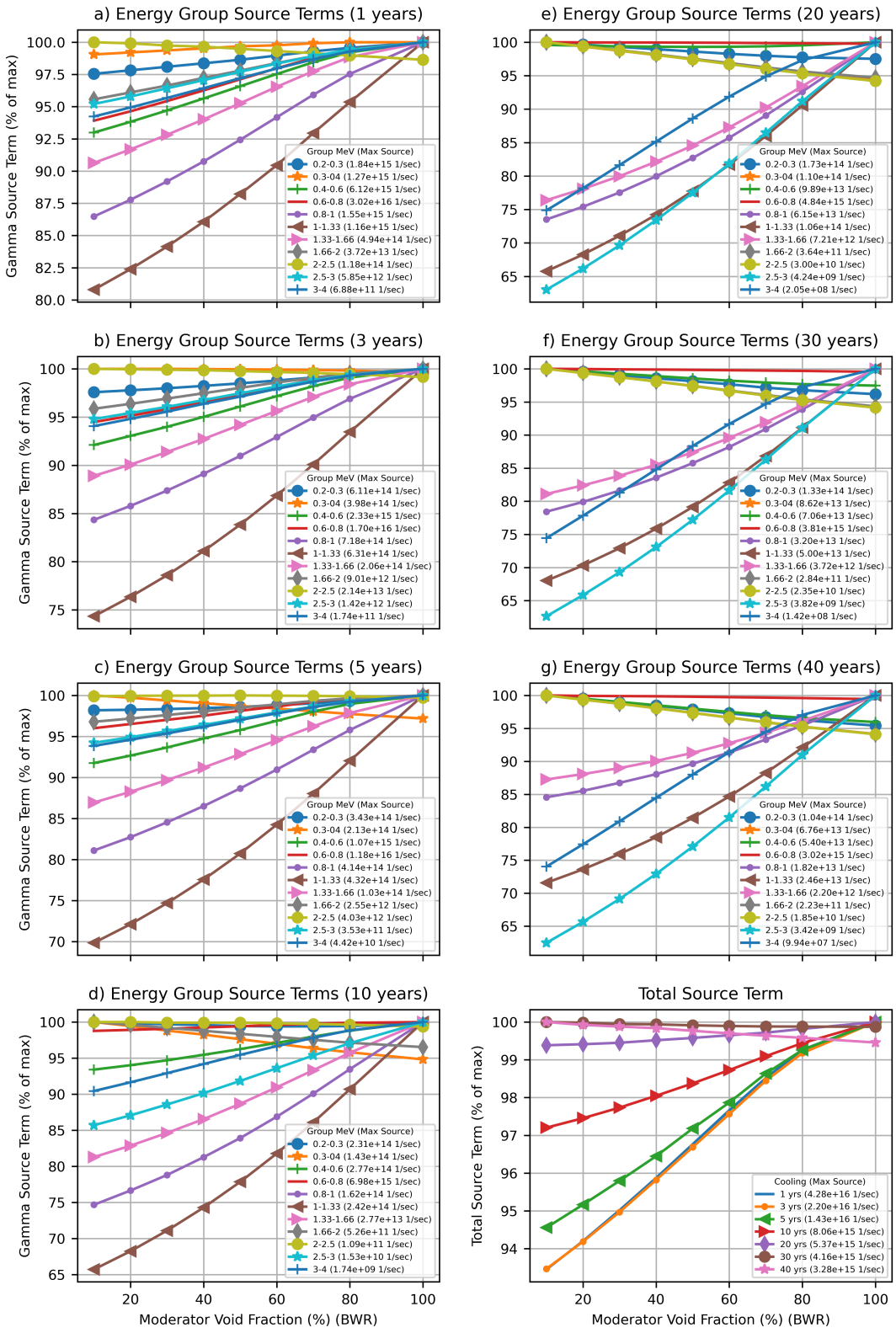

Figure 50. Gamma source terms as a function of moderator void fraction (BWR).

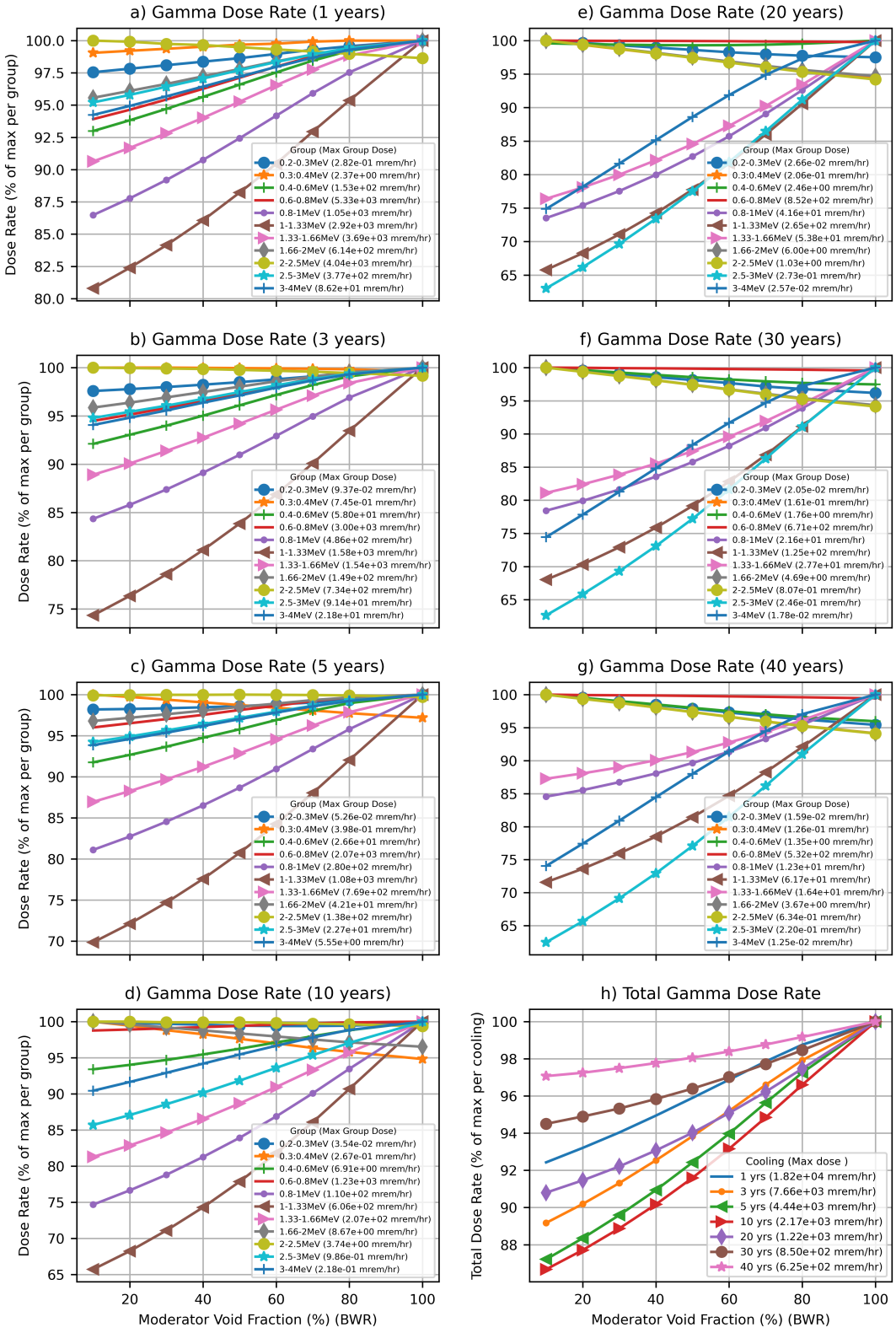

Figure 51. Gamma dose rate as a function of moderator void fraction (BWR).

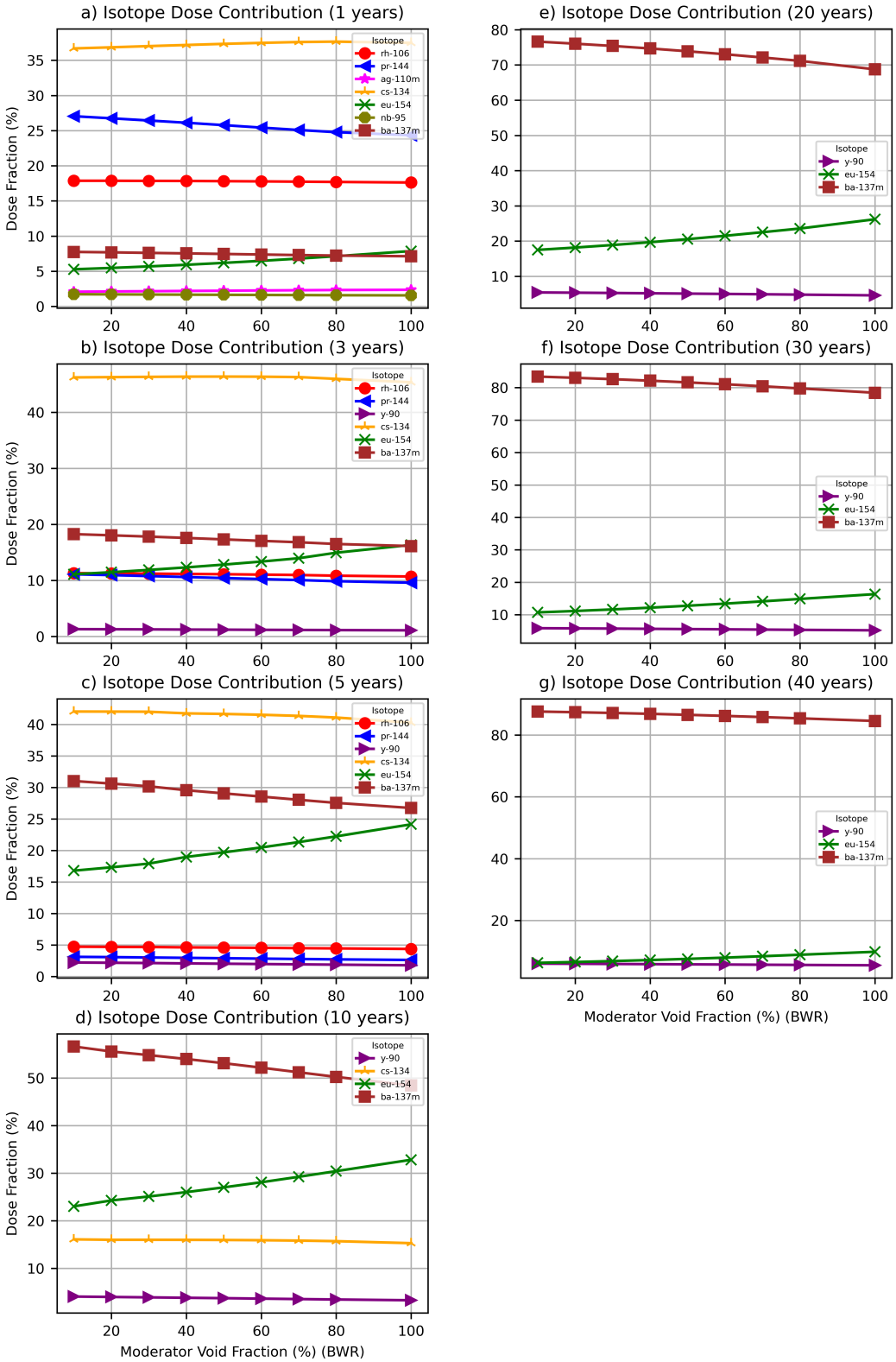

Figure 52. Radionuclide fractional contributions to gamma dose rate as a function of moderator void fraction (BWR).

4.2.5.2 Neutron Radiation and Secondary Gamma Radiation

In Figure 53(h), the total neutron radiation source terms are plotted as a function of moderator void fraction at selected cooling times. In this plot, the maximum total source strength over the entire range of evaluated moderator void fractions is found for each cooling time. The results for that cooling time are then normalized by that maximum value. The total strength of the neutron source terms increases with increasing moderator void fraction.

Figure 53(a–g) shows the trends of neutron radiation sources as a function of moderator void fraction within energy groups. The results show that the neutron sources in all energy groups follow a similar trend to that of the total source term: increasing with moderator void fraction. No significant changes in source terms spectra are indicated by these results over the 40 years of cooling time. Contributions above 1% to neutron source terms from individual isotopes is shown in Figure 54. As discussed above, the main contributors to neutron dose rates are ^{242}Cm, ^{244}Cm, ^{246}Cm and ^{252}Cf, where ^{244}Cm always contributes over 90% of the source. As a result, the spectrum of the neutron source terms does not vary appreciably with respect to the cooling time, although the half-lives of these dominating nuclides vary. The fractional contributions of ^{244}Cm and ^{252}Cf to the neutron source terms at cooling times less than 10 years depend on the void fraction. Contributions from ^{244}Cm decrease with void fraction, whereas contribution from ^{252}Cf and ^{246}Cm tends to increase with void fraction. The production pathway of ^{252}Cf ($T_{1/2}$=2.645 years) consists of neutron absorption reactions and beta decay of ^{244}Cm and other transcurium nuclides. These results indicate that the concentration of ^{252}Cf in fuel per unit of ^{244}Cu consumption is higher for the higher void fraction range compared to the lower void fraction range.

A dose rate calculation was performed using the simple shielded assembly model described in Section 3.5. The neutron dose rates are plotted in Figure 55. The evaluation confirms the similar trends of the source terms.

Neutron source terms give rise to secondary gamma dose rates. Since trends in the secondary gamma dose rates are linked to neutron source terms, the trends are similar. Therefore, this calculation was not performed.

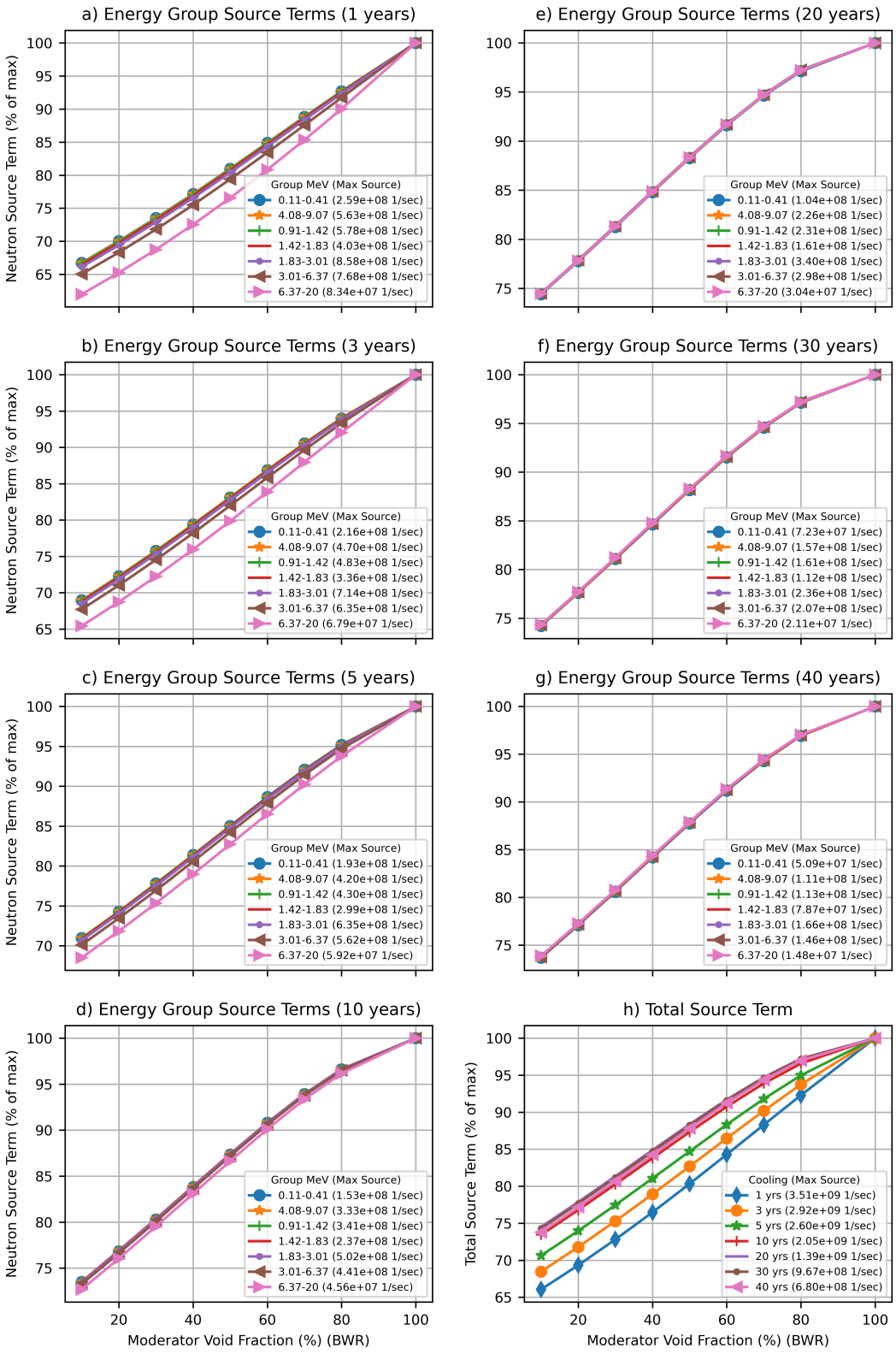

Figure 53. Neutron source terms as a function of moderator void fraction (BWR).

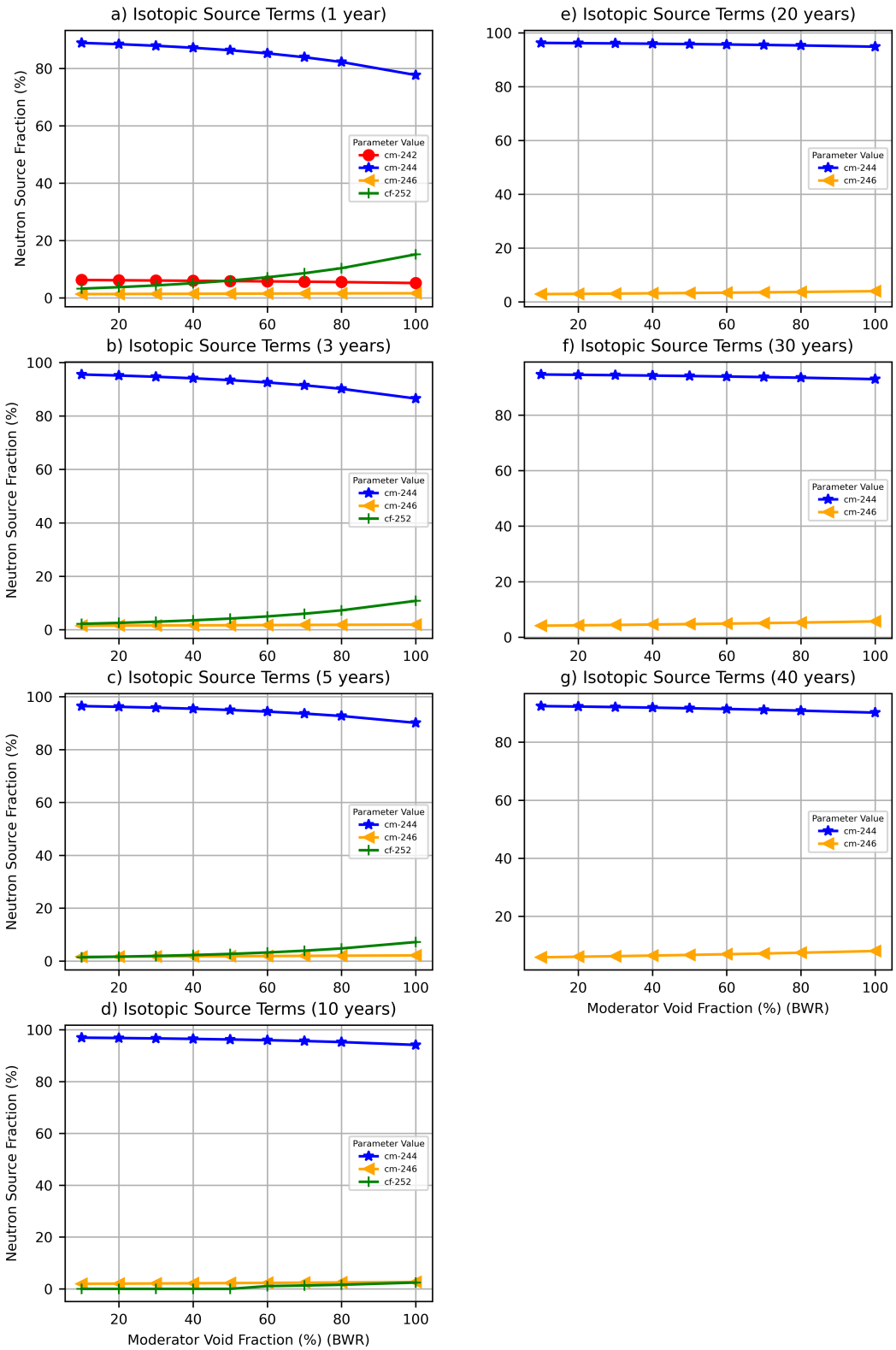

Figure 54. Radionuclide fractional contributions to neutron source as a function of moderator void fraction (BWR).

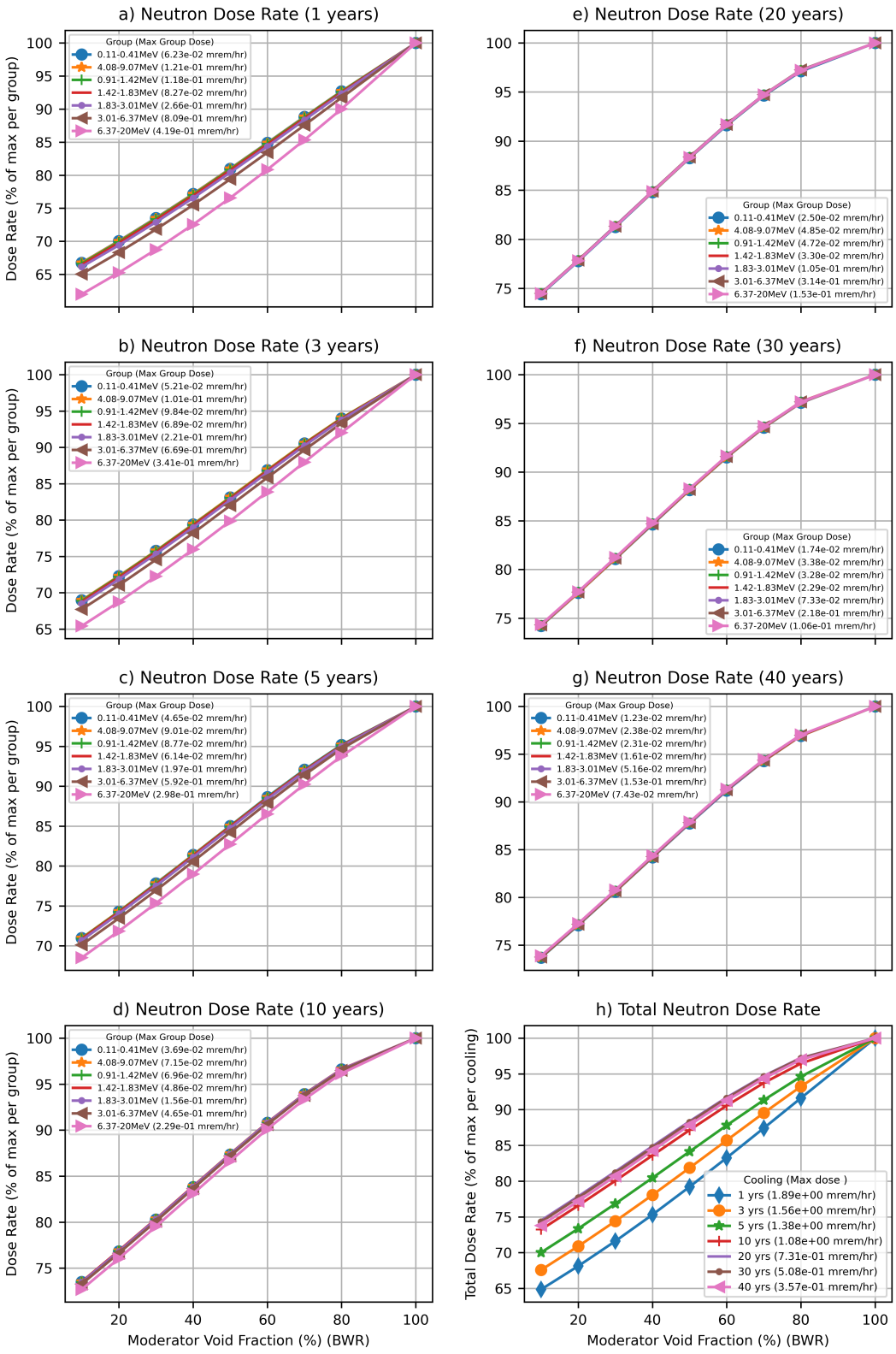

Figure 55. Neutron dose rate as a function of moderator void fraction (BWR).

5. FAR-FIELD DOSE RATE STUDY

Dose rates at the far-field consist of contributions from direct radiation and skyshine. The dose rates as a function of distance from a single vertical concrete storage cask were calculated using the hypothetical storage cask model described in Section 3.4. The results show that the cask surface total dose rate is dominated by the gamma radiation. The B&W 15×15 fuel assembly type was used in the cask model. Although dose rate values may depend on a particular cask design, the dose rate trends and conclusions from this study are considered applicable to all vertical concrete storage casks.

5.1 DOSE RATE VARIATION AS A FUNCTION OF DISTANCE FROM CASK

External cask dose rate was calculated as a function of distance up to 1,600 m from the cask. Varying parameters in these analyses were the following:

- Average fuel assembly burnup (45, 60, and 70 GWd/MTU). The initial fuel enrichments for these burnup values were 3.2, 4, and 5 %, respectively.
- Fuel cooling time (1, 5, and 40 years).
- Air density (1.2 kg/m^3 and 1.108 kg/m^3).

The amount of cobalt impurity assumed for the fuel hardware in the active fuel region (i.e., spacer grids), LEF, GP, and UEF were 15, 12.83, 4.95, and 15.63 grams respectively, based on an assumed 800 ppm cobalt impurity concentration in steel. The ^{60}Co activation sources were uniformly distributed within each region volume. The ORIGEN flux scaling factors for the LEF, GP, and UEF were 0.3, 0.3, and 0.15, respectively, which are the flux scaling factors from the PNL-6906-vol. 1 report [24], including their uncertainty. The hypothetical storage cask model used in skyshine calculations is described in Section 3.4. The geometry of the model and the locations of the mesh and region tallies are illustrated in Figure 3. The maximum dose rate value at one meter from the cask side surface was calculated using a mesh tally. Far-field dose rate was calculated in the air above the ground within thin concentric cylindrical shell regions. The width and height of a tally region were 1 m and 2 m, respectively.

Table 8 through Table 14 provide the estimated total dose rate and fractional contributions from primary gamma, ^{60}Co activation sources in assembly hardware, neutron, and secondary gamma radiation as a function of distance for an air density of 1.2 kg/m^3. The dose rate values are illustrated in the graphs in Figure 56(a) and Figure 57. The dose rate values for the one-year cooling time and the 70 GWd/MTU average fuel burnup value are presented in Table 8. These values for the five-year cooling time are presented in Table 9 (45 GWd/MTU average fuel burnup), Table 10 (60-GWd/MTU average fuel burnup), and Table 11 (70 GWd/MTU average fuel burnup). The values for the 40-year cooling time are presented in Table 12 (45 GWd/MTU average fuel burnup), Table 13 (60 GWd/MTU average fuel burnup), and Table 14 (70 GWd/MTU average fuel burnup). For the analyzed cask model and assembly average burnup range, the maximum dose rate values at 1 m from the cask surface were approximately 500, 110, and 5 mrem/h for the one-year, five-year, and 40-year cooling times, respectively. The external total dose rate decreased by approximately 3–10 orders of magnitude at 100–1,600 m, respectively, from the center of the cask. The statistical uncertainties of the gamma, neutron, secondary gamma, and total dose rate estimates were less than 0.5, 2.5, 6, and 5.5%, respectively. However, for clarity, the statistical uncertainty values of the dose rate estimates are not shown in tables and graphs. Fractional contributions of various radiation sources to the total dose rate are shown as a function of distance in Figure 56(b) and Figure 58.

The percentage contribution of primary gamma radiation produced by fuel assemblies with an average burnup of 70 GWd/MTU and one-year cooling time was between 82% to 89% of the total dose rate at all evaluated locations. Primary gamma radiation also dominated the total dose rates at locations up to 1,600 m from the cask center for the five-year cooling time and up to 500–700 m from the cask center for the 40-year cooling time. The contribution of the secondary gamma radiation to the total dose rate increased with increasing distance from the cask. This contribution significantly increased with increasing burnup and cooling time, as seen in Tables 12–14. Secondary gamma radiation dominates the total dose rate at distances beyond approximately 700 m from the cask loaded with fuel that has a 40-year cooling time. The secondary gamma source consists of gamma radiation from neutron capture reactions with nuclei in fuel, structural, and shielding materials. Secondary gamma radiation is more energetic (i.e., more penetrating) than primary gamma radiation [25]. This source of radiation is directly proportional to the neutron sources. The neutron and secondary gamma dose rates reported in this section also include the contributions from the neutron source produced by subcritical multiplication and the associated secondary gammas. Section 6.3 of this report provides discussions on how the neutron source produced by subcritical multiplication and the associated secondary gammas are accounted for in the shielding calculations.

Far-field dose rates also depend on air density and humidity [26]. The effects of these input parameters on dose rate increase with increasing distance. Therefore, careful consideration of local conditions (e.g., altitude) is necessary to produce reliable far-field dose rate estimates for specific storage facility locations. In this report, the dry air density at standard conditions (1.2 kg/m^3) and a 10% reduction in this value (i.e., 1.108 kg/m^3) were analyzed to illustrate the importance of air density for far-field dose rates. A reduction of 10% in the dry air density produced an increase in the total dose rate from ~4.5% at 100 m to ~100% (5-year cooling) and ~75% (40-year cooling) at 1,600 m from the cask center (see Figure 59).

Table 8. Total dose rate and fractional contributions by type of radiation from a single PWR storage cask as a function of distance: fuel assemblies with a 5.0% initial enrichment, average burnup of 70 GWd/MTU, and a 1-year cooling time; dry air density of 1.2 kg/m^3.

	Fractional contribution to total dose rate by type of radiation						
Distance (m)	**Primary gamma**	**^{60}Co in UEF, GP, and LEF**	**^{60}Co in spacer grids**	**Neutron**	**Secondary gamma**	**Total dose rate (mrem/h)**	**Relative error (%)**
1	0.82	0.11	0.06	0.004	0.004	5.09E+02	0.23
100	0.84	0.10	0.06	0.004	0.004	3.43E-01	0.19
150	0.84	0.09	0.06	0.005	0.005	1.20E-01	0.20
200	0.85	0.09	0.05	0.005	0.005	5.27E-02	0.21
300	0.85	0.09	0.05	0.005	0.006	1.41E-02	0.23
400	0.85	0.09	0.05	0.006	0.008	4.71E-03	0.25
500	0.86	0.08	0.05	0.006	0.009	1.79E-03	0.25
600	0.86	0.08	0.04	0.006	0.011	7.44E-04	0.27
700	0.87	0.07	0.04	0.006	0.014	3.27E-04	0.28
800	0.88	0.06	0.04	0.006	0.017	1.51E-04	0.29
900	0.88	0.06	0.04	0.006	0.021	7.25E-05	0.30
1,000	0.89	0.05	0.03	0.006	0.025	3.58E-05	0.30
1,100	0.89	0.05	0.03	0.006	0.030	1.81E-05	0.31
1,200	0.89	0.04	0.02	0.005	0.037	9.38E-06	0.32
1,300	0.89	0.04	0.02	0.005	0.045	4.96E-06	0.33
1,400	0.89	0.04	0.02	0.005	0.054	2.66E-06	0.36
1,500	0.89	0.03	0.01	0.005	0.065	1.46E-06	0.39
1,600	0.88	0.03	0.01	0.004	0.078	8.03E-07	0.38

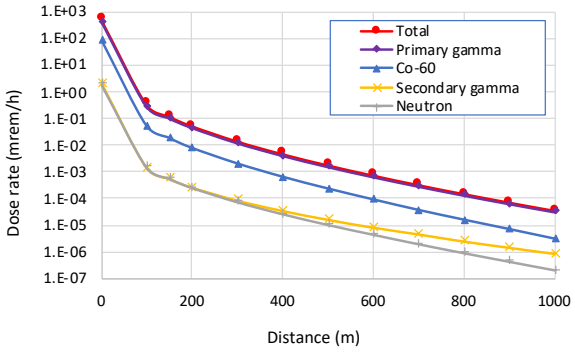

(a)

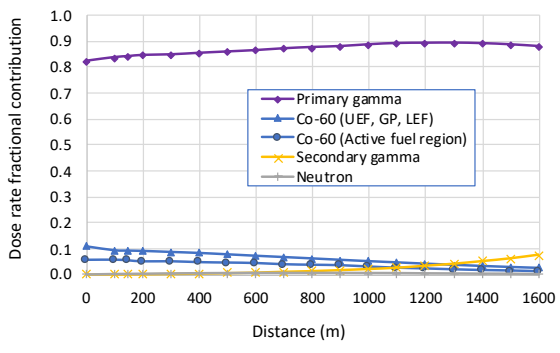

(b)

Figure 56. Dose rate versus distance (a) and fractional contributions of various radiation sources to the total dose rate as a function of distance (b) for fuel burnup of 70 GWd/MTU and cooling time of 1 year.

Table 9. Total dose rate and fractional contributions by type of radiation from a single PWR storage cask as a function of distance: fuel assemblies with a 3.2% initial enrichment, average burnup of 45 GWd/MTU, and a 5-year cooling time; dry air density of 1.2 kg/m^3.

	Fractional contribution to total dose rate by type of radiation						
Distance (m)	**Primary gamma**	**^{60}Co in UEF, GP, and LEF**	**^{60}Co in spacer grids**	**Neutron**	**Secondary gamma**	**Total dose rate (mrem/h)**	**Relative error (%)**
1	0.45	0.35	0.18	0.01	0.01	8.35E+01	0.22
100	0.47	0.32	0.19	0.01	0.01	5.31E-02	0.17
150	0.47	0.33	0.19	0.01	0.01	1.83E-02	0.19
200	0.46	0.33	0.19	0.01	0.01	7.91E-03	0.21
300	0.46	0.33	0.19	0.01	0.01	2.03E-03	0.20
400	0.46	0.32	0.19	0.01	0.02	6.49E-04	0.21
500	0.46	0.32	0.18	0.01	0.02	2.35E-04	0.22
600	0.46	0.32	0.18	0.01	0.03	9.26E-05	0.23
700	0.47	0.31	0.17	0.02	0.04	3.89E-05	0.25
800	0.47	0.30	0.16	0.02	0.05	1.70E-05	0.27
900	0.48	0.29	0.16	0.02	0.06	7.79E-06	0.28
1,000	0.48	0.27	0.15	0.02	0.08	3.69E-06	0.32
1,100	0.49	0.26	0.14	0.02	0.10	1.80E-06	0.38
1,200	0.49	0.24	0.13	0.02	0.13	9.06E-07	0.52
1,300	0.49	0.22	0.11	0.02	0.15	4.64E-07	0.58
1,400	0.49	0.20	0.10	0.02	0.19	2.44E-07	0.79
1,500	0.49	0.18	0.09	0.02	0.23	1.32E-07	1.10
1,600	0.47	0.16	0.08	0.01	0.28	7.40E-08	1.75

Table 10. Total dose rate and fractional contributions by type of radiation from a single PWR storage cask as a function of distance: fuel assemblies with a 4.0% initial enrichment, average burnup of 60 GWd/MTU, and a 5-year cooling time; dry air density of 1.2 kg/m^3.

	Fractional contribution to total dose rate by type of radiation						
Distance (m)	Primary gamma	^{60}Co in UEF, GP, and LEF	^{60}Co in spacer grids	Neutron	Secondary gamma	Total dose rate (mrem/h)	Relative error (%)
1	0.48	0.33	0.17	0.01	0.01	1.02E+02	0.22
100	0.49	0.30	0.18	0.01	0.01	6.52E-02	0.31
150	0.49	0.30	0.18	0.02	0.02	2.25E-02	0.34
200	0.49	0.30	0.18	0.02	0.02	9.71E-03	0.32
300	0.48	0.30	0.18	0.02	0.02	2.48E-03	0.29
400	0.48	0.30	0.17	0.02	0.03	7.88E-04	0.24
500	0.47	0.30	0.17	0.02	0.04	2.86E-04	0.22
600	0.47	0.29	0.16	0.03	0.05	1.13E-04	0.23
700	0.47	0.28	0.16	0.03	0.06	4.72E-05	0.25
800	0.47	0.27	0.15	0.03	0.08	2.09E-05	0.29
900	0.47	0.26	0.14	0.03	0.10	9.57E-06	0.35
1,000	0.47	0.25	0.13	0.03	0.12	4.55E-06	0.37
1,100	0.46	0.23	0.12	0.03	0.15	2.24E-06	0.44
1,200	0.45	0.21	0.11	0.03	0.19	1.14E-06	0.62
1,300	0.45	0.19	0.10	0.03	0.23	5.89E-07	0.58
1,400	0.43	0.17	0.09	0.03	0.28	3.18E-07	0.68
1,500	0.42	0.15	0.08	0.02	0.33	1.75E-07	0.84
1,600	0.39	0.13	0.07	0.02	0.39	9.94E-08	1.03

Table 11. Total dose rate and fractional contributions by type of radiation from a single PWR storage cask as a function of distance: fuel assemblies with a 5.0% initial enrichment, average burnup of 70 GWd/MTU, and a 5-year cooling time; dry air density of 1.2 kg/m^3.

	Fractional contribution to total dose rate by type of radiation						
Distance (m)	Primary gamma	^{60}Co in UEF, GP, and LEF	^{60}Co in spacer grids	Neutron	Secondary gamma	Total dose rate (mrem/h)	Relative error (%)
1	0.50	0.31	0.16	0.01	0.02	1.10E+02	0.23
100	0.52	0.28	0.16	0.02	0.02	6.97E-02	0.20
150	0.52	0.28	0.16	0.02	0.02	2.40E-02	0.20
200	0.51	0.28	0.17	0.02	0.02	1.04E-02	0.20
300	0.51	0.28	0.17	0.02	0.03	2.66E-03	0.20
400	0.50	0.28	0.16	0.02	0.03	8.47E-04	0.21
500	0.49	0.28	0.16	0.03	0.04	3.07E-04	0.22
600	0.48	0.27	0.16	0.03	0.05	1.21E-04	0.24
700	0.48	0.27	0.15	0.03	0.07	5.06E-05	0.27
800	0.47	0.26	0.14	0.03	0.09	2.24E-05	0.34
900	0.47	0.24	0.14	0.03	0.12	1.04E-05	0.39
1,000	0.46	0.23	0.13	0.03	0.15	4.96E-06	0.52
1,100	0.45	0.21	0.12	0.03	0.19	2.46E-06	0.72
1,200	0.44	0.19	0.11	0.03	0.23	1.26E-06	0.84
1,300	0.42	0.17	0.10	0.03	0.28	6.64E-07	0.91
1,400	0.40	0.16	0.09	0.03	0.33	3.59E-07	1.12
1,500	0.38	0.13	0.07	0.03	0.39	1.99E-07	1.33
1,600	0.35	0.11	0.06	0.03	0.45	1.15E-07	1.48

Table 12. Total dose rate and fractional contributions by type of radiation from a single PWR storage cask as a function of distance: fuel assemblies with a 3.2% initial enrichment, average burnup of 45 GWd/MTU, and a 40-year cooling time; dry air density of 1.2 kg/m^3.

	Fractional contribution to total dose rate by type of radiation						
Distance (m)	Primary gamma	^{60}Co in UEF, GP, and LEF	^{60}Co in spacer grids	Neutron	Secondary gamma	Total dose rate (mrem/h)	Relative error (%)
1	0.75	0.10	0.03	0.05	0.06	2.95E+00	0.64
100	0.75	0.09	0.03	0.07	0.06	1.92E-03	0.29
150	0.73	0.09	0.03	0.07	0.07	6.50E-04	0.31
200	0.72	0.09	0.03	0.08	0.08	2.75E-04	0.32
300	0.66	0.10	0.04	0.09	0.11	6.76E-05	0.34
400	0.60	0.10	0.05	0.11	0.15	2.08E-05	0.41
500	0.53	0.10	0.05	0.12	0.19	7.37E-06	0.51
600	0.46	0.10	0.05	0.13	0.25	2.87E-06	0.74
700	0.39	0.10	0.05	0.14	0.32	1.24E-06	1.14
800	0.33	0.09	0.05	0.14	0.39	5.68E-07	1.17
900	0.27	0.08	0.05	0.13	0.47	2.79E-07	1.63
1,000	0.21	0.07	0.04	0.12	0.55	1.45E-07	1.79
1,100	0.17	0.06	0.03	0.12	0.62	7.73E-08	1.96
1,200	0.13	0.05	0.03	0.10	0.69	4.40E-08	2.15
1,300	0.10	0.04	0.02	0.08	0.75	2.59E-08	2.53
1,400	0.08	0.03	0.02	0.07	0.80	1.62E-08	2.90
1,500	0.06	0.02	0.01	0.06	0.84	9.86E-09	2.63
1,600	0.05	0.02	0.01	0.05	0.88	6.29E-09	2.74

Table 13. Total dose rate and fractional contributions by type of radiation from a single PWR storage cask as a function of distance: fuel assemblies with a 4.0% initial enrichment, average burnup of 60 GWd/MTU, and a 40-year cooling time; dry air density of 1.2 kg/m^3.

	Fractional contribution to total dose rate by type of radiation						
Distance (m)	Primary gamma	^{60}Co in UEF, GP, and LEF	^{60}Co in spacer grids	Neutron	Secondary gamma	Total dose rate (mrem/h)	Relative error (%)
1	0.71	0.08	0.03	0.08	0.09	4.06E+00	0.28
100	0.69	0.07	0.05	0.10	0.10	2.69E-03	0.44
150	0.67	0.07	0.04	0.11	0.11	9.14E-04	0.30
200	0.65	0.07	0.05	0.11	0.12	3.90E-04	0.32
300	0.60	0.08	0.04	0.13	0.15	9.67E-05	0.35
400	0.53	0.08	0.05	0.15	0.19	3.06E-05	0.42
500	0.47	0.08	0.04	0.16	0.25	1.10E-05	0.64
600	0.40	0.07	0.04	0.18	0.31	4.46E-06	0.95
700	0.33	0.07	0.04	0.18	0.38	1.93E-06	0.90
800	0.27	0.06	0.03	0.18	0.46	9.21E-07	1.08
900	0.21	0.05	0.03	0.16	0.54	4.73E-07	1.78
1,000	0.17	0.05	0.03	0.15	0.62	2.50E-07	1.97
1,100	0.13	0.04	0.02	0.13	0.68	1.37E-07	2.13
1,200	0.10	0.03	0.02	0.12	0.74	8.03E-08	2.38
1,300	0.08	0.02	0.01	0.10	0.79	4.77E-08	3.06
1,400	0.06	0.02	0.01	0.08	0.83	3.03E-08	3.83
1,500	0.04	0.01	0.01	0.06	0.87	1.96E-08	4.80
1,600	0.03	0.01	0.01	0.05	0.91	1.26E-08	5.64

Table 14. Total dose rate and fractional contributions by type of radiation from a single PWR storage cask as a function of distance: fuel assemblies with a 5.0% initial enrichment, average burnup of 70 GWd/MTU, and a 40-year cooling time; dry air density of 1.2 kg/m^3.

	Fractional contribution to total dose rate by type of radiation						
Distance (m)	**Primary gamma**	**^{60}Co in UEF, GP, and LEF**	**^{60}Co in spacer grids**	**Neutron**	**Secondary gamma**	**Total dose rate (mrem/h)**	**Relative error (%)**
1	0.73	0.07	0.01	0.09	0.10	4.73E+00	0.29
100	0.69	0.06	0.04	0.11	0.10	3.13E-03	0.27
150	0.67	0.06	0.04	0.11	0.11	1.07E-03	0.28
200	0.65	0.06	0.04	0.12	0.12	4.55E-04	0.31
300	0.59	0.07	0.04	0.14	0.16	1.14E-04	0.36
400	0.53	0.07	0.04	0.16	0.21	3.61E-05	0.43
500	0.46	0.06	0.04	0.18	0.27	1.33E-05	0.59
600	0.38	0.06	0.04	0.19	0.33	5.42E-06	0.77
700	0.31	0.06	0.03	0.19	0.41	2.40E-06	0.98
800	0.25	0.05	0.03	0.18	0.49	1.15E-06	1.33
900	0.20	0.04	0.02	0.17	0.56	5.86E-07	1.55
1,000	0.15	0.04	0.02	0.15	0.64	3.18E-07	1.85
1,100	0.12	0.03	0.02	0.13	0.71	1.80E-07	2.19
1,200	0.09	0.02	0.01	0.11	0.76	1.05E-07	2.38
1,300	0.07	0.02	0.01	0.10	0.80	6.12E-08	1.96
1,400	0.05	0.01	0.01	0.08	0.85	3.89E-08	2.21
1,500	0.04	0.01	0.01	0.06	0.88	2.48E-08	2.20
1,600	0.03	0.01	0.00	0.05	0.91	1.61E-08	2.31

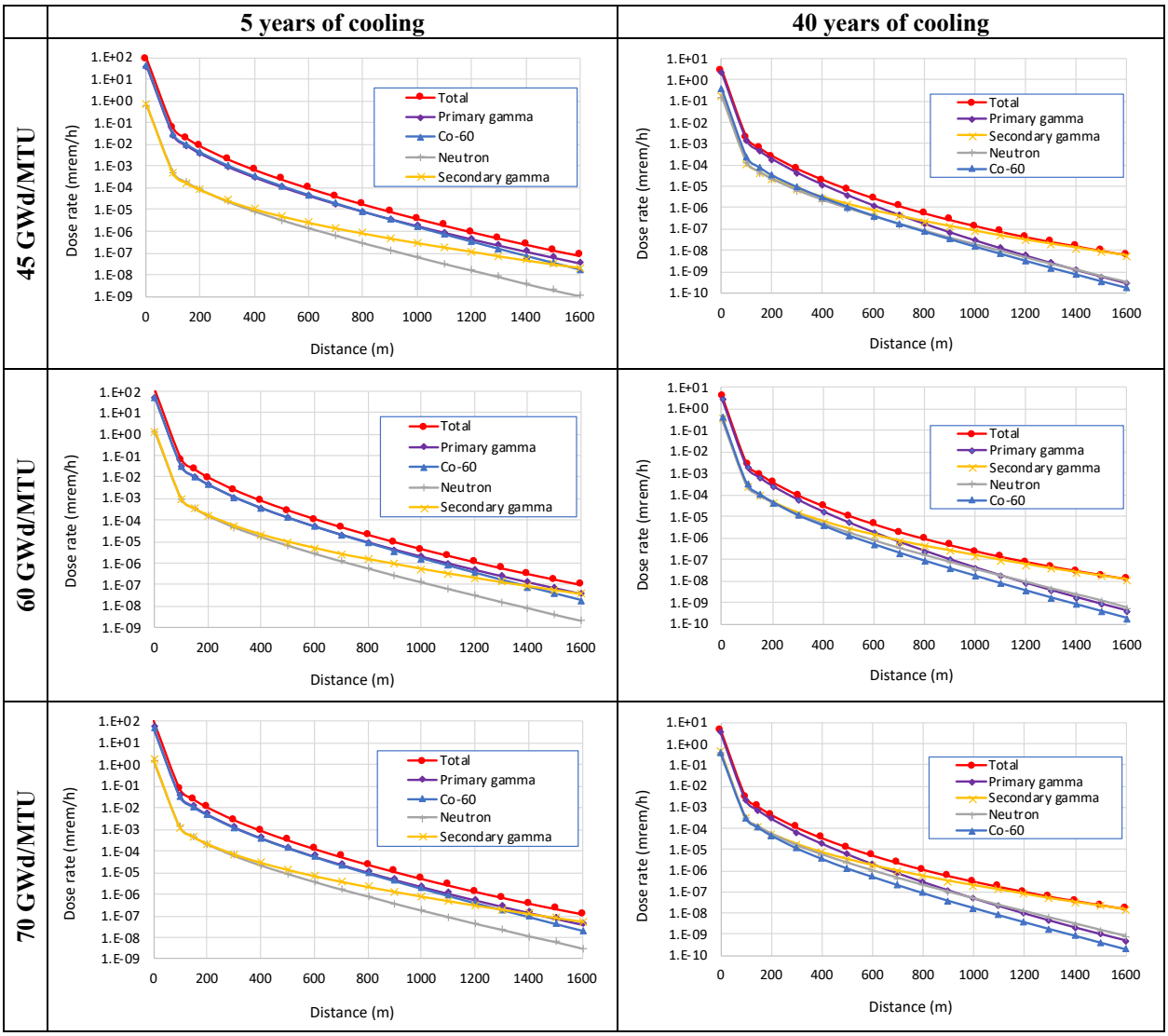

Figure 57. Total dose rate and components versus distance.

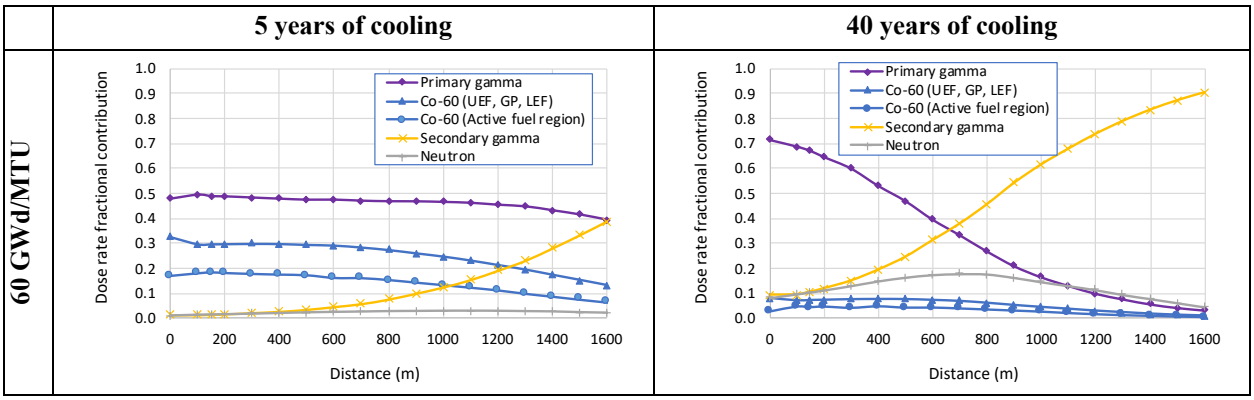

Figure 58. Fractional contributions of various radiation sources to the total dose rate as a function of distance for fuel assemblies with a 60-GWd/MTU average burnup value.

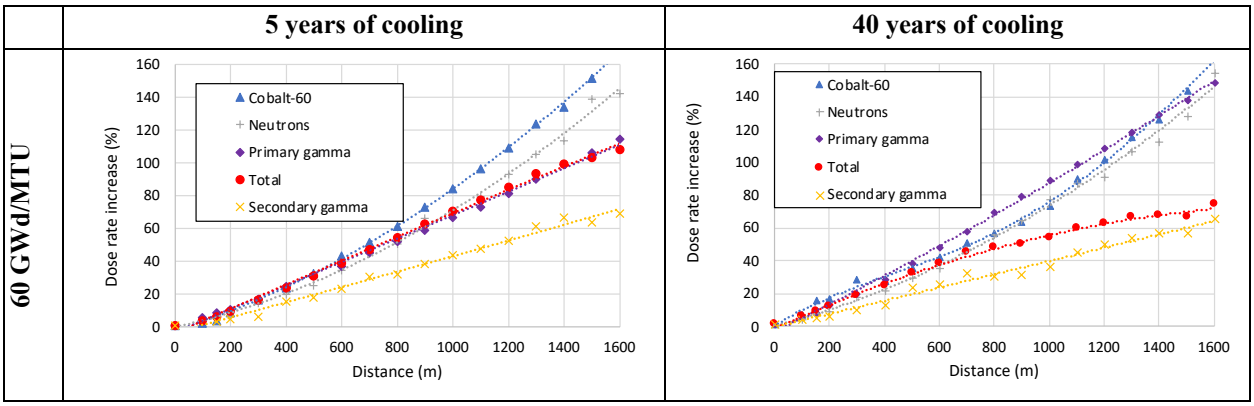

Figure 59. Dose rate increases as a function of distance with a 10% reduction of air density for fuel assemblies with a 60-GWd/MTU average burnup value.

5.2 FAR-FIELD DOSE RATES FROM CASKS WITH SIMILAR NEAR-FIELD DOSE RATE

A study was performed to assess whether cask loadings that produce the same near-field external dose rate values would also produce the same dose rate values at large distances from the cask. For this study, dose rate was calculated as a function of distance up to 1,600 m from the cask center for the storage cask model loaded with B&W 15 × 15 fuel assemblies. Two combinations of assembly average burnup, enrichment, and cooling time produced the same maximum dose rate values, within statistical uncertainty, at 1 m from the cask surface:

- 55 GWd/MTU, 3% ^{235}U, 20 years of cooling.
- 35 GWd/MTU, 3% ^{235}U, 15 years of cooling.

The ratio between the total dose rate values produced by the two fuel assemblies and the percentage contributions to the total dose rate by radiation type for each assembly are provided in Table 15. The two fuel assemblies produced the same dose rates up to 400 m from the cask center. However, beyond 400 m, the dose rates produced by the higher burnup fuel assembly were higher than the dose rates produced by the lower burnup fuel assembly. The percentage contributions of each type of radiation to the total dose rate differ between the two fuel assemblies as a function of distance from the cask.

In these calculations, fuel average burnup and cooling times are factored in. The fuel with higher burnup has a longer cooling time than the fuel with lower burnup. Although the contributions from the different radiation sources to the total dose rates differ between the two fuel assemblies, both fuel loadings produce the same (or similar) total dose rates at shorter distances (<400 m). At these distances the total dose rates are dominated by the direct radiation rather than scattering in air. As seen in Table 15, for distances beyond 400 meters the secondary gammas contribution increases. The secondary gamma radiation is from photon release due to neutron capture in shielding materials and surrounding air. The higher burnup fuel has higher neutron source term. Neutrons scatter to longer distances than gamma and as seen from the Table 15 their proportion in the total dose rate increases with distance. Subsequently, scattering of photons from neutron capture in the air contributes to increased secondary gammas generated at longer distances.

Table 15. Ratio between the dose rate values produced by the two assemblies and percentage contributions to total dose rate by radiation type for each assembly.

		Percentage contribution (%)							
		Assembly 1: 55 GWd/MTU, 3% ^{235}U, 20 years of cooling				Assembly 2: 35 GWd/MTU, 3% ^{235}U, 15 years of cooling			
Distance (m)	Dose rate ratio[a]	Primary gamma	^{60}Co	Neutron	Secondary gamma	Primary gamma	^{60}Co	Neutron	Secondary gamma
1	0.98 ± 0.03	40.19	49.63	4.79	5.39	32.48	65.19	1.09	1.24
100	0.99 ± 0.01	40.54	47.42	6.20	5.84	33.76	63.52	1.37	1.35
150	1.00 ± 0.01	39.51	47.62	6.58	6.28	32.97	64.07	1.48	1.48
200	1.00 ± 0.01	37.99	47.91	7.01	7.09	32.02	64.75	1.59	1.65
300	1.01 ± 0.01	35.07	48.18	7.88	8.87	30.12	66.00	1.80	2.08
400	1.03 ± 0.01	31.94	47.79	8.72	11.54	28.08	67.07	2.10	2.75
500	1.07 ± 0.01	28.37	46.89	9.74	15.00	26.07	67.92	2.42	3.59
600	1.12 ± 0.01	24.86	45.05	10.29	19.79	24.02	68.54	2.63	4.81
700	1.18 ± 0.03	21.50	42.53	10.73	25.24	22.16	68.41	2.92	6.50
800	1.25 ± 0.02	18.53	39.83	11.00	30.64	20.43	67.92	3.09	8.55
900	1.36 ± 0.03	15.61	35.93	10.66	37.80	18.69	66.58	3.32	11.42
1,000	1.49 ± 0.04	12.97	31.79	10.16	45.08	17.07	64.98	3.45	14.51
1,100	1.64 ± 0.06	10.69	27.38	9.55	52.38	15.57	61.65	3.53	19.25
1,200	1.79 ± 0.07	8.79	23.67	8.75	58.79	14.04	58.30	3.56	24.11
1,300	1.98 ± 0.08	7.08	19.63	7.74	65.55	12.31	53.10	3.56	31.04
1,400	2.16 ± 0.12	5.66	16.05	6.62	71.67	10.82	47.58	3.29	38.31
1,500	2.48 ± 0.15	4.34	12.55	5.40	77.71	9.43	42.87	3.10	44.60
1,600	2.62 ± 0.18	3.53	10.03	4.77	81.67	7.90	36.37	2.81	52.92

[a]Ratios of Assembly 1 total dose rate over Assembly 2 total dose rate.

6. EFFECTS OF VARIOUS INPUT PARAMETERS ON CASK EXTERNAL DOSE RATES

SNF cask systems are typically designed for the storage and transportation of a variety of fuel assembly and NFH types with a wide range of irradiation characteristics. Bounding input parameters are typically used in shielding analyses to assess expected bounding dose rates. Subsequently a range of SNF and NFH characteristics can be identified that results in dose rates within an acceptable range. This report provides radiation source term and dose rate analyses that help identify bounding input parameters with respect to external dose rates of storage and transportation casks.

6.1 ASSEMBLY TYPE

Shielding analyses are typically performed based on the initial uranium mass per fuel assembly, average fuel assembly burnup, a fuel assembly type with a higher initial uranium mass, and initial uranium enrichment. However, a heavier fuel assembly also provides greater self-shielding against gamma radiation than lighter fuel assemblies.

Several representative PWR and BWR fuel assemblies have been analyzed in this section with respect to their effects on dose rate at the radial surface and at 2 m from the radial surface of the hypothetical transportation package model under NCT (see Section 3.3). The evaluated PWR fuel assembly types are B&W 15 × 15, WE 17 × 17 low parasitic (LOPAR), WE 17 × 17 OFA, and Combustion Engineering (CE) 16 × 16; the evaluated BWR fuel assembly types are GE 7 × 7, GE 8 × 8, ANF 9 × 9, and GE 10 × 10. The physical characteristics of these fuel assemblies are summarized in ORNL/SPR-2021/2093 [10]. A pin-by-pin representation of the fuel region for these fuel assembly types, shown in Figure 60, was used in the hypothetical transportation package model presented in Section 3.3. The GE 10 × 10 fuel assembly was modeled with full-length rods and uniform axial enrichment. A comparison between the dose rates produced by a 10 × 10 full-length rod fuel assembly and a 10 × 10 partial-length rod fuel assembly is provided in Section 6.7.

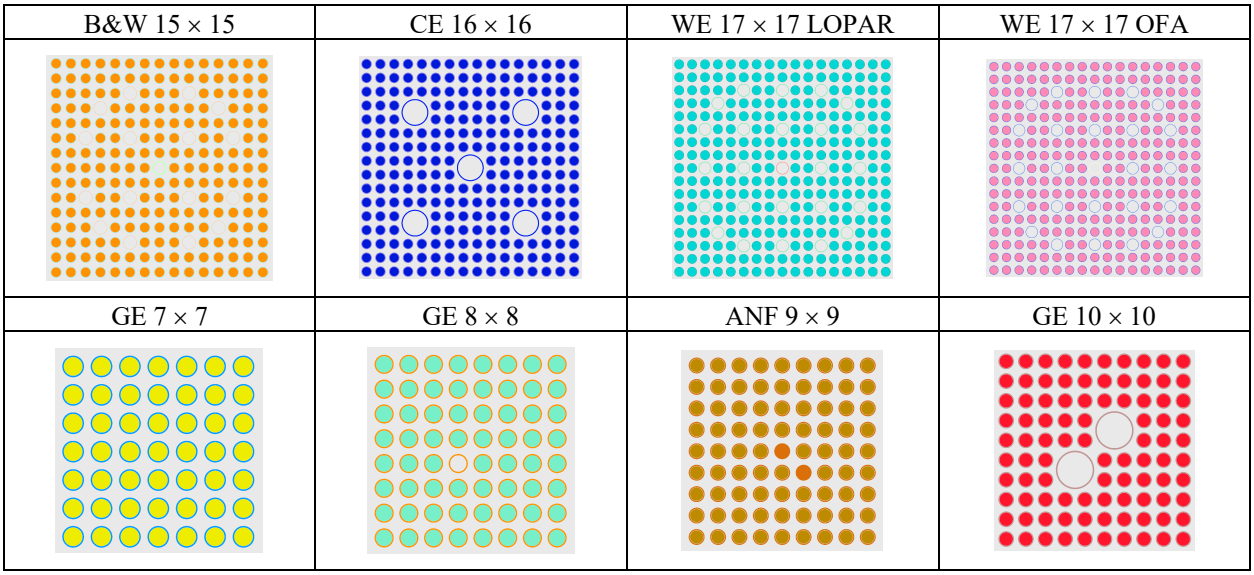

Figure 60. Horizontal cross-sectional views of the PWR and BWR fuel assembly designs used in the analyses.

Identical irradiation and decay conditions were used for each fuel assembly model: an average fuel assembly burnup of 50 GWd/MTU, a 4.2 wt % initial ^{235}U enrichment, and a 10-year decay time. The axial burnup profiles applied to the PWR and BWR fuel assemblies are presented in Table 1 and

Table 2, respectively. The highest initial uranium mass for these assembly types based on the GC-859 survey data, which are presented in Table 16, were used in the geometry models and radiation source term calculations. Only neutron and primary gamma radiation sources originating in the active fuel regions were included in these calculations. The radiation sources were calculated using ORIGAMI and pre-generated ORIGEN cross section libraries for the individual assembly types and bounding irradiation conditions such as those presented in Section 6.5. The assembly total neutron and primary gamma strengths are presented in Table 16. However, the axial burnup profiles used in these analyses did not consider the impact of natural or low enrichment uranium blankets. Although the BWR axial profile was selected from a database containing profiles from both blanketed and unblanketed fuel [12,27], the database does not indicate which profiles are for blanketed and unblanketed fuel. As discussed in Section 9, studies with burnup profiles for the blanketed fuel assemblies will be addressed in future studies pending availability of data in public domain.

The normalized values for the maximum neutron, secondary gamma, primary gamma, and total dose rate values produced by each fuel assembly type at the planar surface and at 2 m from the radial surface of transportation package model are presented in Table 17. Normalization was performed relative to the maximum values produced by the B&W 15 × 15 fuel assembly type for the PWR fuel and the maximum values produced by the GE 7 × 7 fuel assembly type for the BWR fuel because these fuel assemblies produced largest dose rate values among the evaluated PWR and BWR fuel assembly types, respectively. It is also noted that the WE 17 × 17 LOPAR fuel assembly produced approximately the same maximum radial dose rate values within the range of statistical uncertainty as the B&W 15 × 15 fuel assembly type. The evaluated BWR fuel types practically produced the same maximum radial dose rates within the statistical uncertainty.

Table 16. Assembly initial U mass and radiation source strengths.

Assembly code	Initial U mass (kg)	Neutron source strength (n/s)	Photon source strength (p/s)
B&W 15 × 15	491.72	4.88E + 08	4.69E + 15
CE 16 × 16	433.20	4.08E + 08	4.11E + 15
WE 17 × 17 LOPAR	469.20	4.65E + 08	4.47E + 15
WE 17 × 17 OFA	429.58	4.03E + 08	4.08E + 15
GE 7 × 7	197.60	2.89E + 08	1.81E + 15
GE 8 × 8	187.89	2.75E + 08	1.72E + 15
ANF 9 × 9	175.66	2.71E + 08	1.60E + 15
GE 10 × 10	183.37	2.69E + 08	1.67E + 15

Table 17. Normalized[a] maximum neutron, secondary gamma, primary gamma, and total dose rate values at package surface and at 2 m from the NCT transportation package model.

	Radial package surface				2 m from the radial package surface			
Assembly type	**Neutron**	**Secondary gamma**	**Primary gamma**	**Total**	**Neutron**	**Secondary gamma**	**Primary gamma**	**Total**
PWR								
B&W 15 × 15	1.00	1.00	1.00	1.00	1.00	1.00	1.00	1.00
CE 16 × 16	0.82 ± 0.07	0.87 ± 0.07	0.81 ± 0.03	0.85 ± 0.04	0.92 ± 0.06	0.91 ± 0.08	0.90 ± 0.02	0.90 ± 0.04
WE 17 × 17 LOPAR	0.94 ± 0.07	0.92 ± 0.07	1.02 ± 0.04	0.96 ± 0.04	0.96 ± 0.06	0.94 ± 0.08	1.06 ± 0.03	0.96 ± 0.04
WE 17 × 17 OFA	0.85 ± 0.08	0.82 ± 0.07	0.96 ± 0.04	0.87 ± 0.05	0.91 ± 0.07	0.85 ± 0.08	0.97 ± 0.03	0.88 ± 0.04
BWR								
GE 7 × 7	1.00	1.00	1.00	1.00	1.00	1.00	1.00	1.00
GE 8 × 8	0.97 ± 0.07	0.98 ± 0.06	0.99 ± 0.03	0.97 ± 0.05	0.99 ± 0.05	0.98 ± 0.08	0.99 ± 0.03	0.99 ± 0.05
ANF 9 × 9	0.96 ± 0.07	0.99 ± 0.06	0.89 ± 0.03	0.94 ± 0.05	0.96 ± 0.06	0.99 ± 0.08	0.89 ± 0.03	0.95 ± 0.05
GE 10×10	1.02 ± 0.08	1.05 ± 0.07	0.98 ± 0.03	0.98 ± 0.04	1.01 ± 0.04	1.00 ± 0.06	0.94 ± 0.02	0.98 ± 0.04

[a]Maximum dose rate ratio ± 2 sigma uncertainty values. Reference PWR fuel type: B&W 15 × 15. Reference BWR fuel type: GE 7 × 7.

6.2 PIN-BY-PIN MODEL VERSUS HOMOGENEOUS MATERIAL MODEL

The effect on the external cask dose rate of the active fuel zone, represented in the cask model as either pin-by-pin or homogeneous material, was evaluated at one meter from the hypothetical storage cask model (see Section 3.4, Figure 3(a)). This evaluation was performed for the B&W 15 × 15 fuel assembly with a 4% initial enrichment, a 60 GWd/MTU assembly average burnup value, and a five-year cooling time, assuming the fresh fuel composition. The mass density of a UO_2 pellet was 10.8159 g/cm^3 and the mass density of the homogeneous material was of 3.9831 g/cm^3. The uniform fuel zone model produced a higher dose rate than the pin-by-pin model for the gamma radiation originating in the active fuel zone. The ratio of the dose rate from the pin-by-pin model to the dose rate from the homogeneous material model is provided in Table 18 as a function of radiation type. The gamma dose rate produced by the pin-by-pin model was approximately 5% lower than that produced by the homogeneous material model. The total dose rate contributions from neutrons and secondary gamma were practically identical for the two models. Therefore, the homogeneous material model is slightly conservative in comparison with the pin-by-pin model.

Table 18. Ratio of dose rate from the pin-by-pin model to dose rate from the homogeneous material model.

Gamma source in the active fuel region [a,b]	^{60}Co in UEF, GP, and LEF [a]	Neutron [a]	Secondary gamma [a]	Total [a]
0.942 ± 0.007	1.002 ± 0.009	0.986 ± 0.023	1.009 ± 0.029	0.952 ± 0.040

[a]Dose rate ratio ± 2σ.
[b]Contribution from the ^{60}Co in spacer grids is included as primary gamma source.

6.3 NEUTRON SOURCES FROM SUBCRITICAL MULTIPLICATION

In a cask, the neutrons emitted from the spent fuel will further react with the fissile nuclides, ^{235}U, ^{239}Pu, and ^{241}Pu, in the spent fuel to produce neutrons by fission reactions. This neutron source is often called subcritical multiplication neutron source. Because this neutron source is not included in the neutron source term determined with depletion and decay codes, it must be considered as a separate source in dose

rate calculations. This additional neutron source can be treated implicitly or explicitly in dose rate calculations with shielding codes that track the neutrons produced by fission reactions. Another approach to account for this neutron source is to update the neutron source calculated by the depletion code with the $S^* = S/(1-k_{eff})$ formula [2], where S is the neutron source calculated by depletion analysis, S* is the neutron source that includes subcritical multiplication, and k_{eff} is the effective neutron multiplication factor which is determined by a criticality calculation for the specific cask design and fuel loading pattern.

Contributions made by the neutrons from subcritical multiplication to external cask neutron and associated secondary dose rates were determined with MAVRIC Monte Carlo radiation transport calculations. The default behavior for MAVRIC is to create neutrons from fission events and create secondary gammas from neutron collisions. To turn off the creation of fission neutrons in all multiplying media (for example, when the source already includes them), the keyword "fissionMult=0" was specified in the input file. The calculation results presented in this section are based on the following input/output parameters and assumptions:

- B&W 15 × 15 fuel assembly type.
- Homogeneous material (mass density of 3.9831 g/cm^3) and pin-by-pin fuel (UO_2 mass density of 10.8159 g/cm^3) assembly models.
- Fresh fuel compositions.
- Characteristics of the fuel assembly: an initial uranium mass of 491.72 kg, a 60 GWd/MTU average fuel assembly burnup value; a 4% initial enrichment; and a 5-year cooling time; the axial burnup profile provided in Table 1.
- Dose rate at 1 m from the side surface of the storage cask model as described in Section 3.4.

The results of the MAVRIC calculations for the storage cask model are summarized in Table 19. The percentage contribution of the neutron source from subcritical multiplication to the total dose rate was approximately 37% and the percentage contribution of the secondary gamma radiation associated with the neutrons from subcritical multiplication was approximately 60%.

Table 19. Neutron multiplication effects on neutron and secondary gamma dose rate for fresh fuel composition.

	Dose rate increase factor [a]		
Active fuel material	**Neutron**	**Secondary gamma**	**Neutron and secondary gamma**
Homogeneous	1.36 ± 0.02	1.59 ± 0.03	1.49 ± 0.05
Pin-by-pin	1.38 ± 0.02	1.60 ± 0.03	1.51 ± 0.05

[a]Ratio between dose rate with subcritical multiplication contributions and dose rate without subcritical multiplication contributions.

The evaluated subcritical multiplication factor, $1/(1-k_{eff})$, for the analyzed model is approximately 1.67, i.e., an increase of the total neutron source by 67% when including neutrons from subcritical multiplication. It is important to point out that the k_{eff} values used in determining the subcritical multiplication neutron sources were determined based on dry internal of the casks and this modeling approach is consistent with the actual spent fuel dry cask storage system designs and storage conditions.

6.4 FUEL COMPOSITION (FRESH VERSUS IRRADIATED FUEL) SPECIFICATIONS

Typical shielding calculations for SNF use fresh fuel compositions to reduce the complexity of models considering irradiated fuel compositions. The basis for this approach is that the fresh fuel composition is either conservative or produces very similar external cask dose rates as the irradiated fuel composition. The validity of this assumption was evaluated in this report by comparing external storage cask dose rates produced by fuel assembly irradiated and fresh fuel compositions. The irradiated fuel composition includes all actinides and 20 of the most abundant fission product nuclides in the irradiated fuel composition. The mass of the remainder fission products was added to the ^{137}Cs to keep the material weight the same. The calculation results presented in this section are based on the following input/output parameters:

- B&W 15 × 15 fuel assembly type.
- Fuel assembly characteristics are an initial uranium mass of 491.72 kg, a 60 GWd/MTU average fuel assembly burnup value; a 4% initial enrichment; and a five-year cooling time; the axial burnup profile provided in Table 1.
- Same mass density for both fresh and irradiated fuel compositions.
- Dose rate at 1 m from the surface of the generic storage cask model described in Section 3.4.
- Four different calculations were performed for the following input model specifications:
    - Fresh fuel composition and homogeneous material (mass density of 3.9831 g/cm^3).
    - Fresh fuel composition and pin-by-pin fuel (UO_2 mass density of 10.8159 g/cm^3).
    - Irradiated fuel composition and homogeneous fuel material (mass density of 3.9831 g/cm^3). The irradiated fuel compositions vary axially based on the fuel assembly characteristics described above.
    - Irradiated fuel composition and pin-by-pin fuel (UO_2 mass density of 10.8159 g/cm^3). The irradiated fuel compositions vary axially based on the fuel assembly characteristics described above.

Table 20 presents the calculated ratio of dose rate produced by an irradiated fuel composition to dose rate produced by a fresh fuel composition as a function of fuel zone model (i.e., homogeneous material or pin-by-pin fuel model) and radiation type. This study determined that the net effects of the two different fuel composition specifications on the total dose rate are within statistical uncertainty for both the pin-by-pin and homogeneous material fuel assembly representations. However, further studies may be necessary for higher average fuel assembly burnup and to assess the validity of the results of this analysis to other cask designs or transportation packages.

Fresh and irradiated fuel compositions have opposite effects on the dose rates produced by primary gamma and neutron sources. The irradiated fuel composition produced a slightly higher dose rate (i.e., by ~2%, including the statistical uncertainty) than the fresh fuel composition for the primary gamma radiation. This result may be explained by a slightly lower average atomic number of the irradiated fuel composition compared to the fresh fuel composition. It also produced lower dose rate values for neutrons (i.e., by ~15%) and secondary gamma radiation (i.e., by ~17%) than the fresh fuel composition. This result may be explained by a lower subcritical multiplication neutron source and slightly higher neutron

absorption in irradiated fuel compared to fresh fuel. Irradiated fuel produces a lower k_{eff} value (i.e., lower subcritical multiplication factor) than fresh fuel composition because SNF contains a lower fissile amount than fresh fuel. Therefore, the amount of subcritical multiplication neutrons is higher if a fresh fuel composition is specified in the dry cask model compared with irradiated fuel compositions. Similar effects are observed for the secondary gamma dose rate, which is correlated with the neutron source.

Table 20. Ratio of dose rate using irradiated fuel composition to dose rate using fresh fuel composition in the assembly material: average fuel assembly burnup of 60 GWd/MTU, cooling time of 5 years.

	Homogeneous fuel material	Pin-by-pin fuel model
Radiation type	**Dose rate ratio[a]**	
Primary gamma	1.016 ± 0.003	1.022 ± 0.003
^{60}Co	0.996 ± 0.010	1.000 ± 0.003
Neutron	0.844 ± 0.008	0.873 ± 0.010
Secondary gamma	0.816 ± 0.012	0.838 ± 0.011
Total	1.010 ± 0.021	1.009 ± 0.018

[a]Ratio of dose rate produced by irradiated fuel composition to dose rate produced by fresh fuel composition.

6.5 EFFECTS OF PWR BURNABLE POISON RODS AND BWR CONTROL BLADES ON FUEL ASSEMBLY RADIATION SOURCES

This section analyzes the effects of BPRs for PWR fuel and control blades for BWR fuel on fuel assembly radiation sources. These components, which contain neutron absorber, are not an integral part of the fuel assembly, but may be used during operation to enhance neutron absorption. Radiation source terms for PWR fuel assemblies exposed to BPRs and BWR fuel assemblies exposed to control blades were evaluated and compared to the radiation source terms of fuel assemblies with no exposure. However, this study does not include the effect of axial power shaping rods because the complexity of their irradiation histories. The evaluated PWR and BWR fuel assemblies were the WE 17 × 17 (469.20 kg U) and GE 10 × 10 (183.37 kg U) fuel assemblies with average assembly burnup values of 10, 20, 30, 40, 50, and 60 GWd/MTU.

Source terms for a WE 17 × 17 assembly were determined for two different irradiation scenarios:

1) BPRs fully inserted into the assembly guide tubes throughout irradiation history.
2) No burnable absorber present.

Source terms for a GE 10 × 10 assembly were determined for two different irradiation scenarios:

1) The control blade fully inserted throughout irradiation history.
2) No control blade next to the fuel assembly during irradiation.

ORIGEN cross section libraries were generated for each of these scenarios using the deletion parameters provided in Table 21. The ORIGEN cross section libraries were generated with SCALE/TRITON [1]. These cross-section libraries were then used in ORIGAMI calculations to generate radiation source terms for the two fuel assemblies as a function of average assembly burnup.

Table 21. Depletion modeling parameters for ORIGEN cross section libraries.

Parameter/reactor type	WE 17 × 17	WE 17 × 17	GE 10 × 10	GE 10 × 10
Fuel rod mixture	UO_2	UO_2	UO_2	UO_2
Fuel density (g/cm^3)	10.741	10.741	10.741	10.741
Specific power (MW/MTU)	30	30	25	25
Fuel temperature (K)	1,157	1,157	1,200	1,200
Moderator temperature (K)	598.2	598.2	560.7	560.7
Moderator density (g/cm^3)	0.6668	0.6668	0.3	0.3
Soluble boron concentration (ppm)	1,000	1,000	N/A	N/A
Burnable absorber exposure	Pyrex rods fully inserted throughout irradiation time	None	Full-length (B_4C) control blade insertion throughout irradiation time	None. Bypass water density of 0.738 g/cm^3
Type of absorber	SiO_2-B_2O_3	–	B_4C	–
B_4C wt %	12.5	–	70	–

The neutron spectra of the WE 17 × 17 and GE 10 × 10 fuel assemblies with and without exposure to the neutron absorber or a control blade are illustrated in Figure 61 (a) and (b), respectively. The graphs in the figure show the normalized neutron flux per unit lethargy [28] as a function of neutron energy. The figure shows significant differences for the neutron spectra of a GE 10 × 10 fuel assembly in the thermal energy range. The fuel assembly fully exposed to a control blade has a harder spectrum than does the fuel assembly with no absorber exposure.

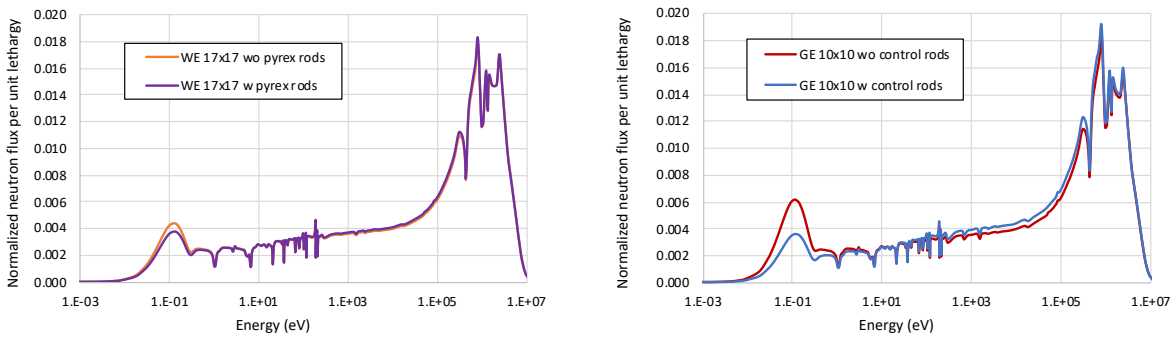

(a) (b)

Figure 61. Normalized neutron flux per unit lethargy for the WE 17 × 17 (a) and GE 10 × 10 (b) fuel assemblies (45 GWd/MTU).

The calculated gamma and neutron source strengths of the WE 17 × 17 and GE 10 × 10 fuel assemblies are presented in Table 22 and Table 23, respectively, as a function of fuel assembly average burnup.

The neutron source strength of a fuel assembly exposed to burnable absorber or control blades during irradiation was significantly higher than that of a fuel assembly without those inserts. The difference is much higher for the GE 10 × 10 fuel assembly than that for the WE 17 × 17 fuel assembly. However, the difference between assembly neutron source strengths with and without burnable absorber or control blade exposures significantly decreased with increasing fuel assembly average burnup and cooling time. For example, from a five-year cooling time to a forty-year cooling time, the relative difference decreases from ~23% to 4% for the WE 17 × 17 assembly over the average assembly burnup of 10 GWd/MTU to

60 GWd/MTU. This relative difference varies from ~70% to 20% in the case of the GE 10 × 10 fuel assembly over the average burnup range of 10 GWd/MTU to 60 GWd/MTU.

For the five-year cooling time, the gamma source strengths were slightly higher for the WE 17 × 17 (i.e., by ~1%) and the GE 10 × 10 (i.e., by ~3%) fuel assemblies with exposure to burnable absorber or control blades compared to no absorber exposure. No significant difference was observed for the gamma source strength at a 40-year cooling time. Overall, burnable absorber exposure had little effect on primary gamma radiation source terms.

Table 22. WE 17 × 17 fuel assembly radiation sources of full and no exposure to burnable absorber during irradiation.

		Primary gamma source strength (s^{-1})					
		5-year cooling time			**40-year cooling time**		
Assembly burnup (GWd/MTU)	**Enrichment (%)**	**Pyrex rods present**	**Pyrex rods absent**	**Relative difference [a] (%)**	**Pyrex rods present**	**Pyrex rods absent**	**Relative difference [a] (%)**
10	2.0	1.51E + 15	1.50E + 15	0.80	3.99E + 14	4.01E + 14	-0.56
20	2.5	3.06E + 15	3.04E + 15	0.63	7.79E + 14	7.82E + 14	-0.37
30	3.0	4.61E + 15	4.59E + 15	0.58	1.15E + 15	1.15E + 15	-0.24
40	3.5	6.14E + 15	6.11E + 15	0.57	1.50E + 15	1.50E + 15	-0.14
50	4.0	7.63E + 15	7.59E + 15	0.58	1.85E + 15	1.85E + 15	-0.07
60	4.5	9.08E + 15	9.03E + 15	0.58	2.19E + 15	2.19E + 15	-0.01
		Neutron source strength (s^{-1})					
		5-year cooling time			**40-year cooling time**		
Assembly burnup (GWd/MTU)	**Enrichment (%)**	**Pyrex rods present**	**Pyrex rods absent**	**Relative difference [a] (%)**	**Pyrex rods present**	**Pyrex rods absent**	**Relative difference [a] (%)**
10	2.0	3.01E + 06	2.44E + 06	23.23	1.78E + 06	1.54E + 06	15.48
20	2.5	3.32E + 07	2.91E + 07	14.32	1.10E + 07	9.75E + 06	12.80
30	3.0	1.27E + 08	1.16E + 08	9.46	3.73E + 07	3.41E + 07	9.19
40	3.5	3.04E + 08	2.85E + 08	6.85	8.60E + 07	8.05E + 07	6.83
50	4.0	5.67E + 08	5.39E + 08	5.11	1.59E + 08	1.51E + 08	5.15
60	4.5	9.10E + 08	8.77E + 08	3.84	2.54E + 08	2.45E + 08	1.93

[a]Relative percentage change between neutron strength values.

Table 23. GE 10 × 10 fuel assembly radiation sources of full and no exposure to a control rod during irradiation.

		Primary gamma source strength (s^{-1})					
		5-year cooling time			40-year cooling time		
Assembly burnup (GWd/MTU)	Enrichment (%)	Control rods present	Control rods absent	Relative difference [a] (%)	Control rods present	Control rods absent	Relative difference [a] (%)
10	2.0	5.86E + 14	5.72E + 14	2.29	1.54E + 14	1.57E + 14	-1.94
20	2.5	1.18E + 15	1.15E + 15	3.08	3.01E + 14	3.04E + 14	-0.96
30	3.0	1.77E + 15	1.71E + 15	3.30	4.45E + 14	4.45E + 14	-0.12
40	3.5	2.34E + 15	2.29E + 15	2.32	5.81E + 14	5.81E + 14	0.01
50	4.0	2.89E + 15	2.80E + 15	3.21	7.14E + 14	7.13E + 14	0.13
60	4.5	3.41E + 15	3.31E + 15	3.03	8.38E + 14	8.40E + 14	-0.24
		Neutron source strength (s^{-1})					
		5-year cooling time			40-year cooling time		
Assembly burnup (GWd/MTU)	Enrichment (%)	Control rods present	Control rods absent	Relative difference [a] (%)	Control rods present	Control rods absent	Relative difference [a] (%)
10	2.0	1.78E + 06	1.05E + 06	69.93	8.67E + 05	6.17E + 05	40.64
20	2.5	1.87E + 07	1.17E + 07	59.44	5.11E + 06	3.86E + 06	32.47
30	3.0	6.58E + 07	4.56E + 07	44.09	1.74E + 07	1.33E + 07	30.25
40	3.5	1.47E + 08	1.10E + 08	33.10	3.94E + 07	3.12E + 07	26.32
50	4.0	2.60E + 08	2.08E + 08	25.08	7.20E + 07	5.82E + 07	23.65
60	4.5	4.01E + 08	3.37E + 08	19.03	1.12E + 08	9.41E + 07	19.50

[a]Relative percentage change between neutron strength values.

Fuel assembly spacer grids and hardware materials may contain cobalt impurity. The cobalt impurity activation was simulated for one gram of cobalt-59 uniformly distributed within the active fuel region. The activated cobalt source in fuel hardware can be determined by multiplying the activity of one gram of cobalt irradiated in the active fuel region by the actual amount of cobalt impurity in the hardware and a flux scaling factor. The calculated ^{60}Co activities at five years after irradiation are provided in Table 24 as a function of fuel assembly average burnup for the WE 17 × 17 and GE 10 × 10 fuel assemblies. The differences in ^{60}Co activity were relatively small (i.e., <1%) in the case of the WE 17 × 17 fuel assembly, but they were important for the BWR fuel assembly. The ^{60}Co activity for a GE 10 × 10 fuel assembly not exposed to a control blade is much higher (e.g., by 75% at 40 GWd/MTU) than that of a GE 10 × 10 fuel assembly with exposure because of differences in the neutron flux and energy spectrum between the two irradiation scenarios (see Figure 61).

This result indicates that fuel assembly exposure to inserts yields conservative neutron source terms and non-conservative ^{60}Co activation sources, primarily for the BWR assemblies. However, the effects decrease with increasing fuel assembly average burnup and cooling time. Overall, fuel assembly exposure to inserts has little effect on primary gamma radiation source terms.

Table 24. ^{60}Co activities for assembly with full and without exposure to inserts [a] during irradiation.

		WE 17 × 17			GE 10 × 10		
		^{60}Co activity [b] (Ci)					
Assembly Burnup (GWd/MTU)	Enrichment (%)	Pyrex rods present	Pyrex rods absent	Relative difference [c] (%)	Control blade present	Control blade absent	Relative difference [c] (%)
10	2.0	26.90	26.88	0.08	15.36	29.35	-91.12
20	2.5	44.07	44.22	-0.34	26.07	48.04	-84.25
30	3.0	56.92	57.13	-0.38	34.69	62.06	-78.90
40	3.5	66.95	67.23	-0.42	41.75	72.91	-74.66
50	4.0	74.97	75.35	-0.51	47.59	81.58	-71.44
60	4.5	81.48	81.95	-0.58	52.43	88.56	-68.90

[a]Burnable poison rods for PWR fuel and control blade for BWR fuel.
[b]1 g of cobalt per fuel assembly.
[c]Relative percentage change between neutron strength values.

6.6 IRRADIATED STEEL REPLACEMENT RODS[†]

In the United States, limited substitutions of Zr alloy or solid stainless-steel filler rods for fuel rods are allowed per Generic Letter 90-02 and its Supplement 1 guidance [29]. The 2013 GC-859 survey data reported that approximately 850 fuel assemblies contained replacement rods [10]. A discharged fuel assembly is not expected to contain more than 10 replacement rods [10]. Depending on the actual number of replacement stainless-steel rods within a fuel assembly, ^{60}Co and other activation products in irradiated steel may be significant contributors to external cask dose rates. Among these activation products, ^{60}Co contributes more than 90% to dose rate produced by activation products in irradiated steel from approximately 30 days to 75 years after discharge [30]. Other steel activation products are primarily important to shielding at cooling times less than 30 days.

The effects of ^{60}Co in irradiated steel replacement rods on the external dose rate of the storage cask model presented in Section 3.4 were evaluated in this report by comparing the external cask dose rates produced by reconstituted fuel assemblies (i.e., fuel assemblies that contain irradiated steel rods) with the external cask dose rates produced by regular fuel assemblies (i.e., fuel assemblies that do not contain irradiated steel rods). Contributions from activation sources in assembly hardware were not modeled in the calculations because these contributions would be approximately identical for both reconstituted and regular fuel assemblies. Therefore, the radiation source of a regular fuel assembly consists of the primary gamma radiation from the active fuel region, whereas the radiation source of a reconstituted fuel assembly consists of the primary gamma radiation from the fuel rods and activation sources from the irradiated steel rods. These effects were evaluated for selected fuel cooling times from 2 to 75 years. The calculation results presented in this section are based on the following input/parameters:

- B&W 15 × 15 fuel assembly type.
- Pin-by-pin fuel assembly model.
- Fresh fuel compositions.
- Characteristics of the regular fuel assembly and fuel rods in assemblies containing replacement rods: an initial uranium mass of 491.72 kg, a 60-GWd/MTU average fuel assembly burnup value; a 4% initial enrichment; and cooling times from 2 to 75 years.
- 800 ppm cobalt impurity in steel [10] (i.e., ~2.15 g of cobalt per steel rod).
- Solid steel rods replacing fuel assembly rods in the reconstituted fuel assembly model.
- Replacement rods located at peripheral assembly locations for maximum impact on cask external dose rate.
- ^{60}Co source intensities based on activation rates from exposure to the neutron flux within a reconstituted fuel assembly with burnup values of 60 and 40 GWd/MTU, where the reconstituted fuel assembly discharge burnup is 60 GWd/MTU. The 60-GWD/MTU burnup value, which corresponds to the regular assembly average value, is a conservative assumption.
- Dose rate at 1 m from the surface of the storage cask model described in Section 3.

Four different canister models with different spatial distributions of the replacement rods were evaluated:

- Case 1: Each fuel assembly containing from 8 to 10 steel rods for a total of 366 steel rods per canister (i.e., 4.75% of the total rods in the canister), as illustrated in Figure 62(a).

[†]Erratum note: In the initial version of this report, there was an error in the cobalt impurity amount assumed for stainless steel replacement rods, which affected the dose rate values in Table 25. The cobalt mass per stainless steel replacement rod and the dose rate values in Table 25 have been corrected in this revision of the report.

- Case 2: Each fuel assembly containing from 3 to 4 steel rods for a total of 136 steel rods per canister (i.e., 1.8% of the total rods in the canister), as illustrated in Figure 62(b).
- Case 3: Only the innermost 9 fuel assemblies contain 8 to 10 steel rods for a total of 84 steel rods per canister (i.e., 1.1% of the total rods in the canister), as illustrated in Figure 62(c).
- Case 4: Only the innermost 9 fuel assemblies contain from 3 to 4 steel rods for a total of 32 steel rods per canister (i.e., 0.4% of the total rods in the canister), as illustrated in Figure 62(d).

The ratio between the gamma dose rate produced by reconstituted fuel assemblies and the gamma dose rate produced by regular fuel assemblies for the Case 1 and Case 2 configurations is shown as a function of cooling time in Table 25. For the analyzed cases, ^{60}Co in irradiated replacement steel rods was a major contributor to the total gamma dose rate up to approximately 30 years of cooling, and its contributions extended up 45 years of cooling. The decay of short-lived fission products in fuel reduces the gamma dose rate from regular fuel assemblies by approximately one order of magnitude within the cooling time interval 2 to 10 years. However, the ^{60}Co activity decreases by a factor of ~ 3 within this time interval. Therefore, the dose rate ratio significantly increases as the cooling time increases from 2 to 10 years. After 10 years of cooling, the dose rate ratio decreases. The reconstituted fuel assemblies produced a maximum gamma dose rate increase of 30% to 130% compared to the regular fuel assemblies, depending on the number of steel rods and reconstituted assembly average burnup. Therefore, detailed fuel assembly models should be used in safety analyses if fuel assemblies are known to contain irradiated steel replacement rods to accurately capture the dose rate from these assemblies. Cases 3 and 4 produced the same dose rate as the cask loaded with regular fuel assemblies because of the shielding provided by the regular assemblies. Therefore, reconstituted fuel assemblies can be loaded into the innermost basket locations to minimize the impact of the cobalt activation sources from irradiated steel replacement rods.

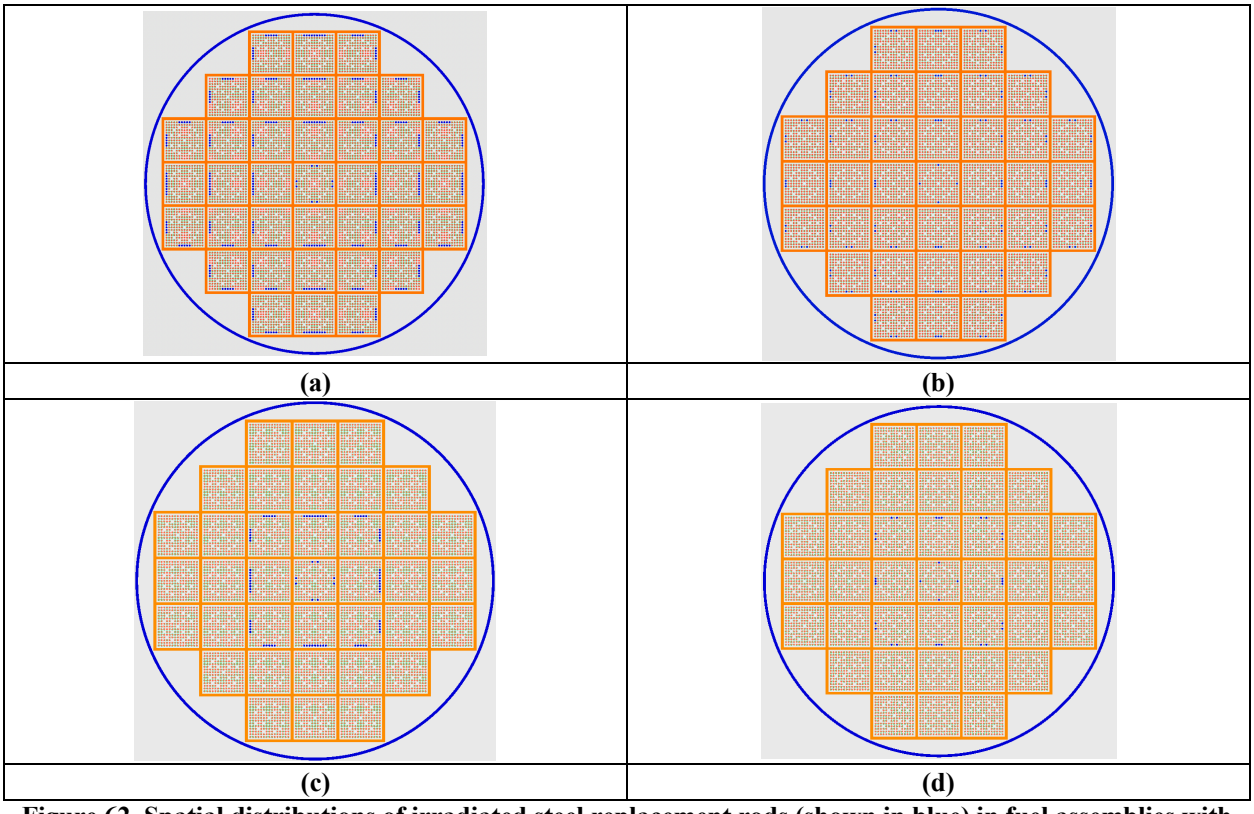

Figure 62. Spatial distributions of irradiated steel replacement rods (shown in blue) in fuel assemblies with (a) eight to 10 rods per assembly, (b) three to four rods per assembly, (c) eight to 10 rods in the nine innermost assemblies, (d) three to four rods in the nine innermost assemblies.

Table 25. Comparison of gamma dose rates produced by the Case 1 and Case 2 configurations with various irradiated steel replacement rods in a storage cask.

		Dose rate ratio [a]	
Average assembly burnup	**Cooling time (years)**	**Up to 10 replacement rods per assembly (Figure 62[a])**	**Up to four replacement rods per assembly (Figure 62[b])**
60 GWd/MTU	2	1.29 ± 0.01	1.10 ± 0.01
	5	1.89 ± 0.02	1.33 ± 0.01
	10	2.30 ± 0.02	1.48 ± 0.01
	20	1.90 ± 0.02	1.33 ± 0.01
	30	1.38 ± 0.01	1.14 ± 0.02
	45	0.99 ± 0.01	0.99 ± 0.01
	55	0.89 ± 0.02	0.96 ± 0.01
	65	0.86 ± 0.01	0.94 ± 0.01
	75	0.85 ± 0.01	0.95 ± 0.01
40 GWd/MTU	2	1.17 ± 0.01	1.06 ± 0.01
	5	1.61 ± 0.01	1.23 ± 0.01
	10	1.91 ± 0.02	1.33 ± 0.01
	20	1.62 ± 0.02	1.23 ± 0.01
	30	1.23 ± 0.01	1.09 ± 0.01
	45	0.95 ± 0.01	0.97 ± 0.01
	55	0.88 ± 0.02	0.95 ± 0.02
	65	0.85 ± 0.01	0.94 ± 0.01
	75	0.84 ± 0.01	0.94 ± 0.01

[a]Ratio of external cask gamma dose rates between reconstituted fuel and regular fuel assemblies.

6.7 BWR FUEL ASSEMBLIES WITH PARTIAL-LENGTH RODS

Modern BWR fuel assemblies contain both full-length and partial-length fuel rods. Calculations of radiation source terms for the vanishing lattice and shielding model development for fuel assemblies with part-length rods require more detailed knowledge of the fuel designs and complicated modeling. This section analyzes the effects on the external dose rates of transportation packages for two different BWR fuel assembly models. The purpose of this study is to determine whether a full-length fuel rod assembly produces bounding dose rates for a fuel assembly with partial-length fuel rods, assuming the same irradiation conditions for both assembly models.

The BWR fuel assembly type used in the study is a BWR 10 × 10 assembly with 78 full-length fuel rods, 14 partial-length fuel rods, and two water rods, each water rod displacing four fuel rods. The irradiation characteristics of the fuel assemblies are the following:

- an average assembly burnup value of 50 GWd/MTU,
- a 4.2 wt % initial ^{235}U enrichment,
- a 10-year cooling time, and
- the axial burnup profile described in Table 2.

The initial uranium weight for the fuel assembly with full-length rods is 183.37 kg. The detailed fresh fuel assembly model has 88.018 kg of uranium in the dominant lattice region and 80.842 kg of uranium in the vanished lattice region. The location of the axial burnup profile peak is within the dominant lattice region.

Two different ORIGEN cross section libraries were generated with TRITON [1], one for the full lattice and another for the vanished lattice. Identical irradiation conditions were used for the full and vanished lattices (e.g., bladed lattice and a moderator density of 0.3 g/cm^3). Neutron and primary gamma radiation source terms were then calculated with ORIGAMI [1] using the pre-generated ORIGEN cross sections. The gamma and neutron source strengths for the 10 axial zones of the two fuel assembly models are shown in Figure 63. The axial neutron and photon dose rate profiles at the radial surface of the hypothetical transportation package model described in Section 3 were calculated for each of the two BWR fuel assembly models. The 3D fuel assembly model includes both full-length and partial-length rod regions. A horizontal cross-sectional view of the transportation package model showing the vanished lattice is illustrated in Figure 64.

The axial dose rate profiles of the primary gamma, neutron, and secondary gamma radiation produced by the two assembly models at the cask surface are illustrated in Figure 65. The relative uncertainty of the dose rate estimate was less than 2% for neutrons and less than 1% for primary gamma radiation; however, the uncertainty values are not shown in the graphs for clarity. The graphs in the figure indicate that a typical BWR full lattice model produces bounding axial dose rate profiles for the detailed partial-length rod fuel assembly model.

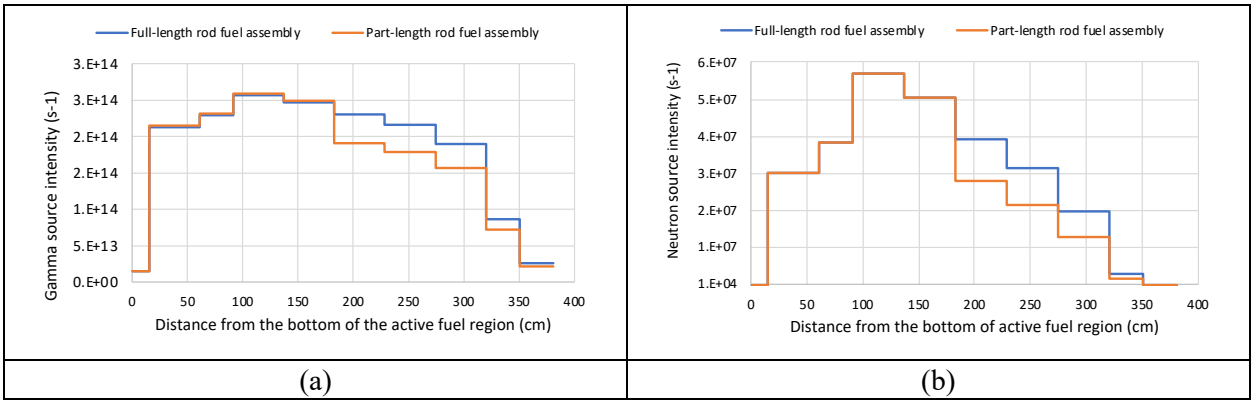

Figure 63. Gamma (a) and neutron (b) source intensities as a function of axial fuel zone.

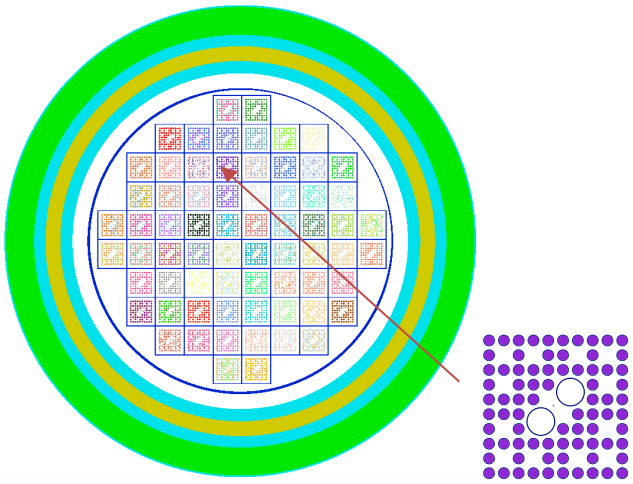

Figure 64. Horizontal cross-sectional view of the cask model through the vanished lattice of the 10 × 10 BWR fuel assembly with 14 partial-length fuel rods.

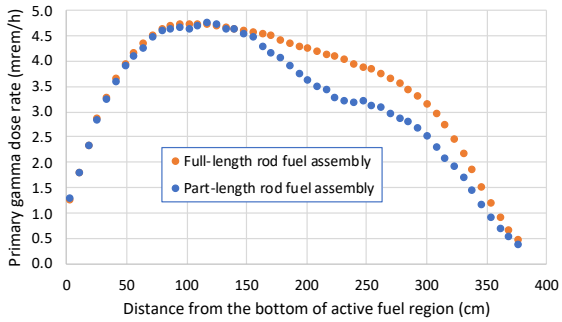

(a)

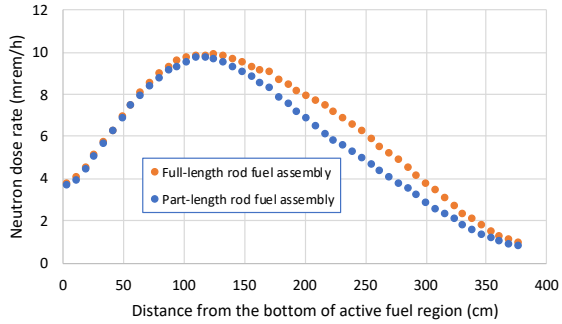

(b)

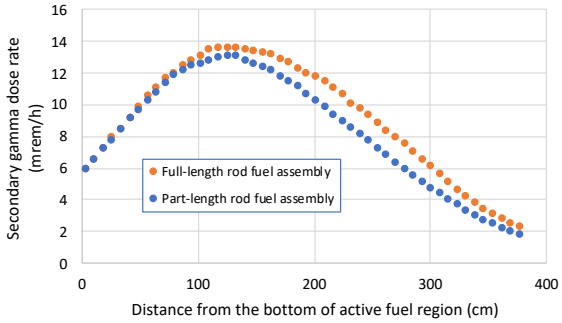

(c)

Figure 65. Axial primary gamma (a), neutron (b), and secondary gamma (c) dose rate profiles produced by full-length rod and part-length rod fuel assemblies at the radial surface of a transportation cask model.

7. ACTIVATION SOURCES ASSOCIATED WITH VARIOUS NFH

Nuclear power reactors use various components to control the reactivity and power distribution and fuel channel to control flow of coolant. These components are called NFH and are not an integral part of the fuel assembly. In dry storage cask or spent fuel transportation packages, irradiated PWR non-fuel components are usually inserted into the guide tubes of the PWR SNF assemblies loaded in storage canisters. Therefore, NFH activation sources contribute to cask external radiation dose rates. The PWR NFH include control rods, axial power shaping rods (APSR), BPR assemblies (BPRAs), neutron source assemblies, ORAs, and TPDs, etc. A limited study, including calculations of ^{60}Co activation sources associated with cobalt impurity in BPRs, ORAs, and TPDs, is provided in this section. Data used in the calculations documented in this section were taken from ORNL/SPR-2021/2093 [10].

7.1 BURNABLE POISON ROD ASSEMBLIES

BPRs are not an integral part of the fuel assembly and are typically removed after one reactor loading cycle. There are several types of BPRs. Only the WE Pyrex BPRs could contain significant ^{60}Co radioactivity because of their steel cladding. An assembly average burnup value of 28.8 GWd/MTU [31], the Pyrex BPRs dimensions summarized in ORNL/SPR-2021/2093 [10], 24 rodlets per BPR assembly, and a cobalt impurity concentration of 800 ppm in stainless-steel were used in an activation calculation. The total amount of cobalt in the active fuel region is approximately 9 grams. The ^{60}Co activity for the 9 grams of cobalt irradiated in the core and cooled for five years was calculated assuming a fuel initial enrichment of 3.59%. The calculated ^{60}Co activity is 447 Ci.

Activated BPRAs are typically inserted in the guide tubes of spent fuel assemblies for storage and transportation. The effect of activated BPRAs on cask external dose rate is determined relative to the dose rate produced by the primary gamma radiation of fuel assemblies without BPRAs. The hypothetical storage cask model containing 37 fuel assemblies, which is described in Section 3, was used in these calculations. The characteristics of the fuel assembly are an initial enrichment of 4.2%, an average burnup of 50 GWd/MTU, and a cooling time of 10 years. Dose rate values were calculated for the cask with irradiated BPRAs in each fuel assembly and for the cask without irradiated BPRAs. The 447 Ci of ^{60}Co in activated BPRA materials increased the dose rate at 1 m from the radial surface of the hypothetical storage cask model by ~13.5%. The BPRA material was neglected in the assembly model.

7.2 ORA AND TPD

ORAs and TPDs are inserted into the guide tubes in B&W and WE power reactors to prevent coolant from flowing through empty tubes. The exposure locations of ORA/TPD are within assembly GP and UEF axial regions. The estimated ORA/TPD exposure lifetime is 20 years [10]. This corresponds to the irradiation time of five cycles, assuming each fuel assembly is irradiated for two 24-month cycles. Mean values for average fuel assembly burnup, specific power, and effective full-power day (EFPD) values of the host assembly [10], which are presented in Table 26, were used in cobalt activation calculations. The neutron flux values at the assembly UEF and GP locations are fractions of the core neutron flux (i.e., ORAs and TPDs are irradiated with a much lower neutron flux than the fuel itself). Therefore, a flux scaling factor was applied to the fuel assembly specific power in the ORIGAMI irradiation history block. The ORIGEN cross section libraries available in SCALE 6.2.4 for the fuel assembly types were used in the ORIGAMI calculations. These calculations simulated the irradiation conditions of ORA/TPD at the GP and UEF locations for five consecutive cycles using a fresh fuel assembly at the beginning of each irradiation cycle. Table 27 provides information on the material composition at the UEF and GP exposure locations [10] and the calculated ^{60}Co activities based on a cobalt impurity concentration in stainless-steel of 800 ppm and cobalt impurity concentrations in Inconel-718 of 4,694 and 500 ppm [10]. The calculated

^{60}Co activity values in Table 27 are provided for five years after hardware discharge from the reactor. These calculations identified irradiated ORA as the bounding component among ORA and various TPDs.

The maximum ^{60}Co activity values in Table 27 for an ORA/TPD assembly in the assembly GP and UEF regions are 93.89 Ci and 73.14 Ci, respectively. Activated ORA/TPD assemblies are typically inserted into the guide tubes of spent fuel assemblies for storage and transportation. The dose rate contributions of activated ORA were evaluated for the hypothetical storage cask model containing 37 fuel assemblies, which is described in Section 3. The characteristics of the fuel assembly are an initial enrichment of 4.2%, an average burnup of 50 GWd/MTU, and a cooling time of 10 years. The maximum external cask dose rate values were determined for the cask with irradiated ORA in each fuel assembly and for the cask without irradiated ORA. Fuel assemblies containing activated ORA increased the dose rate at 1 m from the radial surface of the hypothetical storage cask by ~50% at the axial location of the assembly GP region and by ~16% at the axial location of the assembly UEF region. The ORA material was neglected in the assembly model.

Table 26. Mean values for average fuel assembly burnup, specific power, and EFPD of the host assembly in each irradiation cycle.

Fuel assembly	Assembly code	U mass (kg)	Enrichment (%)	Assembly burnup (GWd/MTU)	Specific power (MW/MTU)	EFPD[a]
B&W 15 × 15	B1515B10	489.30	4.23	56.88	40.31	1,411
WE 14 × 14	W1414WL	405.81	4.39	59.22	41.97	1,411
WE 15 × 15	W1515WL	465.60	4.95	58.60	41.53	1,411
WE 17 × 17	W1717WL	469.20	3.59	58.42	41.40	1,411

[a]Assumed EFPD value.

Table 27. Estimated exposure locations, material composition, and ^{60}Co activation sources for ORA and TPD.

UEF location							
Type	**Material at location**	**Weight (kg) at location**	**Flux scaling factor**	**Cobalt [a] (g)**	**^{60}Co activity [a,b] (Ci)**	**Cobalt [c] (g)**	**^{60}Co activity [c,b] (Ci)**
ORA	SS CF3M	3.5	0.1	2.80	51.81	2.80	51.81
	SS 304	0.07	0.1	0.06		0.06	
TPD for WE 14 × 14	SS 304	1.7	0.1	1.36	57.74	1.36	27.30
	Inconel-718	0.42	0.1	1.97		0.21	
TPD for WE 15 × 15	SS 304	1.8	0.1	1.44	55.61	1.44	26.90
	Inconel-718	0.42	0.1	1.97		0.21	
TPD for WE 17 × 17	SS 304	2.3	0.1	1.84	73.14	1.84	39.34
	Inconel-718	0.42	0.1	1.97		0.21	

GP location					
Type	**Material at location**	**Weight (kg) at location**	**Flux scaling factor**	**Cobalt (g)**	**^{60}Co activity [b] (Ci)**
ORA	SS 304	3.4	0.2	2.72	93.89
TPD for WE 14 × 14	SS 304	2.2	0.2	1.76	54.74
TPD for WE 15 × 15	SS 304	2.7	0.2	2.16	66.92
TPD for WE 17 × 17	SS 304	3.2	0.2	2.56	93.26

[a]Assuming a cobalt impurity of 4,694 ppm in Inconel-718, where applicable.
[b]Activity of ^{60}Co at 5 years after NFH discharge from the reactor.
[c]Assuming a cobalt impurity of 500 ppm in Inconel-718.

8. CONCLUSIONS

SNF storage and transportation systems are designed for a variety of fuel assemblies with wide ranges of irradiation characteristics. A series of parametric calculations was presented in this report to help shielding analysts identify input parameters that are more important with respect to radiation source terms and external cask dose rates. The calculations presented in this report were performed using computer codes and analyses sequences within the SCALE code system, including ORIGEN, ORIGAMI, POLARIS, TRITON, and MAVRIC. A series of hypothetical cask models were used in various MAVRIC calculations.

Radiation Source Terms Sensitivity Analysis

The effect of depletion parameters on source terms from PWR and BWR assemblies and their impact on dose rates outside dry storage casks are evaluated in Section 4. For each evaluated depletion parameter, primary gamma, neutron, and ^{60}Co radiation source terms were calculated. Detailed plots of source terms and dose rates are provided in Section 4. The impact on dose rate of depletion parameters over their evaluated ranges (see Table 5 and Table 6) is concisely summarized in Table 28. The assembly average fuel assembly burnup was 80 GWd/MTU.

Table 28. Change in dose rates (%) over the full range of evaluated parameters.

Parameter [a]	Parameter range	Component	Cooling time (years)						
			1	3	5	10	20	30	40
Specific power (PWR)	10–50 W/g	Gamma [b]	66	54	43	25	17	17	17
		Neutron	11	12	12	12	12	12	12
		^{60}Co [c]	58	58	58	58	58	58	58
Enrichment (PWR)	1–12 %	Gamma	-24	-24	-18	0	8	8	7
		Neutron	-97	-97	-96	-95	-95	-95	-95
		^{60}Co	-76	-76	-76	-76	-76	-76	-76
Fuel density (PWR)	10.0–10.75 g/cm^3	Gamma	0	0	0	0	0	0	0
		Neutron	0	0	0	0	0	0	0
Fuel temperature (PWR)	500–1,100 K	Gamma	0	0	0	1	1	0	0
		Neutron	3	3	3	3	3	3	3
		^{60}Co	0	0	0	0	0	0	0
Soluble boron content (PWR)	0–1,700 ppm	Gamma	2	3	3	3	2	1	0
		Neutron	8	8	8	8	8	8	8
		^{60}Co	2	2	2	2	2	2	2
Moderator density (PWR)	0.6611–0.9996 g/cm^3	Gamma	-6	-8	-8	-6	-3	-2	-1
		Neutron	-37	-38	-38	-38	-38	-38	-37
		^{60}Co	-10	-10	-10	-10	-10	-10	-10
Void fraction (BWR)	0.05–1.0	Gamma	8	11	13	13	9	6	3
		Neutron	35	32	30	27	26	26	26

[a]The values represent a change in dose rate in percent over the full range of the evaluated parameters in Table 5 and Table 6. For the BWR assembly, dose rates are evaluated only for void fraction since the other parameters follow similar trends to the PWR fuel assembly. For detailed results refer to Section 4.
[b]A positive number represents an increase in dose rates with increasing value of the parameter, and a negative value represents a decreasing dose rate with increasing parameter. For example, gamma dose rates increase by 66% when specific power during depletion is increased from 10 to 50 W/g and cooling time is 1 year. After 10 years of cooling time, this effect reduces to 25%, and after 40 years it reduces to 17%.
[c]For fuel hardware and NFH materials containing cobalt impurity, a change in ^{60}Co activity is evaluated.

The parametric analyses in this report are more extensive than those provided in NUREG/CR-6802 [2] because the range of values selected for the analyzed depletion parameters include values anticipated for increased enrichment and high burnup fuel. However, ultimately the validation of source terms for

increased enrichment and higher burnups approaching 80 GWd/MTU will need to be demonstrated via the use of assay measurements. As these enhanced burnup measurements become available, their results should be factored into future analyses.

Far-field dose rates from a single vertical concrete cask

Far-field dose rate from a hypothetical vertical concrete cask loaded with PWR fuel was calculated as a function of distance up to 1,600 m from the cask center. Varying parameters in these analyses were average fuel assembly burnup (45, 60, and 70 GWd/MTU), fuel cooling time (1, 5, and 40 years), and air density (1.2 and 1.108 kg/m^3). For the analyzed cask model and assembly average burnup range, the maximum dose rate values at 1 m from the cask surface were approximately 500, 110, and 5 mrem/h for the one-year, five-year, and 40-year cooling times, respectively. The results show that the dose rate decreases with decreasing fuel burnup, increasing distance from the cask, and increasing air density. The total dose rate decreases by approximately 3 orders of magnitude at 100 m from the cask center and by approximately 10 orders of magnitude at 1,600 m from the cask center. The percentage contribution of primary gamma radiation produced by fuel assemblies with an average burnup of 70 GWd/MTU and one-year cooling time was between 82% and 89% of the total dose rate at all evaluated locations. Primary gamma radiation also dominated the total dose rates at locations up to 1,600 m from the cask center for the five-year cooling time and up to 500–700 m from the cask center for the 40-year cooling time. The contribution of the secondary gamma radiation to the total dose rate increased with increasing distance from the cask. This contribution significantly increased with increasing burnup and cooling time. For a 70 GWd/MTU average assembly burnup value and a 40-year cooling time, secondary gamma radiation dominated total dose rate at distances beyond 700 m. A 10% decrease in air density produced a total dose rate increase at 1,600 m from the cask center of ~110% for the fuel with a 5-year cooling time. This increase was ~70% for the fuel with a 40-year cooling time at 1,600 m from the cask center.

A study was also performed to determine whether cask loadings that produce the same near-field dose rate values would also produce the same dose rate values at large distances from the cask. The characteristics of two fuel assemblies that produce approximately the same dose rates up to 400 m from the cask center are identified in the study (55 GWd/MTU, 3 wt% ^{235}U, 20 years of cooling and 35 GWd/MTU, 3 wt% ^{235}U, 15 years of cooling). However, beyond 400 m, the dose rate values produced by the higher burnup fuel assembly were higher than the dose rate values produced by the lower burnup fuel assembly. More studies considering higher burnup assemblies are needed to confirm this result.

Fuel assembly type

Dose rates produced by eight different fuel assembly types—B&W 15 × 15, WE 17 × 17 LOPAR, WE 17 × 17 OFA, CE 16 × 16, GE 7 × 7, GE 8 × 8, ANF 9 × 9, and GE 10 × 10—were evaluated for a transportation cask model under NCT and a pin-by-pin fuel assembly representation. The same fuel initial enrichment, average assembly burnup, cooling time, and the axial burnup profile for each fuel type (see Table 1 for the PWR fuel and Table 2 for the BWR fuel) were used in these calculations. The study identified the B&W 15 × 15 fuel assembly type as being the bounding assembly for the evaluated PWR fuel assembly types. However, the WE 17 × 17 LOPAR fuel assembly produced approximately the same radial dose rate values within the range of statistical uncertainty as the B&W 15 × 15 fuel assembly type. The evaluated BWR fuel types, including the GE 7 × 7, GE 8 × 8, ANF 9 × 9, and GE 10 × 10 fuel types, practically produced the same dose rates within the statistical uncertainty.

Pin-by-pin model versus homogeneous material model for the active fuel zone

The effect on the external dose rate of the active fuel zone representation in the cask model, as either pin-by-pin or homogeneous material, was evaluated for a storage cask model and the B&W 15 × 15 fuel

assembly type. The gamma dose rate produced by the pin-by-pin model was lower by ~5% than that produced by the homogeneous material model. The total dose rate contributions from neutrons and secondary gamma radiation were practically identical for the two models. Therefore, the homogeneous material model is slightly more conservative than the pin-by-pin model.

Neutron source from subcritical multiplication

Subcritical neutron multiplication refers to the neutrons produced in fission reactions induced by the neutrons from spontaneous fissions and (alpha,n) reactions in spent fuel. This neutron source is not included in the neutron source terms determined with depletion and decay codes and must be considered in dose rate calculations. Historically, the total neutron source was approximated as the product of the neutron source determined with the depletion code and the subcritical multiplication factor, $1/(1-k_{eff})$. Current capabilities of Monte Carlo radiation transport codes, such as MCNP and SCALE/MAVRIC, include explicit simulation of secondary neutrons and secondary gamma radiation in calculations. The effects of the neutron source from subcritical multiplication on dose rate were evaluated for a hypothetical dry cask model. The percentage contribution made by the neutron source from subcritical multiplication to the total neutron dose rate was approximately 37% and the percentage contribution to the total secondary gamma dose rate of the secondary gamma radiation associated with the neutrons from subcritical multiplication was approximately 60%.

Irradiated fuel compositions

Typical shielding calculations for SNF use fresh fuel compositions to reduce the need to obtain the irradiated fuel compositions. The basis for this approach is that the fresh fuel composition is either bounding or produces very similar external cask dose rates as the irradiated fuel composition. The validity of this assumption was evaluated in this report by comparing external storage cask dose rates produced by irradiated and fresh fuel compositions using SCALE/MAVRIC. The irradiated fuel composition included all actinides and the 20 most abundant fission product nuclides in the irradiated fuel composition. The mass of the remainder fission products was added to the ^{137}Cs mass. The fuel mass densities were identical for both compositions. The irradiated fuel composition produced a slightly higher value (i.e., by ~2%) than the fresh fuel composition for the dose rate from primary gamma radiation. This result may be explained by a slightly lower average atomic number of the irradiated fuel composition compared to the fresh fuel composition (i.e., slightly less attenuation in irradiated fuel compositions). It also produced lower dose rate values for neutrons (i.e., by ~15%) and secondary gamma radiation (i.e., by ~17%) than the fresh fuel composition. This result may be explained by lower neutron multiplication and the presence of nuclides with higher absorption cross sections in the irradiated fuel composition compared to the fresh fuel composition. However, the total dose rate values from the two fuel compositions were identical within statistical uncertainty for the hypothetical storage cask model because gamma radiation dominates external cask dose rate for this cask model.

Effects of removable burnable absorber on fuel assembly radiation sources

Radiation source terms for a PWR fuel assembly exposed to BPRs during irradiation as well as radiation source terms for a BWR fuel exposed to a control blade were evaluated and compared to the radiation source terms of fuel assemblies with no absorber (PWR) or control blade (BWR) exposure. The neutron source strength of a fuel assembly exposed to burnable absorber/control blade was significantly higher than that of a fuel assembly not exposed to burnable absorber/control blade during irradiation. This difference was much higher for the BWR fuel assembly than for the PWR fuel assembly. Conversely, this exposure yielded non-conservative ^{60}Co activation sources, especially for the BWR assemblies. However, the difference between assembly neutron source strengths with and without burnable absorber/control blade exposures significantly decreased with increasing fuel assembly average burnup and cooling time.

Burnable absorber/control blade exposure had little effect on primary gamma radiation source terms. The physical explanation is that the fuel assemblies with burnable absorber or control blade would contain more transuranic elements because of neutron spectrum hardening.

Irradiated steel replacement rods

The effects of ^{60}Co in irradiated steel replacement rods on the external dose rate of a hypothetical storage cask model were evaluated for different canister loading scenarios and selected fuel cooling times from 2 to 75 years. These effects were evaluated relative to dose rates produced by regular fuel assemblies with the same irradiation characteristics as the fuel assembly containing irradiated replacement rods. Two different canister models with different spatial distributions for the irradiated steel replacement rods inside assemblies were analyzed. In one canister model, each fuel assembly contained from eight to ten irradiated steel replacement rods, for a total of 366 steel rods per canister (i.e., 4.75% of the total rods in the canister). In the other canister model, each fuel assembly contained from three to four irradiated steel replacement rods, for a total of 136 steel rods per canister (i.e., 1.8% of the total rods in the canister). The irradiated replacement rods were located in assembly peripheral locations for maximum dose rate impact. Additionally, two irradiation scenarios for the steel replacement rods were analyzed for each canister model. In these scenarios, the ^{60}Co source intensities were based on reconstituted assembly burnup values of 60 GWd/MTU and 40 GWd/MTU, where the reconstituted fuel assembly discharge burnup is 60 GWd/MTU. For the analyzed cases, ^{60}Co in irradiated replacement steel rods was a major contributor to the total gamma dose rate up to approximately 30 years of cooling, and its contributions extended up 45 years of cooling. The fuel assemblies containing irradiated replacement steel rods produced a maximum dose rate increase of 30% to 130% relative to regular fuel assemblies, depending on the number of steel rods and the burnup of the assembly with replacement steel rods. Additional evaluations for the storage cask model containing only nine reconstituted fuel assemblies in the innermost locations of the basket showed no increase in the external dose rate relative to the external dose rate of the cask containing regular assemblies. Therefore, reconstituted fuel assemblies with irradiated fuel rods can safely be placed in the inner locations of the fuel basket inside the cask because these reconstituted assemblies are shielded by the regular fuel assemblies.

BWR fuel assemblies with partial-length fuel rods

Modern BWR fuel assemblies contain both full-length and partial-length fuel rods. The study presented in this report shows that a full-length fuel rod assembly model produces the same maximum dose rate as a fuel assembly with partial-length fuel rods, for a given assembly average burnup, axial burnup profile, and cooling time.

Effects of PWR Burnable Poison Rods and BWR Control Blades on Fuel Assembly Radiation Sources

Calculations of ^{60}Co activation sources associated with Co impurity in BPRAs, ORAs, and TPDs—which often serve as bounding PWR NFH radiation sources in cask shielding analyses—are also provided. These calculations identified irradiated ORA as the bounding component among ORA and various TPDs because of its slightly higher weight. Fuel assemblies containing activated BPRA materials increased the dose rate at 1 m from the radial surface of a hypothetical storage cask model by ~13.5%. Fuel assemblies containing activated ORA increased the dose rate at 1 m from the radial surface of the hypothetical storage cask by ~50% at the axial location of the assembly GP and by ~16% at the axial location of the assembly UEF. The characteristics of the fuel assembly used in the dose rate calculations are an initial enrichment of 4.2%, an average burnup of 50 GWd/MTU, and a cooling time of 10 years; the BPRA and ORA/TPD material was neglected in the assembly model.

9. FUTURE WORK

Additional studies are recommended for future work, including:

- Analyses of far-field dose rate from storage casks that produce similar near-field dose rates, focusing on high burnup fuel assemblies (70 GWd/MTU burnup). The analyses presented in Section 5.2 showed that spent fuel assemblies with different burnup and cooling time characteristics can produce approximately the same near-field dose rates but different far-field dose rates. This phenomenon is primarily caused by an increase contribution to dose rate of neutron and secondary gamma radiation as distance from the cask increases.

- Activation sources for PWR control rod assemblies and for the APSRs used in B&W power reactors. Control rods are typically in a fully withdrawn position relative to the active fuel region during normal operation. Therefore, only the bottom end of a control rod is irradiated in the upper regions of the fuel assembly, i.e., the GP and upper tie plate region. APSRs are often inserted in the core for multiple cycles. Therefore, irradiated APSRs when loaded in a spent fuel storage cask or spent fuel transportation package could be a significant activation gamma source and contributor to the dose rate external to the storage cask or transportation package.

- Studies evaluating the impact on radiation source terms and dose rates of partial-length rods in the BWR fuel assemblies with increased enrichment and higher burnup fuel.

- Studies on the source terms axial distribution of fuel assemblies containing natural or lower enrichment uranium blankets and their impacts on dose rates outside the cask.

ACKNOWLEDGMENTS

The work described in this report was accomplished with funding provided by the US Nuclear Regulatory Commission. The authors acknowledge review and useful comments by Lucas Kyriazidis of the Office of Nuclear Regulatory Research, Division of Systems Analysis, and Zhian Li of the Office of Nuclear Material Safety and Safeguards, Division of Fuel Management.

10. REFERENCES

1. B. T. Rearden and M. A. Jessee, Eds. 2016. *SCALE Code System*, ORNL/TM-2005/39, Version 6.2.1, Oak Ridge National Laboratory. Available from the Radiation Safety Information Computational Center as CCC-834.
2. B. L. Broadhead, *Recommendations for Shielding Evaluations for Transport and Storage Packages*, NUREG/CR-6802 (ORNL/TM-2002/31), US Nuclear Regulatory Commission (2003).
3. "Nuclear Fuel Data Survey Form GC-859," Energy Information Administration, US Department of Energy, [Online]. Available: http://www.eia.gov/survey/form/gc_859/proposed/form.pdf. [Accessed 9/30/2020].
4. G. Ilas and B. Hiscox, Validation of SCALE 6.2.4 and ENDF/B-VII.1 Data Libraries for Nuclide Inventory Analysis in PWR Used Fuel, 2021 ANS Virtual Annual Meeting, June 14-16 (2021).
5. I. C. Gauld and U. Mertyurek, Validations of BWR spent fuel isotopic predictions with applications to burnup credit, Nucl. Eng. and Design, 345 (2019) 110-124. doi.org/10.1016/j.nucengdes.2019.01.026.
6. D. E. Peplow. 2011. "Monte Carlo Shielding Analysis Capabilities with MAVRIC." *Nucl. Technol.* 174(2): 289–313. doi.org/10.13182/NT174-289
7. J. C. Wagner, D. E. Peplow, and S. W. Mosher. 2014. "FW-CADIS Method for Global and Regional Variance Reduction of Monte Carlo Radiation Transport Calculations." *Nucl. Sci. Eng.*, 176(1): 37–57. doi.org/10.13182/NSE12-33.
8. T. M. Evans, A. S. Stafford, R. N. Slaybaugh, and K. T. Clarno. 2010. "Denovo: A New Three-Dimensional Parallel Discrete Ordinates Code In SCALE." *Nucl. Technol.* 171(2): 171–200.
9. *American National Standard Neutron and Gamma-Ray Flux-to-Dose-Rate Factors*, ANSI/ANS 6.1.1-1977, American Nuclear Society (1977).
10. G. Radulescu, B. R. Grogan, and K. Banerjee, *Fuel Assembly Reference Information for SNF Radiation Source Term Calculations*, ORNL/SPR-2021/2093, Oak Ridge National Laboratory (2021).
11. R. J. Cacciapouti and S. Van Volkinburg, "Axial Burnup Profile Database for Pressurized Water Reactors," YAEC-1937, Yankee Atomic Electric Company (May 1997).
12. L. B. Wimmer and C. W. Mays, BWR Axial Burnup Profile Evaluation, 32-5045751-00, Framatome ANP, Lynchburg, VA (2004).
13. G. Radulescu, H. Liljenfeldt, and L. Paul Miller, *FY2016 Dose Rate Report for Selected Loaded Transportation Casks*, FCRD-NFST-2016-000095, Oak Ridge National Laboratory (2016).
14. R. Hall et all., *Isotopic and Fuel Lattice Parameter Trends in Extended Enrichment and Higher Burnup LWR Fuel, Vol. I: PWR Fuel*, ORNL/TM-2020/1833, Oak Ridge National Laboratory (2021).
15. R. Cumberland et al., *Isotopic and Fuel Lattice Parameter Trends in Extended Enrichment and Higher Burnup LWR Fuel, Vol. II: BWR Fuel*, ORNL/TM-2020/1835, Oak Ridge National Laboratory (2021).

16. I. C. Gauld and J. C. Ryman, *Nuclide Importance to Criticality Safety, Decay Heating, and Source Terms Related to Transport and Interim Storage of High-Burnup LWR Fuel*, NUREG/CR-6700 (ORNL/TM-2000/284), US Nuclear Regulatory Commission (2000).

17. O. W. Hermann and C. W. Alexander, *A Review of Spent-Fuel Photon and Neutron Source Spectra*, ORNL/CSD/TM-205, Oak Ridge National Laboratory (1986).

18. *Standard Review Plan for Transportation Packages for Spent Fuel and Radioactive Material*, NUREG-2216, US Nuclear Regulatory Commission (2020).

19. S. J. Rimshaw and E. E. Ketchen, Curium Data Sheet, ORNL-4357, Oak Ridge National Laboratory (1969).

20. A. L. Nichols, D. L. Aldama, and M. Verpelli, Handbook of Nuclear Data for Safeguards: Database Extensions, August 2008, INDC(NDS)-0534, International Atomic Energy Agency, Vienna, Austria.

21. M. W. Francis et al., Reactor Fuel Isotopics and Code Validation for Nuclear Applications, ORNL/TM-2014/464, Oak Ridge National Laboratory (2014).

22. https://t2.lanl.gov/nis/data/endf/endfvii.1-n-pdf/co59.pdf. Accessed on Feb. 13, 2022.

23. M. D. DeHart, *Sensitivity and Parametric Evaluations of Significant Aspects of Burn-up Credit for PWR Spent Fuel Packages*, ORNL/TM-12973, Oak Ridge National Laboratory (1996).

24. A. Luksic, "Spent Fuel Assembly Hardware: Characterization and 10CFR 61 Classification for Waste Disposal," Volume 1: Activation Measurements and Comparison with Calculations for Spent Fuel Assembly Hardware, PNL-6906-vol. 1, Pacific Northwest Laboratory, June 1989.

25. J. K. Shultis and R. E. Faw, *Radiation Shielding*, American Nuclear Society edition (2000).

26. G. Radulescu, K. Banerjee, D. Peplow, and T. M. Miller, "Skyshine Calculations for a Large Spent Nuclear Fuel Storage Facility," *Nucl. Technol*., (2020). doi.org/10.1080/00295450.2020.1842702

27. D. E. Mueller et al., Review and Prioritization of Technical Issues Related to Burnup Credit for BWR Fuel, NUREG/CR-7158 (ORNL/TM-2012/261), US Nuclear Regulatory Commission (2012).

28. *Neutron Fluence Measurements*, Technical Report Series No. 107, International Atomic Energy Agency, Vienna (1970).

29. Generic Letter 90-02, Supplement 1, "Alternative Requirements for Fuel Assemblies in Design Features Section of Technical Specifications," US Nuclear Regulatory Commission (1992).

30. G. Radulescu, and K. Banerjee, *Best Practices for Shielding Analyses of Activated Metals and Spent Resins from Reactor Operation*, ORNL/SPR-2020/1586, Oak Ridge National Laboratory (2020).

31. J. R. Secker et al., Optimum Discharge Burnup and Cycle Length for PWRs, *Nucl. Technol*. 151:2, 109–119 (2005).

APPENDIX A. SECONDARY GAMMA DOSE RATES

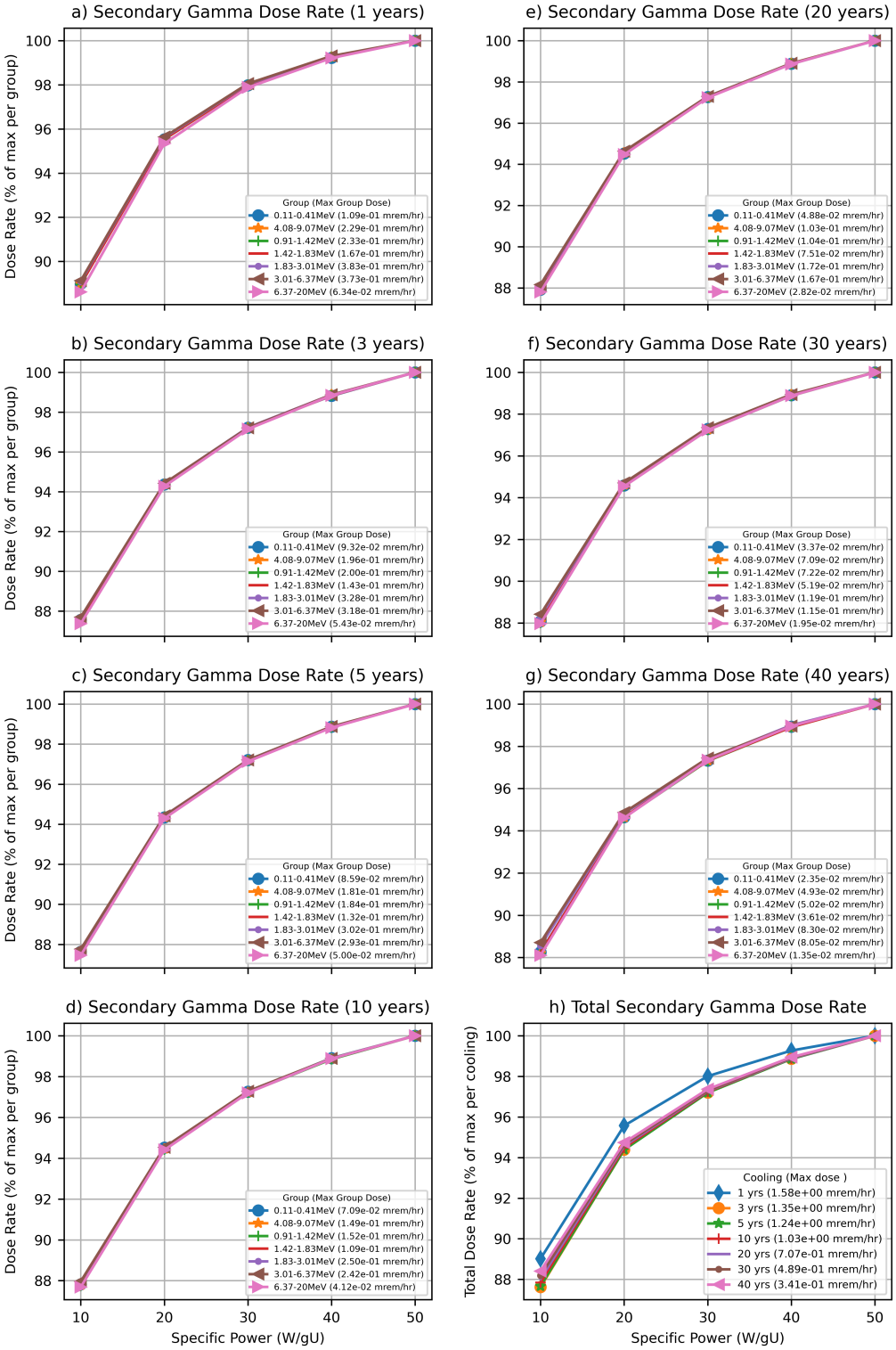

Figure A-1. Secondary gamma dose rate as a function of specific power.

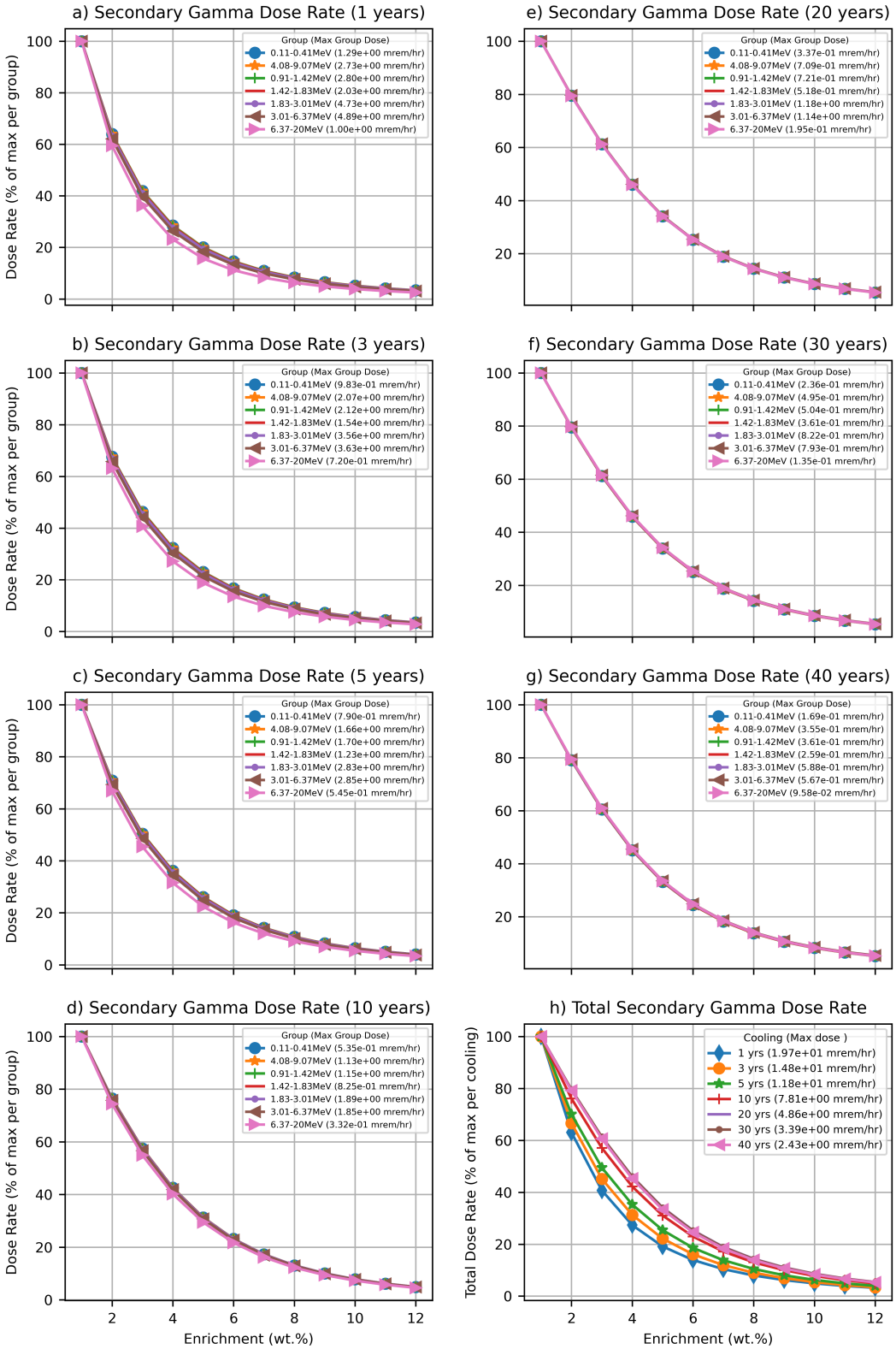

Figure A-2. Secondary gamma dose rates as a function of initial enrichment.

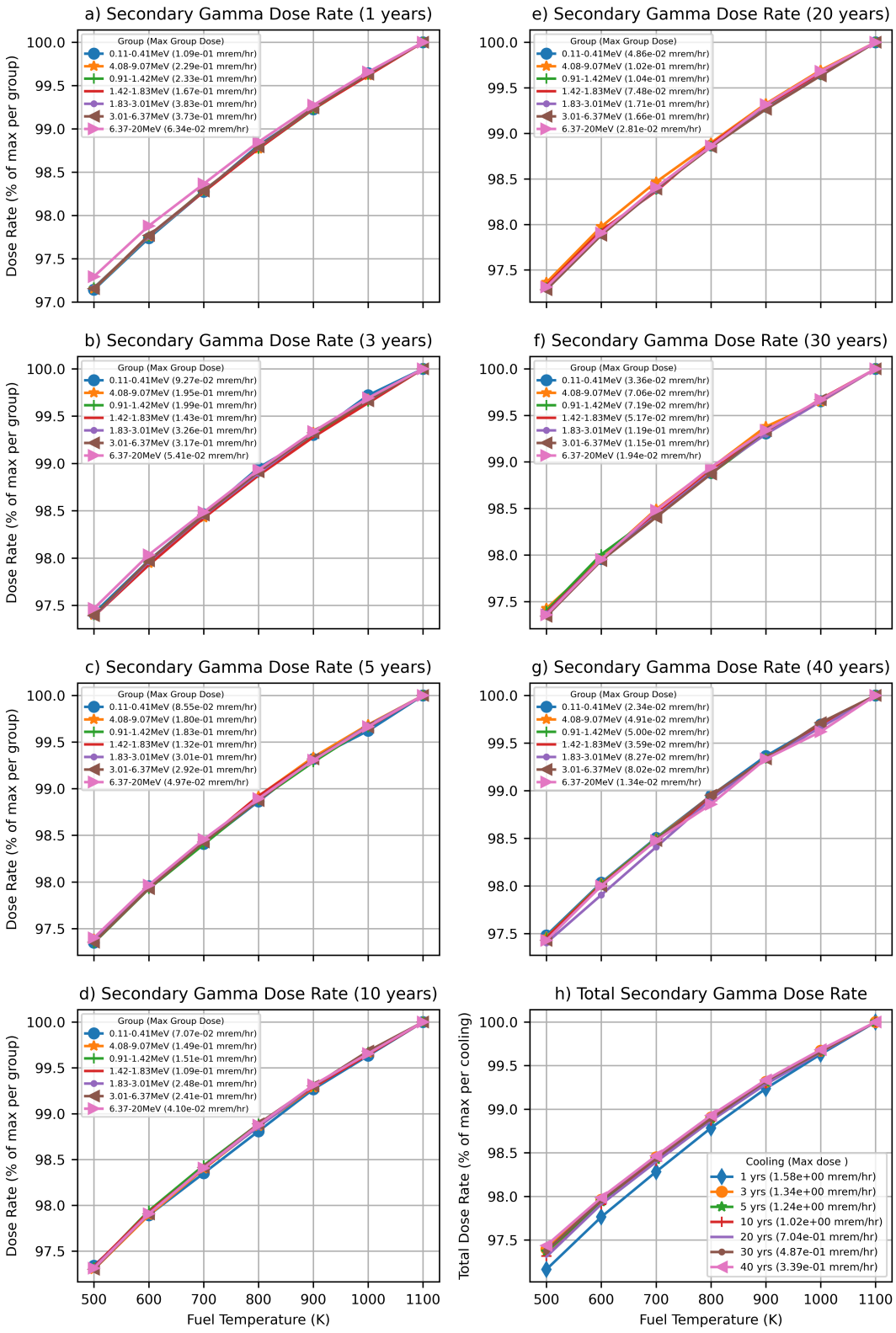

Figure A-3. Secondary gamma dose rate as a function of fuel temperature.

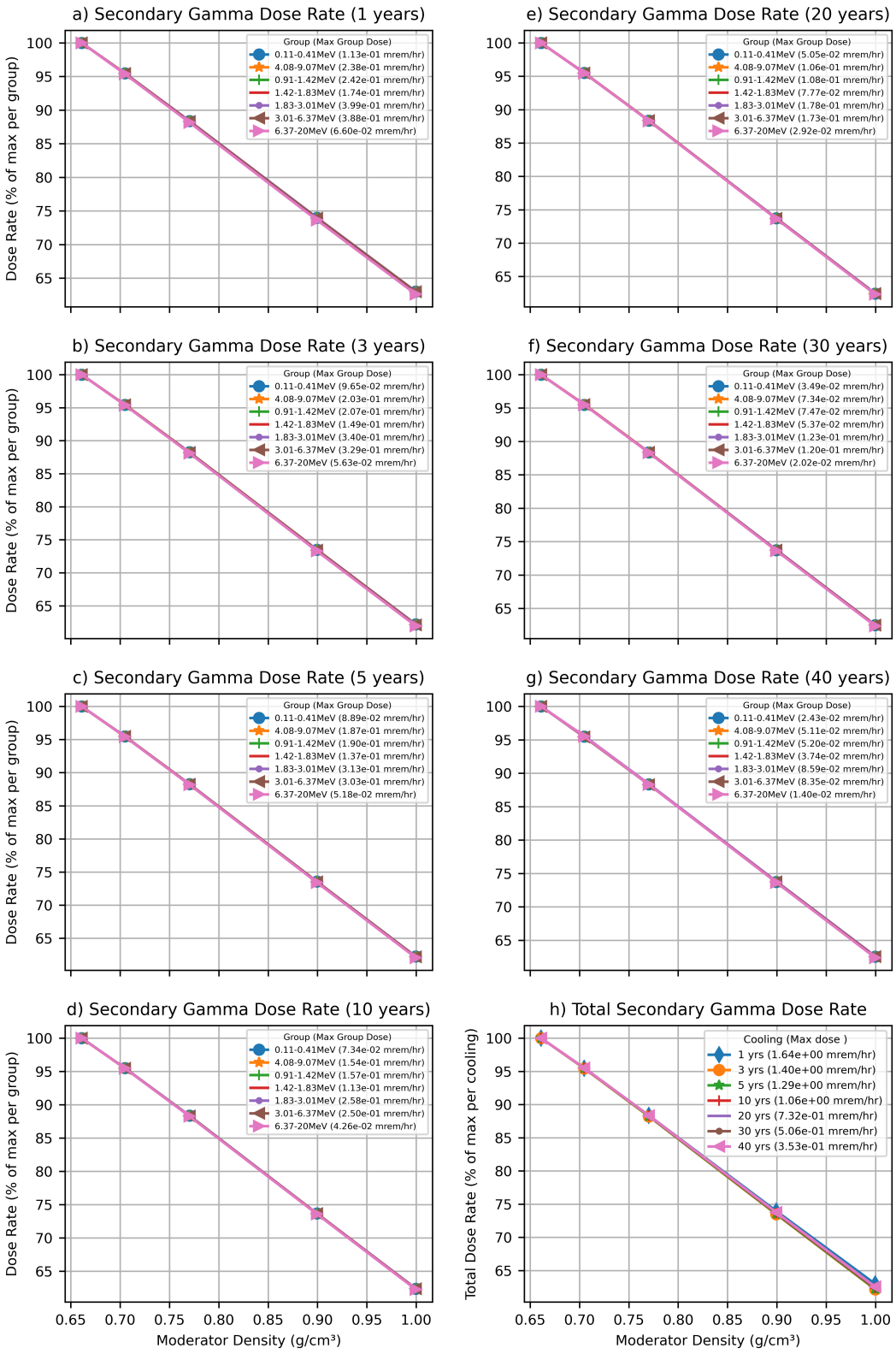

Figure A-4. Secondary gamma dose rate as a function of moderator density.

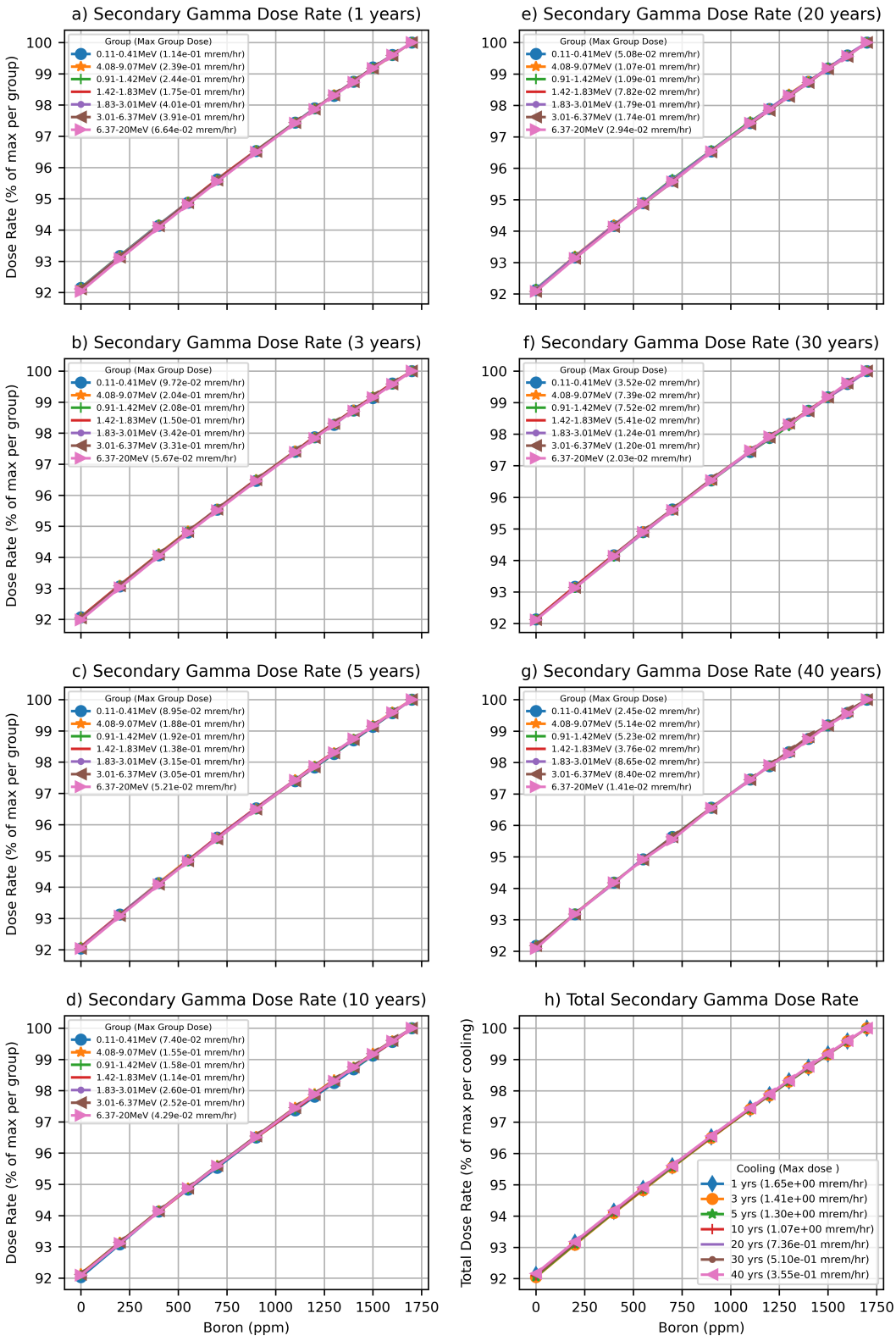

Figure A-5. Secondary gamma dose rate as a function of boron content.

APPENDIX B. DESCRIPTION OF NORMALIZED PLOTS

Source terms are plotted as a function of variables listed in Table 2 and as a function of cooling time. An example of source terms data $S_{i,j,k}$ from a sensitivity study with specific powers SP_i, energy groups EG_j and cooling time of CT_k years from Figure 5 is shown in Table B.1. The energy group plots are normalized for a given cooling time CT_k and within the given energy group EG_j. The normalized source terms are: $Sn_{i,j,k} = \frac{S_{i,j,k}}{\max(S_{i,j,k})}$, where j is held constant and represents a specific energy group EGj, and k is held constant and represents the cooling time (e.g., in this example, $CT_{k=3} = 5$ years). The maximum source term: $\max(S_{i,j=const.,k=3})$ is the maximum from source terms for all specific powers within given energy group EGj and given cooling time $CT_{k=3} = 5$ years. This maximum is also shown in the plot legend next to the energy group. The total source terms $St_{i,k}$ are calculated as a sum of all energy group specific source terms $St_{i,k} = \sum_j S_{i,j,k}$. The total source terms are normalized by the maximum total source term for the given cooling time. The normalized source terms are: $Stn_i = \frac{St_{i,k=c.}}{\max(St_{i,k=c})}$. The maximum source term, $\max(St_{i,k=c.})$, from all specific powers for given cooling time is shown in the plot legend.

Similarly, dose rates are plotted as a function of variables listed in Table 2, and as a function of cooling time. An example of dose rates $D_{i,j,k}$ from a sensitivity study with specific powers SP_i, energy groups EG_j and cooling time of CT_k years from Figure 6 is shown in Table B.2. The energy group plots are normalized for a given cooling time CT_k and within the given energy group EG_j. The normalized dose rates are $Dn_{i,j,k} = \frac{D_{i,j,k}}{\max(S_{i,j,k})}$, where j and k are held constant. The maximum dose rate $\max(D_{i,j=const.,k=const.})$ is the maximum from dose rates from all specific powers within given energy group j and given cooling time k. This maximum is also shown in the plot legend. The total dose rates $Dt_{i,k}$ are calculated as a sum of all energy group specific dose rates $Dt_{i,k} = \sum_j D_{i,j,k}$ and are normalized by the maximum dose rate for the given cooling time. The normalized dose rates are: $Dtn_i = \frac{St_{i,k=c.}}{\max(St_{i,k=c})}$. The maximum dose rate, $\max(Dt_{i,k=c.})$, from all specific powers for given cooling time is shown in the plot legend.

Table B-1. Source terms for specific power sensitivity analysis.

Source terms $S_{i,j,k}$ (photon/s) for 5 years of cooling (Note 3)

	Energy group (MeV) → *j*	*1*	*2*	*3*	*4*	*5*	*6*	*7*	*8*	*9*	*10*	*11*	
i	**Specific power (W/gU)** ↓	$S_{i,j=1,k=3}$ **0.2-0.3**	$S_{i,j=2,k=3}$ **0.3-0.4**	$S_{i,j=3,k=3}$ **0.4-0.6**	$S_{i,j=4,k=3}$ **0.6-0.8**	$S_{i,j=5,k=3}$ **0.8-1**	$S_{i,j=6,k=3}$ **1-1.33**	$S_{i,j=7,k=3}$ **1.330-1.66**	$S_{i,j=8,k=3}$ **1.66-2**	$S_{i,j=9,k=3}$ **2-2.5**	$S_{i,j=10,k=3}$ **2.5-3**	$S_{i,j=11,k=3}$ **3-4**	**Total** St_i
1	**10**	2.68E + 14	1.60E + 14	5.87E + 14	8.56E + 15	2.58E + 14	3.00E + 14	5.83E + 13	1.27E + 12	1.64E + 12	1.42E + 11	1.75E + 10	9.18E + 15
2	**20**	3.28E + 14	2.00E + 14	9.11E + 14	1.09E + 16	3.51E + 14	3.56E + 14	8.79E + 13	2.09E + 12	3.24E + 12	2.69E + 11	3.34E + 10	1.17E + 16
3	**30**	3.65E + 14	2.26E + 14	1.13E + 15	1.23E + 16	4.10E + 14	3.88E + 14	1.07E + 14	2.78E + 12	4.80E + 12	3.82E + 11	4.75E + 10	1.32E + 16
4	**40**	3.94E + 14	2.47E + 14	1.30E + 15	1.32E + 16	4.51E + 14	4.11E + 14	1.21E + 14	3.40E + 12	6.30E + 12	4.82E + 11	5.97E + 10	1.41E + 16
5	**50**	4.18E + 14	2.64E + 14	1.43E + 15	1.38E + 16	4.81E + 14	4.27E + 14	1.32E + 14	3.93E + 12	7.72E + 12	5.69E + 11	7.02E + 10	1.48E + 16
	Maximum max ($S_{i,j=const.,k=3}$) (Note 1) and max(St_i) (Note 2)	4.18E + 14	2.64E + 14	1.43E + 15	1.38E + 16	4.81E + 14	4.27E + 14	1.32E + 14	3.93E + 12	7.72E + 12	5.69E + 11	7.02E + 10	1.48E + 16

Normalized source terms $Sn_{i,j,k}$ for 5 years of cooling (Note 3)

i	**Specific power (W/gU)** ↓	$Sn_{i,j=1,k=3}$ **0.2-0.3**	$Sn_{i,j=2,k=3}$ **0.3-0.4**	$Sn_{i,j=3,k=3}$ **0.4-0.6**	$Sn_{i,j=4,k=3}$ **0.6-0.8**	$Sn_{i,j=5,k=3}$ **0.8-1**	$Sn_{i,j=6,k=3}$ **1-1.33**	$Sn_{i,j=7,k=3}$ **1.330-1.66**	$Sn_{i,j=8,k=3}$ **1.66-2**	$Sn_{i,j=9,k=3}$ **2-2.5**	$Sn_{i,j=10,k=3}$ **2.5-3**	$Sn_{i,j=11,k=3}$ **3-4**	**Total** Stn_i (Note 2)
1	**10**	64%	61%	41%	62%	54%	70%	44%	32%	21%	25%	25%	60%
2	**20**	78%	76%	64%	79%	73%	83%	67%	53%	42%	47%	48%	78%
3	**30**	87%	86%	80%	89%	85%	91%	82%	71%	62%	67%	68%	88%
4	**40**	94%	93%	91%	95%	94%	96%	92%	86%	82%	85%	85%	95%
5	**50**	100%	100%	100%	100%	100%	100%	100%	100%	100%	100%	100%	100%

k	*1*	*2*	***3***	*4*	*5*	*6*	*7*
Cooling times (years)	1	3	**5**	10	20	30	40

Note 1: Values are plotted in Figure 4(c), with the "Maximum" value provided in the legend.
Note 2: Values are included in Figure 4(h), with the "Maximum" St_i provided in the legend.
Note 3: Absolute source terms values are per 1 MTU.

Table B-2. Dose rates for specific power sensitivity analysis.

Dose rates $D_{i,j,k}$ (mrem/h) for 5 years of cooling (Note 3)

	Energy group (MeV) → *j*	*1*	*2*	*3*	*4*	*5*	*6*	*7*	*8*	*9*	*10*	*11*	
i	**Specific power (W/gU)** ↓	$D_{i,j=1,k=3}$ **0.2-0.3**	$D_{i,j=2,k=3}$ **0.3-0.4**	$D_{i,j=3,k=3}$ **0.4-0.6**	$D_{i,j=4,k=3}$ **0.6-0.8**	$D_{i,j=5,k=3}$ **0.8-1**	$D_{i,j=6,k=3}$ **1-1.33**	$D_{i,j=7,k=3}$ **1.330-1.66**	$D_{i,j=8,k=3}$ **1.66-2**	$D_{i,j=9,k=3}$ **2-2.5**	$D_{i,j=10,k=3}$ **2.5-3**	$D_{i,j=11,k=3}$ **3-4**	**Total** Dt_i
1	**10**	0.04	0.30	14.62	1,508.55	174.44	752.18	434.70	20.93	56.37	9.17	2.20	2,973.49
2	**20**	0.05	0.37	22.69	1926.66	237.63	893.23	655.56	34.36	111.20	17.30	4.19	3,903.25
3	**30**	0.06	0.42	28.25	2,162.87	277.42	974.30	801.08	45.88	164.68	24.60	5.95	4,485.51
4	**40**	0.06	0.46	32.36	2,317.99	305.03	1,030.77	904.76	55.96	216.31	31.04	7.48	4,902.24
5	**50**	0.06	0.49	35.50	2,427.28	325.12	1,072.18	980.84	64.73	265.03	36.65	8.80	5,216.69
	Maximum max $(D_{i,j=const.,k=3})$ (Note 1) and max(Dt_i) (Note 2)	0.06	0.49	35.50	2,427.28	325.12	1,072.18	980.84	64.73	265.03	36.65	8.80	5,216.69
Normalized dose rates $Dn_{i,j,k}$ for 5 years of cooling (Note 3)													
i	**Specific power (W/gU)** ↓	$Dn_{i,j=1,k=3}$ **0.2-0.3**	$Dn_{i,j=2,k=3}$ **0.3-0.4**	$Dn_{i,j=3,k=3}$ **0.4-0.6**	$Dn_{i,j=4,k=3}$ **0.6-0.8**	$Dn_{i,j=5,k=3}$ **0.8-1**	$Dn_{i,j=6,k=3}$ **1-1.33**	$Dn_{i,j=7,k=3}$ **1.330-1.66**	$Dn_{i,j=8,k=3}$ **1.66-2**	$Dn_{i,j=9,k=3}$ **2-2.5**	$Dn_{i,j=10,k=3}$ **2.5-3**	$Dn_{i,j=11,k=3}$ **3-4**	**Total** Dtn_i (Note 2)
1	**10**	64%	61%	41%	62%	54%	70%	44%	32%	21%	25%	25%	57%
2	**20**	78%	76%	64%	79%	73%	83%	67%	53%	42%	47%	48%	75%
3	**30**	87%	86%	80%	89%	85%	91%	82%	71%	62%	67%	68%	86%
4	**40**	94%	93%	91%	95%	94%	96%	92%	86%	82%	85%	85%	94%
5	**50**	100%	100%	100%	100%	100%	100%	100%	100%	100%	100%	100%	100%

k	*1*	*2*	***3***	*4*	*5*	*6*	*7*
Cooling times (years)	1	3	**5**	10	20	30	40

Note 1: Values are plotted in Figure 5(c), with the "Maximum" value provided in the legend.
Note 2: Values are included in Figure 5(h), with the "Maximum" Dt_i provided in the legend.
Note 3: Dose rate values are from source term per 1 MTU. Shielding is provided by a concrete cask discussed in Section 3.5